Towards automation and quantification of reperfusion assessment in medical images of the brain, heart, and reconstructed gastric tube

Prasetya, H.

Publication date
2023

Document Version
Final published version

Towards Automation and Quantification of Reperfusion Assessment in Medical Images

of the brain, heart, and reconstructed gastric tube

Haryadi Prasetya

Towards automation and quantification of reperfusion assessment in medical images

of the brain, heart, and reconstructed gastric tube

Haryadi Prasetya

Cover design: Haryadi Prasetya & DALL·E 2
Lay-out: Haryadi Prasetya

Printed by: ProefschriftMaken

ISBN: 978-94-6469-374-4

The work in this thesis was supported by the Indonesia Endowment Fund for Education (LPDP), Ministry of Finance, Republic of Indonesia through LPDP Scholarship Program for Doctorate Students and by the grant from the Netherlands Organization for Health Research and Development (ZonMw).

Financial support by the Dutch Heart Foundation for the publication of this thesis is gratefully acknowledged.

DALL·E 2 is an AI system that can create realistic images and art from a description in natural language developed by OpenAI. OpenAI assigns to Haryadi Prasetya all its right, title and interest in and to the output generated and returned by the services.

Towards automation and quantification of reperfusion assessment in medical images of the brain, heart, and reconstructed gastric tube

ACADEMISCH PROEFSCHRIFT

ter verkrijging van de graad van doctor
aan de Universiteit van Amsterdam
op gezag van de Rector Magnificus
prof. dr. ir. P.P.C.C. Verbeek
ten overstaan van een door het College voor Promoties ingestelde commissie,
in et openbaar te verdedigen in de Agnietenkapel
op woensdag 21 juni 2023, te 10.00 uur

door Haryadi Prasetya
geboren te Laxou

Promotiecommissie

Promotores:	prof. dr. H.A. Marquering	AMC-UvA
	prof. dr. E.T. van Bavel	AMC-UvA
Copromotor:	prof. mr. dr. B.A.J.M. de Mol	AMC-UvA
Overige leden:	prof. dr. J.A. Reekers	AMC-UvA
	prof. dr. ir. H.W.A.M de Jong	Universiteit Utrecht
	prof. dr. R.J. de Winter	AMC-UvA
	prof. dr. ir. A.G. Hoekstra	Universiteit van Amsterdam
	prof. dr. L. Reneman	AMC-UvA
	prof. dr. ir. T.L.E. Rajab	Institut Teknologi Bandung

Faculteit der Geneeskunde

For my parents, Aya, and Milarose.

CONTENTS

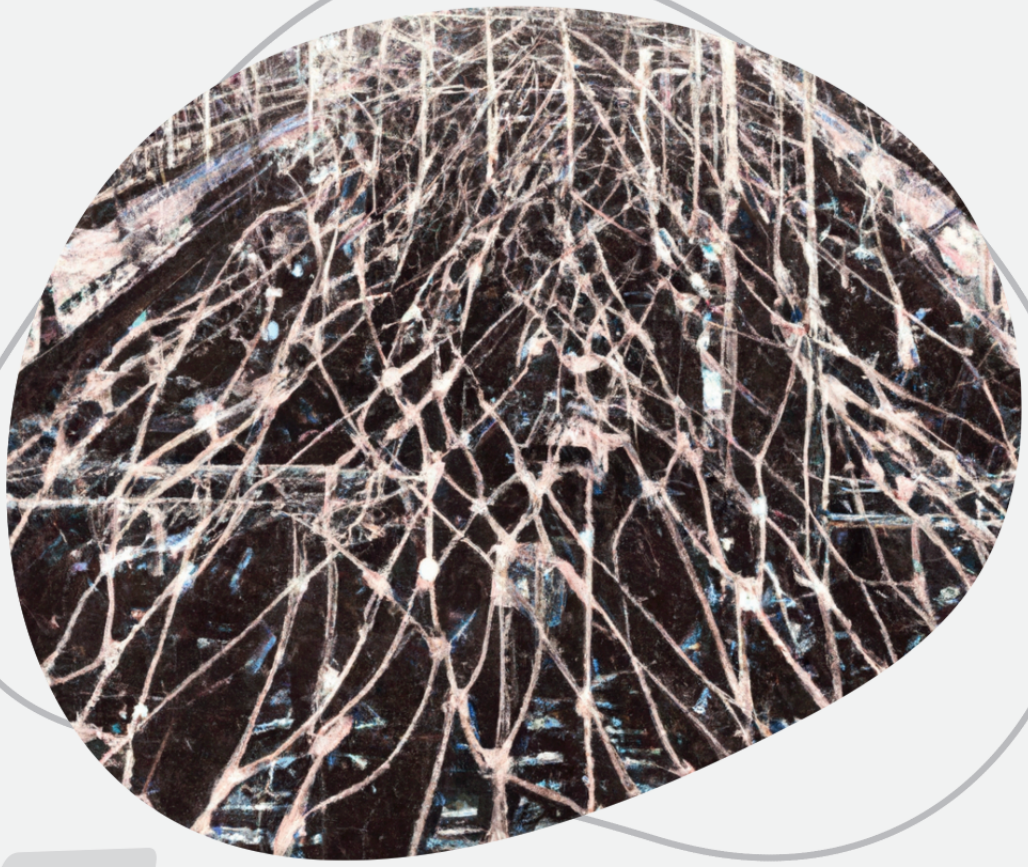

DALL·E 2: "A neural network made of train railways, digital art"

Chapter 1

GENERAL INTRODUCTION

TISSUE PERFUSION PHYSIOLOGY

Tissue perfusion refers to the delivery of oxygen-rich blood to tissue via the arterial network and, subsequently, the capillaries. With the exception of lung tissue, in all organs, oxygen diffuses from the capillaries to the parenchyma to fulfil the oxidative requirements. Afterwards, the generated carbon dioxide diffuses back to the capillaries, where it is transported through the venular system and eventually leaves the body through the lungs. Impaired perfusion causes the disruption of several important cellular processes, eventually leading to tissue necrosis. If such an event occurs in critical organs such as the brain or heart, it may prove to be lethal.[1]

The perfusion flow is regulated by local and central mechanisms. Local control is referred to as autoregulation of microvascular blood flow and involves, among others, metabolic, myogenic and shear stress-dependent mechanisms.[2] According to the classic metabolic theory, the flow through the microvascular bed is controlled by a direct relationship between the parenchymal cell partial pressure of oxygen (pO_2) and arteriolar smooth muscle cell contraction.[3] In case of oxygen deprivation, arterioles respond to the low pO_2 by dilation, reducing microvascular resistance and increasing local flow and capillary perfusion, returning the oxygenation level to normal. This relationship persists in the opposite case, wherein contracted arterioles lower excessive tissue oxygenation. In specifically the brain, such local control is not a mere oxygen response but involves a complex interplay between neurons, astrocytes and several vascular and perivascular cells.[4] In addition to these metabolic responses, the classic myogenic theory explains vasoregulation by the inherent response of arteriolar smooth muscle to its transmural pressure.[5] An increase in transmural pressure constricts the arterioles and a decrease in transmural pressure dilates them. A third important response is a dilation induced by increased wall shear stress. Wall shear stress refers to the dragging force of the flowing blood, which is sensed by the endothelial cells that form the inner cell layer of all blood vessels. There is a strong interplay of such local mechanisms. As an example, studies found that metabolic mechanisms explain microvessel dilation during subnormal tissue oxygenation while myogenic mechanisms account for microvessel constriction during overoxygenization of the tissue.[6,7] Also, individual segments within the

arterial and arteriolar network are differentially sensitive to pressure, shear stress and metabolites. A true understanding of local flow regulation requires a network analysis of the vascular bed.[8,9] In addition to local control, central mechanisms regulate organ perfusion at a more global level. These processes include autonomic nervous innervation and hormonal pathways and are relevant for, among others, the regulation of total peripheral resistance and mean arterial pressure.[10]

One important component of autoregulation is the development of vasodilator reserve, i.e., the ability to increase flow by vasodilation. Vasodilator reserve can be determined by measuring blood flow in autoregulation and during maximal pharmacological vasodilation. In slowly developing ischemic diseases like coronary artery disease, the vasodilator reserve is gradually lost. This results in stable angina and eventually in unstable angina, with chest pain and oxygen shortage at rest. In the brain, the effects of exhausted vasodilator reserve are far less clear, but it has been argued that chronic brain underperfusion is associated with dementia.[11] During acute vascular events, such as myocardial infarction and stroke, vasodilator reserve becomes irrelevant in light of complete occlusion.

Natural bypass vessels, so-called collaterals, may become available for recruitment when the main feeding artery is failing. The collaterals play roles in both chronic and acute conditions. In chronic underperfusion, they may remodel structurally to a much larger diameter, a process known as arteriogenesis.[12] In acute myocardial infarction and stroke, perfusion relies on the current state of collaterals, although slight vasodilation may occur.

MEASURING TISSUE PERFUSION

Since adequate perfusion is critical for organ function, it is important to have robust and accurate perfusion assessment methods. Advancements in medical imaging technologies, such as higher resolution and faster imaging, allow both direct measurements of perfusion by visual inspection of the images and indirect measurements by analyzing contrast dynamics from which perfusion parameters are derived. Perfusion measures and their derivatives have been widely

investigated for their clinical utility in determining intervention strategy, evaluating treatment, stratifying risks, and predicting patient outcome.[13–15]

Perfusion can be measured by a myriad of medical imaging modalities, each with its own spatial and temporal resolution for the detection of intravascular flow and perfusion of contrast agents. These contrast agents have been used to enhance the visibility of the vessels through which they travel and help differentiate the vessels from the rest of the organs. Medical imaging with the use of contrast agents is commonly known as angiography. Additionally, contrast injection allows kinetic analysis of the concentration-time characteristics measured in an individual voxel or area of interest in the image where the contrast is detected. Such analysis enables the derivation of hemodynamic parameters, which are proxy measures for perfusion.

KINETIC ANALYSIS OF DYNAMIC CONTRAST ENHANCEMENT

Let us consider a region of interest in the image where the contrast perfuses the tissue. In principle, signal intensity as a function of time of this region of interest can be used to approximate the contrast concentration over time, although the complexity of such a measurement depends on the imaging modality. The so-called concentration-time curve is quantifiable by deriving summary properties such as contrast arrival time, time-to-peak, maximum concentration, and transit time. However, these parameters are influenced by several factors in addition to the tissue properties, including contrast injection rate and volume and contrast dispersion.[16] Therefore, to accurately measure the perfusion parameters of the tissue, these confounding effects need to be removed by separating arterial and tissue contributions in the perfusion model. This is achievable by deconvolution of the concentration-time curve by the arterial input function (AIF). AIF is measured at a reference point proximal to the region of interest, commonly preferred to be a major artery.[17] However, this problem is non-trivial and conceptually challenging. The most obvious concern is to solve a single-state equation of indicator-dilution theory with two unknown variables: blood flow and residue function.

$$C_t(t) = AIF \otimes [BF \cdot R(t)]$$

$C_t(t)$ is the concentration-time curve in tissue, BF is blood flow, and $R(t)$ is the residue function which describes the fraction of the instantaneous bolus of contrast agent that remains in the tissue at time t. $R(t)$ is dimensionless and decays from unity at $t = 0$ to zero at $t = \inf$. The product of BF and $R(t)$ is called the impulse response function (IRF).[18] This equation can be solved using a deconvolution method. In the absence of a general solution, multiple methods have been proposed to solve this so-called inverse problem: model-dependent approaches that estimate parameters for residue function with maximum likelihood or Bayesian methods and model-independent approaches such as singular value decomposition.[19,20] After the residue function is determined, BF and mean transit time (MTT) can be calculated as follows[21]:

$$\mathrm{BF} = \max\big(\mathrm{IRF}(t)\big)$$

$$\mathrm{MTT} \overset{\text{def}}{=} \int R(t)dt = \frac{1}{\max\left(\mathrm{IRF}(t)\right)} \int \mathrm{IRF}(t)dt$$

Vascular volume (VV) can then be calculated from BF and MTT using the central volume theorem or derived directly from the residue function.[18,22]

$$\mathrm{VV} = \mathrm{MTT} \cdot \mathrm{BF}$$

$$\mathrm{VV} = \int \mathrm{IRF}(t)dt$$

Another practical perfusion parameter, time-to-maximum of residue function (Tmax), can also be computed from the residue function.

$$\mathrm{Tmax} = \arg\max_t(R(t))$$

This parameter essentially reflects the delay and dispersion of the contrast agent during its passage from the arterial input location to the tissue, which depends on the blood flow. The relations between the perfusion parameters and residue function are illustrated in **Figure 1b**. Although the kinetic analysis provides a theoretical framework as a basis for deriving perfusion parameters, it is important to note that deconvolution is an ill-posed problem. This implies that there are

many approximate solutions that can reproduce the deconvolved signals; the correct values of perfusion parameters are difficult to find.

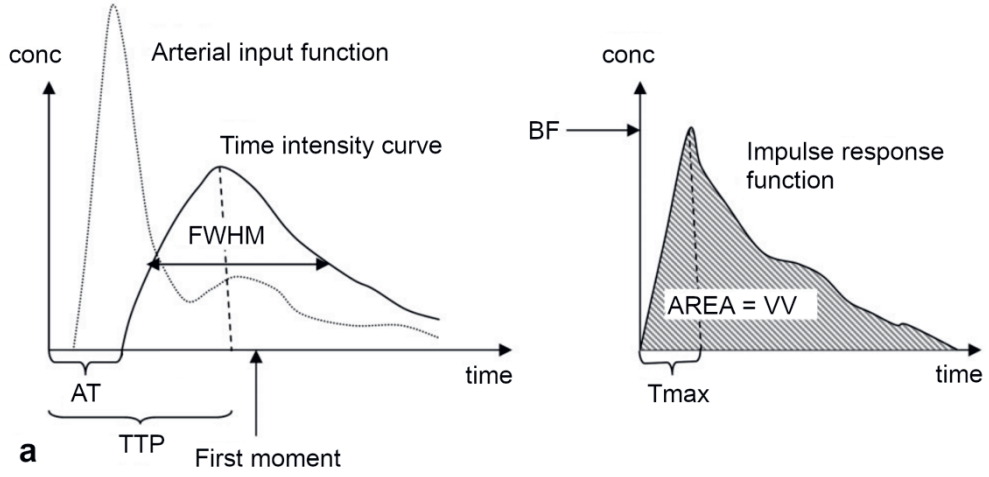

Figure 1. Tracer kinetic analysis. The concentration-time curve is the measured intensity in a tissue of interest over time. This curve can be characterized into summary parameters such as arrival time (AT), time-to-peak (TTP), full-width half maximum (FWHM), and first moment (centroid of the area under the curve) (a). This concentration-time curve depends on the contribution from both the arterial input function and the tissue impulse response function. The dependence on the arterial input function is removed by deconvolving the concentration-time curve with the arterial input function, resulting in the tissue impulse response function (b). From this impulse response function, perfusion parameters such as blood flow (BF), vascular volume (VV), and time-to-maximum (Tmax) can be derived.

PERFUSION IMAGING MODALITIES

Multiple imaging modalities support dynamic angiographic visualization via contrast administration that allows perfusion assessment. These modalities include x-ray angiography, computed tomography (CT), magnetic resonance imaging (MRI), and fluorescence imaging.

X-ray angiography is a fluoroscopy-based imaging technique that leverages contrast agent injection to visualize blood vessels over time. All tissues in the body, including blood vessels, absorb X-ray radiation at varying rates. The appearance of blood vessels and their adjacent tissues in the resulting radiographic image is almost indistinguishable. Therefore, a radiopaque vascular contrast agent is required to differentiate the vessels from the rest of the tissues.

The generated radiographic image that highlights blood vessels is called an angiogram. In such an angiogram, the tissue perfusion is expressed as a blush appearance around and at the end of arterial trees. The visibility of vessels and perfusion can be further increased using digital subtraction to remove bones and other obfuscating tissues, a technique called digital subtraction angiography.

CT provides an additional spatial dimension to conventional X-ray, among other things, as it provides volumetric data of the scanned body part. This is achieved by rotating the X-ray tube around the gantry during which the X-ray passes through the patient body and is received by detectors. Similar to X-ray angiography, the administration of a contrast agent enhances the visualization of the vasculature in the scan. In CT Perfusion (CTP), a series of images of the vasculature enhanced with a contrast agent are acquired over time. The acquisition time is determined to capture the wash-in and wash-out of contrast agent at any individual brain voxel in the scan, assuring a full-time attenuation curve.[23] The time attenuation curve of a voxel or region of interest where a major intracranial artery is located is selected as the arterial input function. The availability of the time attenuation curves and the arterial input function allows tracer kinetic analysis which eventually computes voxel-wise perfusion parameters such as cerebral blood flow (CBF), cerebral blood volume (CBV), MTT, and Tmax. These perfusion parameters form a basis for localized perfusion assessment on CTP.

A common perfusion technique on MRI is dynamic susceptibility contrast (DSC-MRI). Perfusion parameters derived from this technique are generally based on similar principles of tracer kinetic models as used in CTP. The contrast agent concentration is calculated in terms of relaxivity and the measured T2 or T2* signal decrease on the voxel of interest.[24] Another MRI technique for measuring perfusion that has been gaining traction is arterial spin labeling (ASL). This technique is non-invasive and uses magnetically tagged arterial blood water protons as an alternative tracer to exogenous contrast agent.[25]

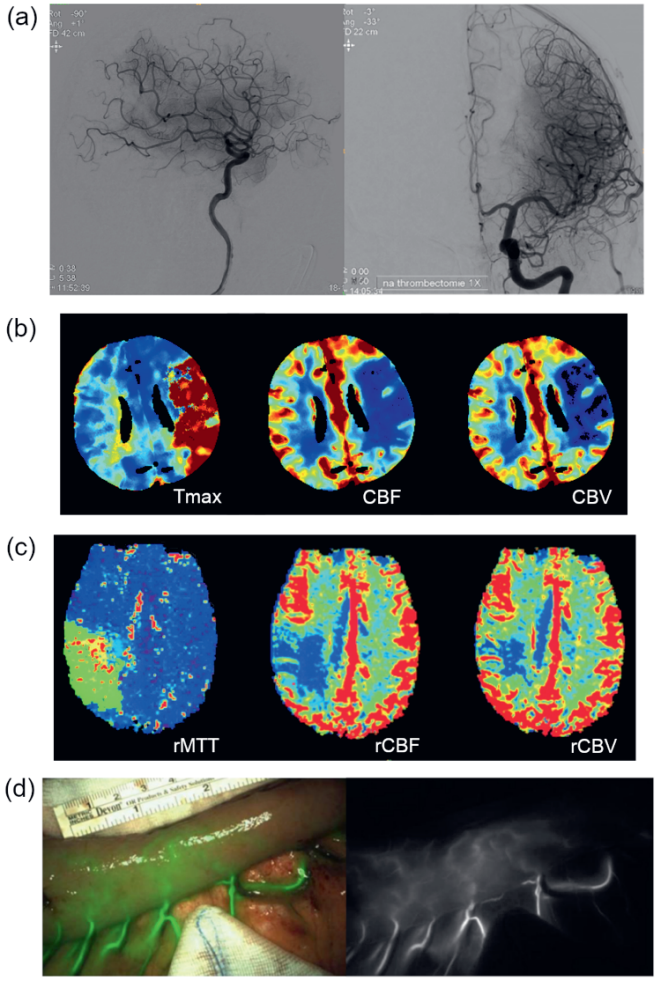

Figure 2. Examples of perfusion imaging modalities. Digital subtraction angiography images (a) highlight cerebral arteries and antegrade perfusion in lateral (left) and anteroposterior (right) projections. CT Perfusion maps (b) show a hypoperfused lesion on the left hemisphere as indicated by a high Tmax (left), low CBF (middle) and low CBV (right). Similarly, hypoperfusion is depicted in dynamic susceptibility contrast of MR T2* images (c) as a lesion with prolonged relative mean transit time (left) and low in both relative CBF (middle) and relative CBV (right). Finally, fluorescence imaging (d) on a gastric tube after esophagectomy following administration of indocyanine green (left) shows fluorescent dye distribution along the tube. The dye pattern is useful for intraoperative evaluation of perfusion on anastomoses as a non-homogenous pattern may be indicative of anastomotic failure. CT Perfusion maps were generated using StrokeViewer Perfusion, Nicolab. MR Perfusion maps and fluorescence imaging figures are reprinted with permission.[15,27]

Finally, near-infrared fluorescence imaging is an emerging perfusion technique useful for intraoperative applications including angiography, vessel patency and soft tissue perfusion assessment.[26] This imaging technique supports real-time display with a high spatial resolution that captures emitted fluorescence due to ultraviolet excitation following the administration of the fluorescent agent, e.g., indocyanine green.

Various perfusion measures based on dynamic contrast assessment have been introduced, and a critical evaluation of their value and usefulness in clinical settings is needed. In the absence of a true quantitative and validated perfusion measure based on contrast dynamics, visual perfusion grading systems have been suggested.

VISUAL PERFUSION GRADING SCALES

Based on the used modality and the disease, multiple visual perfusion grading systems have been established. In patients with myocardial infarction, a four-point scale named myocardial blush grade is used to grade the perfusion after percutaneous coronary intervention.[28] This scale was found to be a strong angiographic predictor of mortality in patients after primary angioplasty. For patients undergoing esophagectomy, intraoperative assessment of perfusion allows risk stratification of necrosis, therefore avoiding post-surgery complications such as anastomotic leakage.[29] Such intraoperative perfusion assessment, for instance, may be achieved by optical fluorescence imaging.[30] A similar rationale applies in the case of acute ischemic stroke, where the result of perfusion assessment factors in treatment selection and evaluation. The commonly used grading system here is the modified treatment in cerebral ischemia (TICI) scale, which is an estimate of the perfusion area visible in digital subtraction angiography relative to the target downstream territory.[31] This scale had since been refined and reintroduced as extended TICI (eTICI).[32] Additional grading scales are used to account for retrograde perfusion by proxy of collateral grading on digital subtraction angiography or CT angiography images.[33]

Although the visual perfusion grading scores have been found to have prognostic value in clinical applications, they have several problems that need to be

addressed. First, they mostly have an ordinal and low-resolution scale, i.e., minimal myocardial blush vs moderate myocardial blush in myocardial blush grade. This lack of resolution may translate to a loss of clinically relevant information. Subsequent resolution improvements to the TICI scale that called for redefinitions of successful reperfusion treatment have provided evidence that a more precise measure of perfusion is necessary. Second, visual grading scores are inherently dependent on the observer who is performing the grading. This is particularly true as the assessment with a high degree of complexity may necessitate a more experienced observer to achieve good interrater agreement.[34] Many studies reported varying results for interobserver agreement on TICI scoring, ranging from poor to good agreement. A recent study illustrated how the operators tend to overestimate the perfusion status after the intervention compared to core lab adjudication.[35] Finally, visual perfusion assessment is often time-consuming.

AIM AND OUTLINE

The aim of this thesis is to form a base for new automated and quantitative alternatives to the qualitative perfusion scores. Several visual perfusion grading scales in multiple organs including the heart, gastric circulation, and the brain are used as references to extract relevant information from medical images. The exploration towards the formation of a base for new automated and quantitative perfusion measure alternatives includes:

- dissecting the existing quantitative methods in assessing myocardial perfusion;
- modeling microvascular hemodynamics of a gastric conduit to predict reduced flow post-esophagectomy;
- developing and validating a new quantitative score in brain perfusion for stroke patients; and
- validating a new collateral assessment method based on CT Perfusion parameters.

In chapter 3, the initial assessment of the myocardial perfusion assessment computer program called Quantitative Blush Evaluator (QuBE) revealed that the

claimed performance of QuBE was not reproducible in our dataset of HEBE trial patients.[36] We provided evidence as to why QuBE, at its current state, may not yet be appropriate to evaluate reperfusion success in a patient with myocardial infarction after percutaneous coronary intervention.

Chapter 2 exhibits the potential of fluorescence dynamics to identify impaired perfusion in the anastomosis of gastric conduit after esophagectomy. In order to investigate the relations between fluorescence dynamics and the reduced flow, we developed a perfusion model as well-mixed compartments of arteries and veins and observed the dynamics of well-perfused sites and anastomotic sites.

The perfusion assessment of acute ischemic stroke patients is studied in chapter 4. We used the TICI methodology to develop a new semi-automated quantitative score, namely quantitative TICI (qTICI), that provides a perfusion assessment on digital subtraction angiography images of patients with a proximal large vessel occlusion. In chapter 5, we implemented a collateral scoring method based on CT Perfusion using multiple perfusion parameters within a hypoperfused volume. These last two chapters are part of the multicenter clinical registry of endovascular treatment for acute ischemic stroke in the Netherlands substudies.[37]

We conclude this thesis with a general discussion and provide recommendations for future research pertaining to the automation and quantification of perfusion assessment.

REFERENCES

1. Granger HJ, Schelling ME, Lewis RE, Zawieja DC, Meininger CJ. Physiology and pathobiology of the microcirculation. *Am J Otolaryngol*. 1988;9(6):264-277. doi:10.1016/S0196-0709(88)80035-8

2. Davis MJ, Hill MA, Kuo L. Local Regulation of Microvascular Perfusion. In: *Microcirculation*. Elsevier; 2008:161-284. doi:10.1016/B978-0-12-374530-9.00006-1

3. Gutterman DD, Chabowski DS, Kadlec AO, et al. The Human Microcirculation: Regulation of Flow and beyond. *Circ Res*. 2016;118(1):157-172. doi:10.1161/CIRCRESAHA.115.305364

4. Iadecola C, Nedergaard M. Glial regulation of the cerebral microvasculature. *Nat Neurosci*. 2007;10(11):1369-1376. doi:10.1038/nn2003

5. Clifford PS. Local control of blood flow. Am J Physiol - *Adv Physiol Educ*. 2011;35(1):5-15. doi:10.1152/advan.00074.2010

6. Reglin B, Pries AR. Metabolic control of microvascular networks: Oxygen sensing and beyond. *J Vasc Res*. 2014;51(5):376-392. doi:10.1159/000369460

7. Davis MJ, Hill MA. Signaling mechanisms underlying the vascular myogenic response. *Physiol Rev*. 1999;79(2):387-423. doi:10.1152/physrev.1999.79.2.387

8. Cornelissen AJM, Dankelman J, Vanbavel E, Spaan JAE. Balance between myogenic, flow-dependent, and metabolic flow control in coronary arterial tree: A model study. *Am J Physiol - Hear Circ Physiol*. 2002;282(6 51-6):2224-2237. doi:10.1152/ajpheart.00491.2001

9. Pries AR, Secomb TW. Microvascular adaptation - Regulation, coordination and function. *Z Kardiol*. 2000;89(SUPPL. 9):117-120. doi:10.1007/s003920070016

10. Hill CE, Phillips JK, Sandow SL. Heterogeneous control of blood flow amongst different vascular beds. *Med Res Rev*. 2001;21(1):1-60. doi:10.1002/1098-1128(200101)21:1<1::AID-MED1>3.0.CO;2-6

11. Duncombe J, Kitamura A, Hase Y, Ihara M, Kalaria RN, Horsburgh K. Chronic

cerebral hypoperfusion: A key mechanism leading to vascular cognitive impairment and dementia. Closing the translational gap between rodent models and human vascular cognitive impairment and dementia. *Clin Sci*. 2017;131(19):2451-2468. doi:10.1042/CS20160727

12. Heil M, Schaper W. Insights into Pathways of Arteriogenesis. *Curr Pharm Biotechnol*. 2007;8(1):35-42. doi:10.2174/138920107779941408

13. Maaniitty T, Knuuti J, Saraste A. Improvement in quantitative myocardial perfusion metrics after revascularization in chronic coronary artery disease. E*ur Heart J Cardiovasc Imaging*. 2022;23(6):753-754. doi:10.1093/ehjci/jeac014

14. Demeestere J, Wouters A, Christensen S, Lemmens R, Lansberg MG. Review of perfusion imaging in acute ischemic stroke: From time to tissue. *Stroke*. 2020;51:1017-1024. doi:10.1161/STROKEAHA.119.028337

15. Jansen SM, de Bruin DM, Wilk LS, et al. Quantitative Fluorescence Imaging of Perfusion - An Algorithm to Predict Anastomotic Leakage. *Life*. 2022;12(249). doi:10.3390/life

16. Ingrisch M, Sourbron S. Tracer-kinetic modeling of dynamic contrast-enhanced MRI and CT: A primer. *J Pharmacokinet Pharmacodyn*. 2013;40(3):281-300. doi:10.1007/s10928-013-9315-3

17. Calamante F. Arterial input function in perfusion MRI: A comprehensive review. *Prog Nucl Magn Reson Spectrosc*. 2013;74:1-32. doi:10.1016/j.pnmrs.2013.04.002

18. Ostergaard L. Principles of Cerebral Perfusion Imaging by Bolus Tracking. *J Magn Reson Imaging*. 2005;(22):710-717. doi:10.1002/jmri.20460

19. Knutsson L, Ståhlberg F, Wirestam R. Absolute quantification of perfusion using dynamic susceptibility contrast MRI: Pitfalls and possibilities. *Magn Reson Mater Physics, Biol Med*. 2010;23(1):1-21. doi:10.1007/s10334-009-0190-2

20. Østergaard L, Weisskoff RM, Chesler DA, Gyldensted G, Rosen BR. High resolution measurement of cerebral blood flow using intravascular tracer bolus passages. Part I: Mathematical approach and statistical analysis. *Magn*

Reson Med. 1996;36(5):715-725. doi:10.1002/mrm.1910360510

21. Fieselmann A, Kowarschik M, Ganguly A, Hornegger J, Fahrig R. Deconvolution-based CT and MR brain perfusion measurement: Theoretical model revisited and practical implementation details. *Int J Biomed Imaging*. 2011;2011. doi:10.1155/2011/467563

22. Konstas AA, Goldmakher G V., Lee TY, Lev MH. Theoretic basis and technical implementations of CT perfusion in acute ischemic stroke, part 1: Theoretic basis. *Am J Neuroradiol*. 2009;30(4):662-668. doi:10.3174/ajnr.A1487

23. Kämena A, Streitparth F, Grieser C, et al. Dynamic perfusion CT: Optimizing the temporal resolution for the calculation of perfusion CT parameters in stroke patients. *Eur J Radiol*. 2007;64(1):111-118. doi:10.1016/J.EJRAD.2007.02.025

24. Kiselev VG. On the theoretical basis of perfusion measurements by dynamic susceptibility contrast MRI. *Magn Reson Med*. 2001;46(6):1113-1122. doi:10.1002/mrm.1307

25. Petcharunpaisan S. Arterial spin labeling in neuroimaging. *World J Radiol*. 2010;2(10):384. doi:10.4329/wjr.v2.i10.384

26. Marshall M V., Rasmussen JC, Tan I-C, et al. Near-Infrared Fluorescence Imaging in Humans with Indocyanine Green: A Review and Update. *Open Surg Oncol J*. 2020;2(1):12-25. doi:10.2174/1876504101002010012

27. Parsons MW, Yang Q, Barber PA, et al. Perfusion magnetic resonance imaging maps in hyperacute stroke: Relative cerebral blood flow most accurately identifies tissue destined to infarct. *Stroke*. 2001;32(7):1581-1587. doi:10.1161/01.STR.32.7.1581

28. Henriques JPS, Zijlstra F, Hof AWJ Van, Boer M De, Dambrink JE, Gosselink M. Angiographic Assessment of Reperfusion in Acute Myocardial Infarction by Myocardial Blush Grade. *Circulation*. 2003:107:2115-2119. doi:10.1161/01.CIR.0000065221.06430.ED

29. Zehetner J, DeMeester SR, Alicuben ET, et al. Intraoperative Assessment of Perfusion of the Gastric Graft and Correlation With Anastomotic Leaks After Esophagectomy. *Ann Surg*. 2014;00(00):1-5.

doi:10.1097/SLA.0000000000000811

30. Quan YH, Kim M, Kim HK, Kim BM. Fluorescent image-based evaluation of gastric conduit perfusion in a preclinical ischemia model. *J Thorac Dis*. 2018;10(9):5359-5367. doi:10.21037/jtd.2018.08.46

31. Almekhlafi MA, Mishra S, Desai JA, et al. Not all "successful" angiographic reperfusion patients are an equal validation of a modified TICI scoring system. *Interv Neuroradiol*. 2014;20(1):21-27. doi:10.15274/INR-2014-10004

32. Liebeskind DS, Bracard S, Guillemin F, et al. eTICI reperfusion: defining success in endovascular stroke therapy. *J Neurointerv Surg*. 2019;11:433-438. doi:10.1136/neurintsurg-2018-014127

33. Jansen IGH, Berkhemer OA, Yoo AJ, et al. Comparison of CTA- and DSA-Based Collateral Flow Assessment in Patients with Anterior Circulation Stroke. *Am J Neuroradiol*. 2016;37(11):2037-2042. doi:10.3174/ajnr.A4878

34. Volny O, Cimflova P, Szeder V. Inter-Rater Reliability for Thrombolysis in Cerebral Infarction with TICI 2c Category. *J Stroke Cerebrovasc Dis*. 2017;26(5):992-994. doi:10.1016/J.JSTROKECEREBROVASDIS.2016.11.008

35. Zhang G, Treurniet KM, Jansen IGH, et al. Operator Versus Core Lab Adjudication of Reperfusion After Endovascular Treatment of Acute Ischemic Stroke. *Stroke*. 2018;49(10):2376-2382. doi:10.1161/STROKEAHA.118.022031

36. van der Laan A, Hirsch A, Nijveldt R, et al. Bone marrow cell therapy after acute myocardial infarction: the HEBE trial in perspective, first results. *Neth Heart J*. 2008;16(12):436-439. doi:10.1007/BF03086194

37. Jansen IGH, Mulder MJHL, Goldhoorn RJB. Endovascular treatment for acute ischaemic stroke in routine clinical practice: prospective, observational cohort study (MR CLEAN Registry). *BMJ*. 2018;360. doi:10.1136/BMJ.K949

DALL·E 2: “A stomach stranded on an island underneath milky way, by van Gogh”

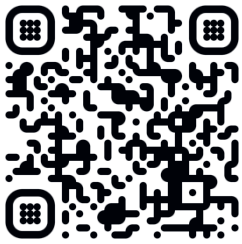

Chapter 2

ESTIMATION OF MICROVASCULAR PERFUSION AFTER ESOPHAGECTOMY

A QUANTITATIVE MODEL OF DYNAMIC FLUORESCENCE IMAGING

Haryadi Prasetya, Sanne M. Jansen, Henk A. Marquering, Ton G. van Leeuwen, Suzanne S. Gisbertz, Daniel M. de Bruin, Ed van Bavel

As published in MBEC 2019;57:1889-1900
DOI: 10.1007/s11517-019-01994-z

This work was supported by Indonesia Endowment Fund for Education (LPDP), Ministry of Finance, Republic of Indonesia through LPDP scholarship Program for Doctorate Students and by the grant from The Netherlands Organization for Health Research and Development (ZonMw project# 104002006).

ABSTRACT

Most common complications of esophagectomy stem from a perfusion deficiency of the gastric conduit at the anastomosis. Fluorescent tracer imaging allows intraoperative visualization of tissue perfusion. Quantitative assessment of fluorescence dynamics has the potential to identify perfusion deficiency. We developed a perfusion model to analyze the relation between fluorescence dynamics and perfusion deficiency. The model divides the gastric conduit into two well-perfused and two anastomosed sites. Hemodynamics and tracer transport were modeled. We analyzed the value of relative time-to-threshold (RTT) as a predictor of the relative remaining flow (RRF). Intensity thresholds for RTT of 20% to 50% of the maximum fluorescence intensity of the well-perfused site were tested. The relation between RTT and RRF at the anastomosed sites was evaluated over large variations of vascular conductance and volume. The ability of RTT to distinguish between sufficient and impaired perfusion was analyzed using c-statistics. We found that RTT was a valuable estimate for low RRF. The threshold of 20% of the maximum fluorescence intensity provided the best prediction of impaired perfusion on the two anastomosed sites (AUC = 0.89 and 0.86). The presented model showed that for low flows, relative time-to-threshold may be used to estimate perfusion deficiency.

Keywords: Fluorescence imaging, indocyanine green, gastric conduit model, perfusion, esophagectomy

INTRODUCTION

Esophagectomy, despite the arduous nature of the procedure, is a commonly used surgical technique to treat esophageal cancer.[1] The procedure involves gastric transposition to the thorax and removal of major arterial and venous connections. Anastomotic leakage, necrosis, and stricture are major complications of this procedure. The success of esophagectomy depends on maintenance of perfusion of the whole gastric tube.[2,3] Particularly, in the fundus, i.e., the proximal end of the gastric tube that is anastomosed with the remaining esophagus, perfusion is hampered as in this region, the perfusion fully depends on the presence of collateral connections. Insufficient perfusion hinders anastomotic healing or may even cause tissue necrosis. Early detection of insufficient perfusion could assist clinical decision making on additional surgical intervention, such as determination of the level of the anastomosis and primary anastomotic repair, consequently improving post-operative outcomes.[4] Accordingly, intra-operative monitoring of local perfusion in the gastric tube is needed to predict success of the procedure.

Recent developments in fluorescence imaging (FI) allow intra-operative visualization of local tissue perfusion in the gastric conduit.[5–9] This technique involves intravenous injection of indocyanine green (ICG) and monitoring of its appearance dynamics in gastric tissue. FI has shown a difference in fluorescence dynamics between native and anastomosed areas in the gastric conduit during surgery.[4] Preliminary experiments showed later time-to-peak of contrast arrival, suggesting lower perfusion, in areas closer to the fundus. However, the quantitative relation between contrast dynamics and actual perfusion of the gastric tissue has not been investigated. Moreover, alternative methods for detection of perfusion in this setting are not available.

Impaired perfusion results in slower contrast appearance compared to normal perfusion. Although time-to-peak is commonly used in dynamics measurements to assess perfusion, we hypothesize that time to intensity threshold is a valuable alternative because this measure can be performed in a shorter acquisition window of FI.[4] However, the validity of time to intensity threshold to assess local perfusion is unknown and may be complicated by the complexity of gastric tube

vascular network, which includes collateral connections. In this study, we present a comprehensive model that describes the deteriorated perfusion after esophagectomy and its relation with temporal ICG fluorescence intensity profiles. This model was used to explore the relation between reduced perfusion and slower fluorescence enhancement at anastomosed areas. Because the volumes of these vascular compartments affect the dynamics, the effect of variations in the vascular architecture of the gastric conduit on the relation between contrast dynamics and local perfusion was studied as well.[10,11] We included a wide range of vascular resistances and volumes in order to identify general trends in ICG enhancement dynamics as a measure for perfusion. Finally, those trends were used to evaluate the usefulness of time to intensity threshold as an estimate for local perfusion.

METHODS

Essentially, we defined a simulation model of the gastric tube that includes perfusion and ICG transport in four regions. Local perfusion in this model was determined for a large range of model parameters. RRF, the relative remaining flow, is the calculated flow after the intervention relative to the flow to that compartment before the intervention and is considered to be a predictor of clinical outcome. RTT, the relative time to threshold, is the calculated time to a threshold signal for local ICG appearance, normalized to the time to threshold in the first, well-perfused compartment. RTT is considered to be a surrogate for RRF. We analyzed how well RTT predicts RFF, how this depends on the chosen parameters, and which threshold should be taken.

Gastric Conduit Model

The reconstruction of the gastric conduit generally preserves the right gastroepiploic vessels and right gastric artery as the main source of blood supply to the gastric wall. Consequently, part of the gastric conduit close to the anastomosis is only supplied with blood from collateral connections in the gastric wall. We modeled the gastric conduit by introducing four sites, as shown in **Figure 1**. This choice was based on the four regions of interest (ROIs) for measurement of fluorescence intensity performed on constructed gastric conduit in the

prospective clinical study in Amsterdam Medical Center from October 2015 to June 2016.[12] **Figure 1a** shows a frame of constructed gastric conduit of a patient with the ICG visualizing the tissue perfusion. The ROI was a 300 pixels circle with #1 3 cm below the watershed, #2 the watershed, #3 3 cm above the watershed, and #4 the fundus. The measured fluorescence enhancement curves at the four ROIS are shown in **Figure 1b**. In the model, the four sites are connected through collateral arteries and veins. Site 3 and site 4 represent the anastomosed areas and perfusion here depends completely on collateral vessels. The distributed nature of the arterial, capillary and venous networks at each site is represented by a single lumped resistance thought to be situated in the arterioles and capillaries, connecting a proximal arterial volume to a distal capillary/venous volume. The vascular bed in the gastric tube is thus represented by eight compartments, four microvascular connections, three arterial collateral connections, and three venous collateral connections. The system is supplied and drained by large arteries and veins of the lower two sites (**Figure 1c**).

Parameter Space of The Model

We assumed identical vascular conductances and volume for each site and varied multiple model parameters including collateral artery and vein conductance relative to microvascular conductance (G_{ca}/G_c and G_{cv}/G_c), relative large vessel conductance (G_{LV}/G_c), and vascular volume including arterial and venous volume (AV and VV). Quantitative information on gastric vascular branching patterns is not available, but we considered that the above conductance ratios are likely to be highly variable between patients. We therefore evaluated the model over a large parameter space, including the presumed physiological range. Determining the physiological range for vessel conductance is difficult. Total conductance of the arterial and venous system depends on the network connectivity and the diameter of the individual segments in this network. Such data are, to the best of our knowledge, not available for the human stomach. We therefore covered a very wide range of values for G_{ca}/G_c and G_{cv}/G_c, spanning 0.01 to 100 for both ratios. The low end of the chosen spectrum reflects absence of collaterals, while the high end indicates a model with identical perfusion of all four sites. Physiological values were estimated to be less than 10, with no definitive lower boundary.[13, 14] The large vessels (LV) include terminal arteries, i.e., right gastric

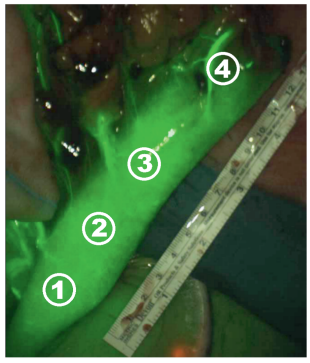

(a)

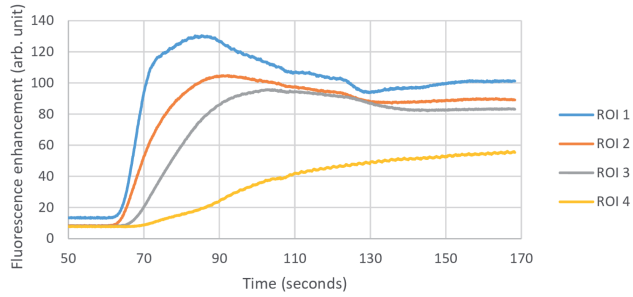

(b)

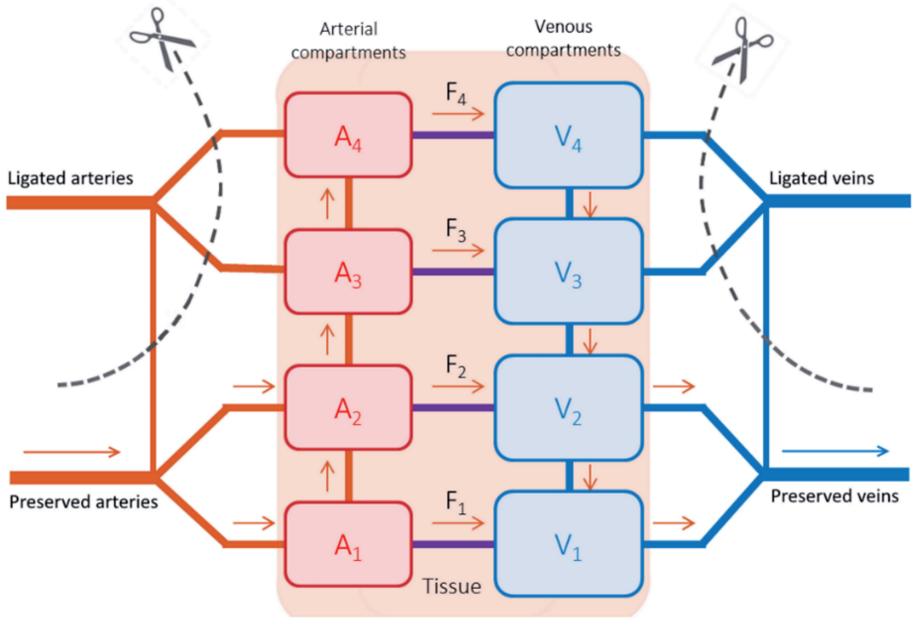

(c)

Figure 1. An image of constructed gastric conduit (a), obtained intraoperatively during fluorescence imaging post-esophagectomy, demonstrated perfusion with ICG and reduced fluorescence in the collateral-dependent upper part. The corresponding fluorescence enhancement curves of each ROI were measured at the gastric conduit (b). The model (c): From bottom to top: the sites 1-4, which correspond respectively to the ROIs. A site consists of an arterial and a venous compartment directly connected through a capillary bed (horizontal line between compartments). Collaterals, as depicted by vertical lines between compartments, connect the adjacent sites. In this figure, site 1 and 2 are well perfused, whereas site 3 and 4 are anastomosed. Arrows indicate direction of flow after the intervention.

artery and right gastroepiploic terminal artery, and initial veins, i.e., pyloric vein and right gastroepiploic initial vein. Relative conductance of the combined large arteries (G_{LV}/G_c) was 3 by default and spanned 1 to 100 when studying the effect of this parameter. Large vein conductance was fixed at twice the large artery conductance. We used physiological data describing the proportion of artery, capillary, and vein in a given volume in the systemic circulation to determine the physiological vascular volumes.[14, 15] The total volume of a site was calculated based on the volume of the ROI in the preceding clinical study.[12] The default vascular volumes were taken as 0.24 mL and 0.56 mL for arterial (AV) and venous (VV) compartments, respectively, spanning 0.12 mL to 1.12 mL when studying the effect of vascular volume to contrast dynamics.

ICG Transport Simulation

Pressure at each branching point in **Figure 1c** and flow in each segment was calculated using Kirchhoff's first law combined with Ohm's law, assuming laminar flow of a Newtonian fluid.[16] These calculated hemodynamic parameters depend on the pressures in the right gastroepiploic artery and vein and on the conductance of all segments. Arterial input and venous outflow pressure were taken as 70 mmHg and 0, respectively. Conductances were varied to evaluate their influence on perfusion. For each segment, after the pressure gradient was obtained, the flow was calculated. Tissue perfusion at the four sites is reflected by the predicted flow in the segments connecting arterial and venous compartments (F_1 to F_4).

The ICG enters the system from the hepatic artery into the gastroduodenal artery (greater curvature), which leads into right gastroepiploic artery, and the right gastric artery (lesser curvature). The ICG then flows into the various compartments from A_1 and A_2 towards capillaries in the native sites and collateral-dependent sites, and leaves the system via V_1 and V_2. ICG from the right gastric and the right gastroepiploic veins drains into the portal and the superior mesenteric vein, respectively. This ICG transport was simulated using the above vessel configuration and well-mixed arterial and venous compartments, where dynamics of dye concentration obey the following differential equation:

$$\frac{dC_k}{dt} = \frac{\sum_{j=1}^{m} UC_j \cdot UF_j - C_k \sum_{i=1}^{n} DF_i}{V_k} \quad (1)$$

with C_k the concentration of the dye in compartment k, m, and n the number of upstream and downstream vessel of compartment k, respectively, UC_j the concentration of upstream compartment j, UF_j upstream flow from this compartment, DF_i flow through i-th downstream vessel, and V_k the volume of compartment k.[17] This ordinary differential equation was numerically solved with a single-step solver based on the Dormand-Prince algorithm of Runge-Kutta method which computed C(t) from [C(t-Δt)].[18] The algorithm had six stages of function evaluation for each partial step and generated fourth-order and fifth-order approximation of C(t). The two approximations was subsequently compared to estimate the error which provides the basis to accept or reject the tentative C(t). The error estimate also modulated the step size, Δt, for the next time step.

The ICG signal intensity for each site was defined as the amount of ICG in both the arterial and venous compartments at time t:

$$\varphi_i(t) = AC_i(t) \cdot AV_i + VC_i(t) \cdot VV_i \quad (2)$$

where ϕ indicates the ICG signal, AC and AV denote the ICG concentration and the volume of the arterial compartment, respectively. VC and VV represent the ICG concentration and the volume of the venous compartment and i denotes the number of site. **Figure 2** shows an example of the simulated temporal profile of ϕ for each site.

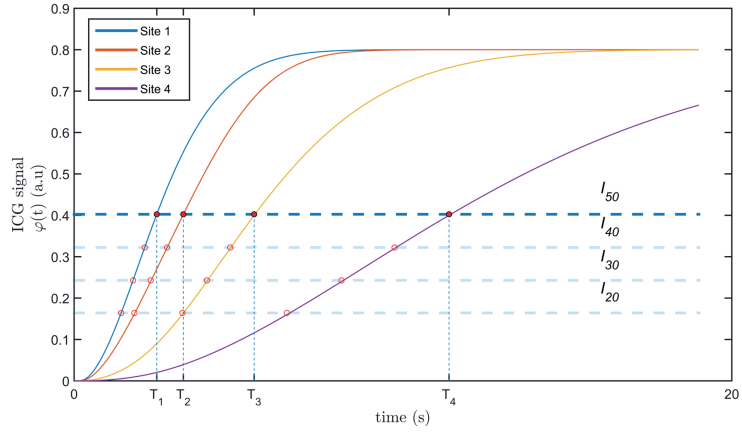

Figure 2. Example of contrast dynamics at the four sites with derivation of the respective times to threshold. Sites 1 and 2 have native perfusion, while sites 3 and 4 depend on collateral flow, and accordingly have slower contrast dynamics

Time Based Perfusion Estimate

For each simulation, the temporal profile of ϕ at each site was analyzed. This signal forms the base for the estimation of remaining perfusion after surgery. We propose a measure to describe relative impairment of flow in a collateral-dependent site. This measure was based on the time to threshold T_n which was defined as the time at which ϕ of site n reaches a fraction of the maximum of ϕ of site 1. For example, in **Figure 2**, T_4 is defined as the time it takes for ϕ to reach 50% of the maximum intensity in site 1 (I_{50}). This approach ensures that T_n can be calculated as long as the maximum ϕ in site 1 is recorded. We introduce RTT as a parameter on which RRF estimation can be based:

$$RTT_3 = T_1/T_3 \qquad RTT_4 = T_1/T_4$$

$$RRF_3 = F_3/F_{3\ presurgery} \qquad RRF_4 = F_4/F_{4\ presurgery} \tag{3}$$

With T_i the time to threshold and F_i the flow in site i. $F_{presurgery}$ is the flow prior to the ligation. It was calculated from the same model and using the same set of parameter values but with A_3 and A_4 still supplied by the large arteries and V_3 and V_4 still drained by the large veins. A range of intensity thresholds were tested: 20%, 30%, 40%, and 50% of the maximum ϕ of site 1. The starting point (t = 0) was defined as the first inflection of contrast intensity in site 1. RRF is the ratio of post- and pre-intervention flow. We hypothesized that for a large range of variation in vascular conductances and volumes, RTT is closely related to RRF, such that RTT is a possible measure for the effect of surgery on local perfusion.

Using the simulation scenarios detailed in the **Table 1**, we first evaluated the effect of G_{ca}/G_c and G_{cv}/G_c on the remaining perfusion in anastomosed sites by fixing G_{LV}/G_c, AV and VV to their default values (simulation 1). The effect of G_{LV}/G_c was tested while fixing AV and VV to 0.24 and 0.56 ml respectively (simulation 2). Finally, G_{LV}/G_c was maintained at its default value (3) while examining the effect of AV and VV (simulation 3). All tests were performed using all intensity

Table 1. Parameters of the model, simulation scenarios, and generated variables

Parameters	Definitions [unit]	Default	Min	Max
G_{ca}/G_c	Relative collateral artery conductance [-]		0.01	100
G_{cv}/G_c	Relative collateral vein conductance [-]		0.01	100
G_{LV}/G_c	Relative large vessel conductance [-]	3	1	100
AV	Arterial volume [ml]	0.24	0.12	1.12
VV	Venous volume [ml]	0.56	0.12	1.12
Simulation 1				
Model parameters varied: G_{ca}/G_c, G_{cv}/G_c Model parameters fixed to default: G_{LV}/G_c, AV, VV				
Simulation 2				
Model parameters varied: G_{ca}/G_c, G_{cv}/G_c, G_{LV}/G_c Model parameters fixed to default: AV, VV				
Simulation 3				
Model parameters varied: G_{ca}/G_c, G_{cv}/G_c, AV, VV Model parameters fixed to default: G_{LV}/G_c				
Generated variables				
Solving Kirchhoff's first law + Ohm's law	F_1, F_2, F_3, F_4			
	$F_{presurgery}$*			
Solving eq.1 & eq.2	T_1, T_2, T_3, T_4; for threshold 20% of maximum φ of site 1 (I_{20})			
	T_1, T_2, T_3, T_4; for threshold 30% of maximum φ of site 1 (I_{30})			
	T_1, T_2, T_3, T_4; for threshold 40% of maximum φ of site 1 (I_{40})			
	T_1, T_2, T_3, T_4; for threshold 50% of maximum φ of site 1 (I_{50})			

* $F_{presurgery}$ were similar across the sites

thresholds over the full range of collateral conductances. We then computed the RRF for all possible combinations of parameters for a range of possible outcomes (sample space) from Ohm's and Kirchhoff's laws. We included curve fits of the relation between RRF and RTT to illustrate the nature of the relation over collateral conductance space. We included curve fits of the relation between RRF and RTT to illustrate the nature of the relation over collateral conductance space. We tested the curve fit using linear, polynomial, and exponential function while evaluating the goodness-of-fit. A good fit was defined as a model that has low sum of squared of errors and high R^2. The prediction interval was calculated by taking into account the sample mean, sample standard deviation, sample size, and critical value of Student's t distribution at 95% confidence level. It should be noted that the indicated relations merely described the data and were not a

result of mathematical analysis of the model. Hence, these fits do not affect the further outcomes in this study. Finally, we performed receiver operating characteristic (ROC) curve analysis to select the best intensity threshold to estimate perfusion impairment. We arbitrarily chose RRF values to dichotomize the outcome into lacking versus adequate perfusion. For site 3, RRF < 50% was defined as lacking perfusion, and RRF ⩾ 50% was adequate perfusion. For site 4, RRF < 40% was defined as lacking perfusion, and RRF ⩾ 40% was adequate perfusion. The area of physiological sample space was treated as predictor variables on which logistic regression was applied to produce the ROC curve. The simulation was performed in Matlab on a standard PC running on Windows 7 with 3 GHz 16 CPUs, 32 GB RAM, and NVIDIA Quadro K4200 GPU.

RESULTS

The relation between RRF and RTT for sites 3 and 4 is shown in **Figure 3**, where the estimates are based on time to reach 20% (**Figure 3a**) to 50% (**Figure 3d**) of the maximum ϕ. The increase in collateral conductance correlates with higher RTT and RRF. Interestingly, aside from negligible variation in the resulting RRF, the varying balance of conductance between collateral arteries and collateral veins seems to be inconsequential (see Appendix). As can be seen, the relation between RTT and RRF is far from linear, with RRF being lower than RTT for low flows. For high flows, RTT becomes stable and insensitive to flow changes. We obtained good fits of the relation at site 3 by second-order polynomials, while for site 4, an exponential fit was needed. The RTT-RRF relation for various values of G_{LV} is illustrated in **Figure 4**. For low values of G_{LV}, the large vessels limit perfusion, thereby reducing the maximum possible levels of RRF. **Figure 5** shows the RTT-RRF relation for various vascular volumes. The RTT-RRF relation for low flows is relatively independent of the volumes. However for higher flows, i.e., better collaterals, the volumes indeed have an influence but rather than the absolute volume values, it is the ratio of arterial and venous volume that matters.

Figure 6 shows the relation between RTT and RRF for all above variations in conductances and volumes (4 sets of parameters). The pink area indicates the sample space for the full range of variations, while the green area denotes

possible outcomes when the parameters were varied between more realistic values.

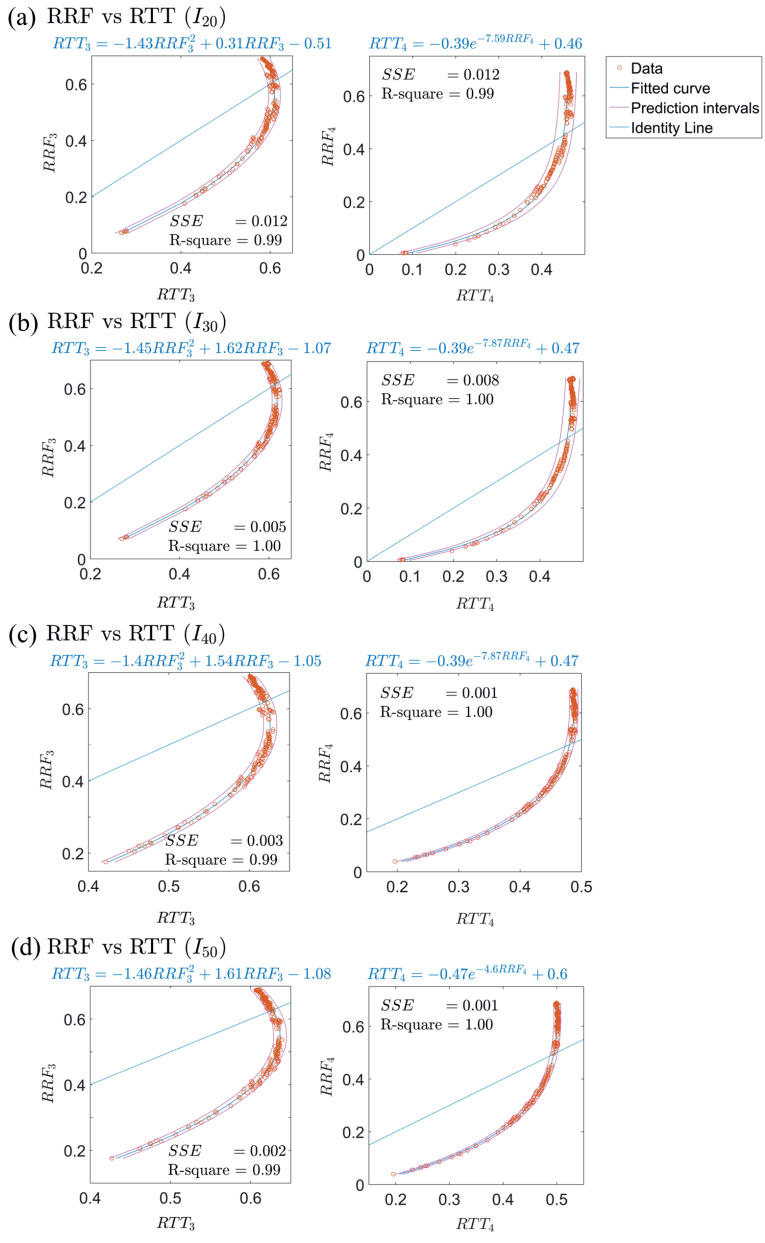

Figure 3. Result of simulation 1: relation between RTT and RRF over collateral conductance space, for site 3 (left) and 4 (right). The plots show RTT for thresholds of contrast arrival at 20% (a), 30% (b), 40% (c) and 50% (d) of the maximum contrast signal at site 1 as a function of RRF. The corresponded fitting functions and the respective goodness-of-fit parameters were also displayed.

The highest accuracy of RTT as RRF estimator resides in both extrema of RTT, particularly in the lower values. As example, for an observed RTT with I_{20} at site 4 of 0.2, the true RRF may have been 0.038 to 0.04, as compared to RTT of 0.5 which may have resulted from a larger range of true RRF from 0.31 to 0.5. Assessed by ROC, all four logistic regression models demonstrated good discriminatory capacity in both sites (see **Figure 7**). Although all intensity thresholds performed comparably well, I_{20} yielded the highest concordance of predictions with actual outcomes (AUC = 0.89 and 0.86 for sites 3 and 4, respectively).

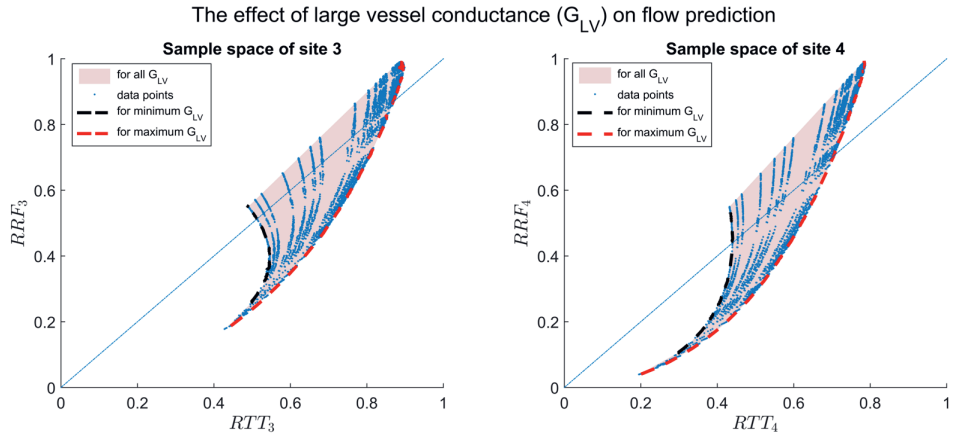

Figure 4. Result of simulation 2: variation in large vessels conductance changes the relation between true RRF and its estimate (RTT)

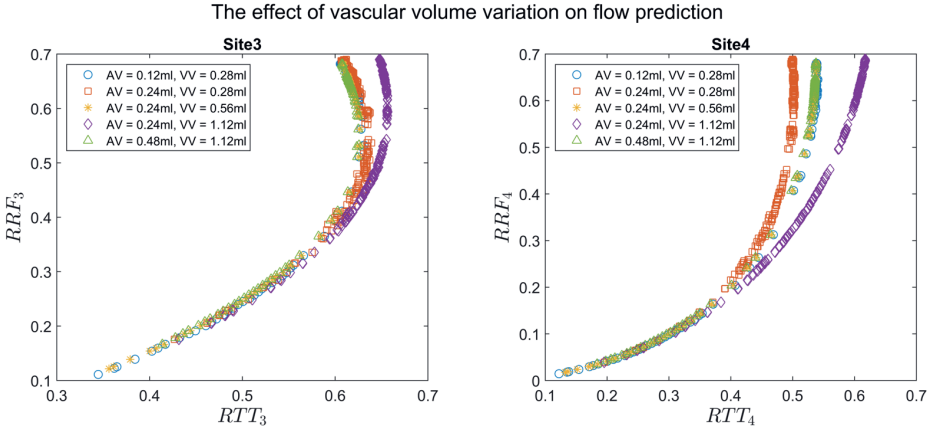

Figure 5. Result of simulation 3: RRF and RTT relation as a function of the ratio of arterial volume (AV) and venous volume (VV). Note that not every symbol/color is visible due to the overlay

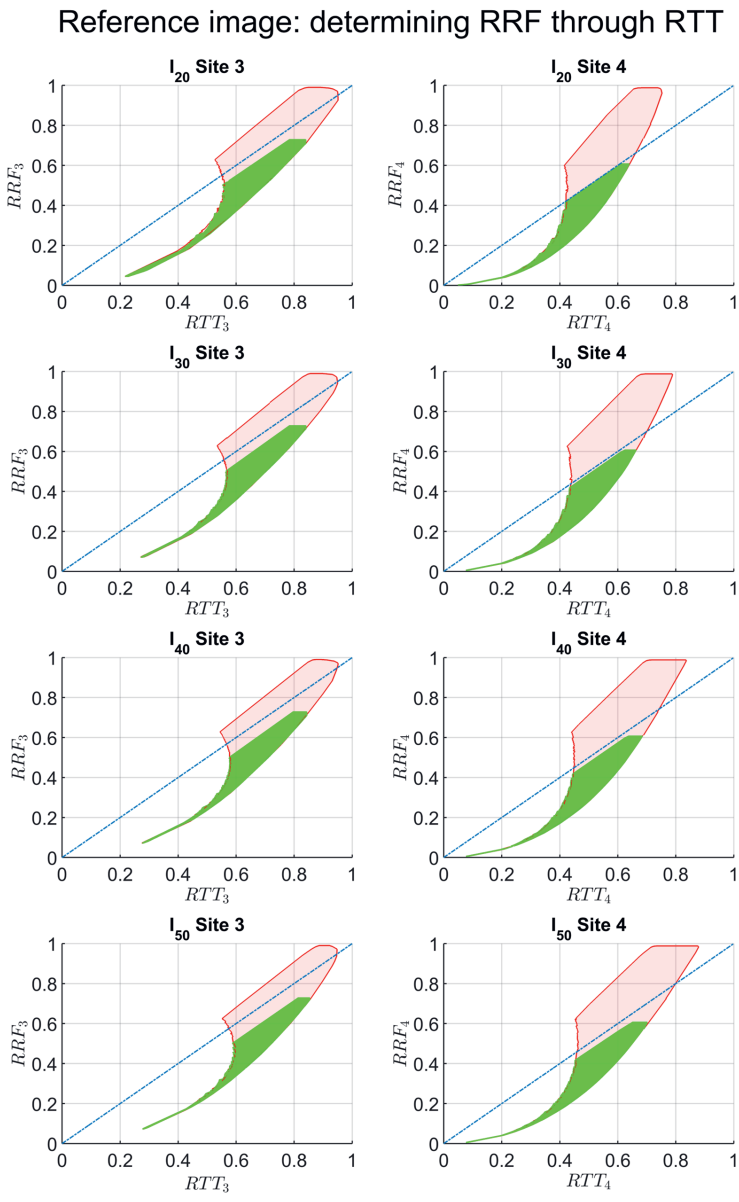

Figure 6 The sample space of the model from the complete (pink) and physiological (green) parameter space of collateral conductances (G_{ca}, G_{cv}), large vessel conductance (G_{LV}), and vascular volume (AV, VV). Was calculated from I_{20} to I_{50} (top to bottom).

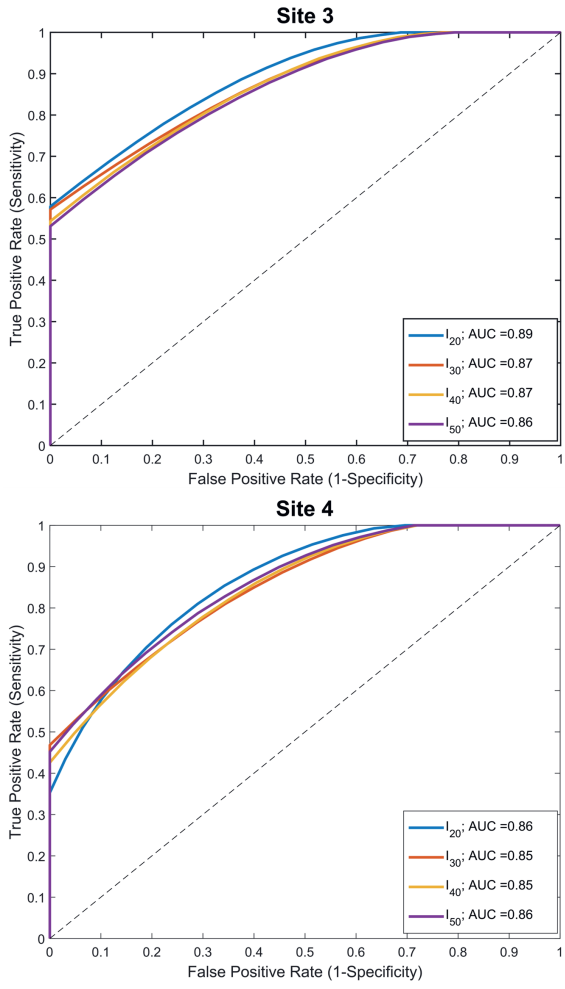

Figure 7 ROC curve of four threshold for site 3 (top) and 4 (bottom). The cutoff value was determined hypothetically as 0.5 and 0.4 for site 3 and 4 respectively

DISCUSSION

In this study, we introduced a gastric conduit model and used this to identify the effects of various combinations of vascular conductance and volume on ICG dynamics. The results indicate that the relation between delayed time-to-threshold (indicated by RTT) and reduced flow (indicated by RRF) is not trivial. We have shown a strong dependency of this relation on collateral conductance, large vessel conductance, and vascular volume. Despite this dependency, we found that time-to-threshold at the collateral-dependent sites can be used to estimate whether remaining perfusion is sufficient.

Perfusion Model Analysis

The vascular tree can be modeled using several choices for the level of detail of the branching network. One extreme is to have a full network of vessel segments, with poroelastic models for the smallest vessels.[19–21] The other extreme would be a single-vessel lumped model that disregards the detailed geometric structure of vascular tree thus reducing the complexity of the model.[10, 22, 23] We believe that the current choice for a limited set of compartments is optimal for the current purpose since the actual small vessel structure in the ROI of the gastric conduit is not well-defined and likely to be highly variable. The four ROIs used in this study, which account for both arterial and venous volumes, are based on a preliminary study using clinical data.[12] The ROI 1, 2, and 3 were equidistant (3 cm apart), while ROI 4 was located in the fundus. We separated arterial and venous network into two compartments of lumped vessels since these compartments influence the contrast dynamics in each ROI. Hence, this model allowed us to evaluate the role of the arterial and venous collateral on the tissue perfusion. Other configuration of the model was not investigated (for instance an eight-site model). This choice would affect the values of the modeling parameters, since clearly the volumes and conductances in each site would be different. Yet, there seems little reason to suspect that the modeling outcomes and further analysis would be fundamentally different for such a more detailed model. Considering the clinical setting we therefore used the four site model.

Limitations

The validity of the presented model remains a limitation as this study only uses hypothetical data. We partly addressed this limitation by varying several model parameters over large ranges. Yet, many other choices would have been possible. Thus, the assumption of identical collateral conductances for all sites is an oversimplification of real cases. Patient data also show high variability in vascular volume between sites. These variations may yield different relations between RTT and RRF. The accuracy of the predictive value of RTT to predict RRF was based on perfusion thresholds of 50% and 40% of the pre-intervention perfusion. Currently, we do not have data for realistic values of this threshold.

A strong point of this study is that we have created a model in which many parameters can be tested. Therefore, alternative measures (such as intensity based, or absolute times) for estimating the perfusion can be evaluated with this model. However, in the context of the complex surgery, observation periods are limited to 2–3 min and longer periods are a concern.[24] In the fluorescence enhancement curve in **Figure 1b**, the fluorescence yield is reasonably similar between the sites and a maximum is obtained in also the fourth site but these are not always the case. Thus, alternative measures of perfusion that rely on normalization to the maximal fluorescence at site 4 or generally the full enhancement curve may have been impractical.

Potential Use of Gastric Conduit Model

A large number of studies have employed fluorescence imaging in intraoperative applications to assist visualization of blood flow or anatomical features.[6, 25–28] However, quantitative analysis of ICG fluorescence imaging of the gastric conduit is still limited. Yukaya et al. introduced a quantitative parameter describing the decay of luminance as analyzed with the software tool LumiView to predict anastomotic leakage.[29] They could not find an association between blood flow and anastomotic leakage. A study on quantitative assessment of free jejunal graft used the time-fluorescence intensity curve, showing that time to half maximum is an indicative parameter for venous malperfusion.[30] However, that study had a population of only five patients suffering from venous anastomotic failure. Furthermore, in that study, no direct relation between perfusion deficit and ICG intensity dynamics was studied. A more recent study had been performed to predict anastomotic leakage by quantitatively measuring ICG speed between four predetermined points in the gastric conduit.[8] Also, this study suffered from limited data especially in the anastomotic leakage/malperfusion group.

While there clearly are several limitations to consider, quantitative analysis of contrast dynamics could provide a useful prognostic tool in determining treatment success. We found that time to 20% of the maximum intensity is optimal in the discrimination between intermediate and low perfusion as indicated by the area under the ROC curve. Additionally, if adopted in clinical practice, this low threshold requires only a relatively short measurement time of

fluorescence imaging after maximum intensity is reached in ROI 1, which alleviates surgery-related risks.

Since fluorescence imaging allows assessment of temporal ICG intensity for different areas of gastric conduit intraoperatively, the operating clinician can evaluate intensity profiles for selected ROIs. This allows the calculation of the RTT at the anastomosed site and this value can be used to estimate the range of perfusion reduction (**Figure 6**). The actual usefulness of RTT as an estimate for local perfusion and predictor of final outcome in esophagectomy remains to be established.

CONCLUSION

Our model demonstrated the effects of vascular conductance and volume on contrast dynamics in gastric conduit in relation to perfusion in anastomosed areas. After evaluating ICG dynamics for numerous different model parameters, we found that the relation between the dynamics and perfusion is not trivial. However, the model showed that for low flows, a low time to threshold intensity is predictive of flow deterioration. This estimation of remaining perfusion may form the base for clinical evaluation of a successful esophagectomy.

APPENDIX

The effect of collateral artery and vein conductance ratio and total collateral conductance to capillary perfusion

The balance ratio between collateral artery and vein conductance (G_{ca}/G_{cv}) reflects the contribution of one side of collateral over another in determining perfusion. We compared the RRF modeled with a specific collateral conductance ratio with its inverse to test whether a certain side of collaterals is more favorable for perfusion. The result has shown negligible difference between RRF of two conductance configuration. Eventually, it was apparent that the total collateral conductance is a more consequential factor in determining the portion of contrast flowing through the capillary. Total collateral conductance was

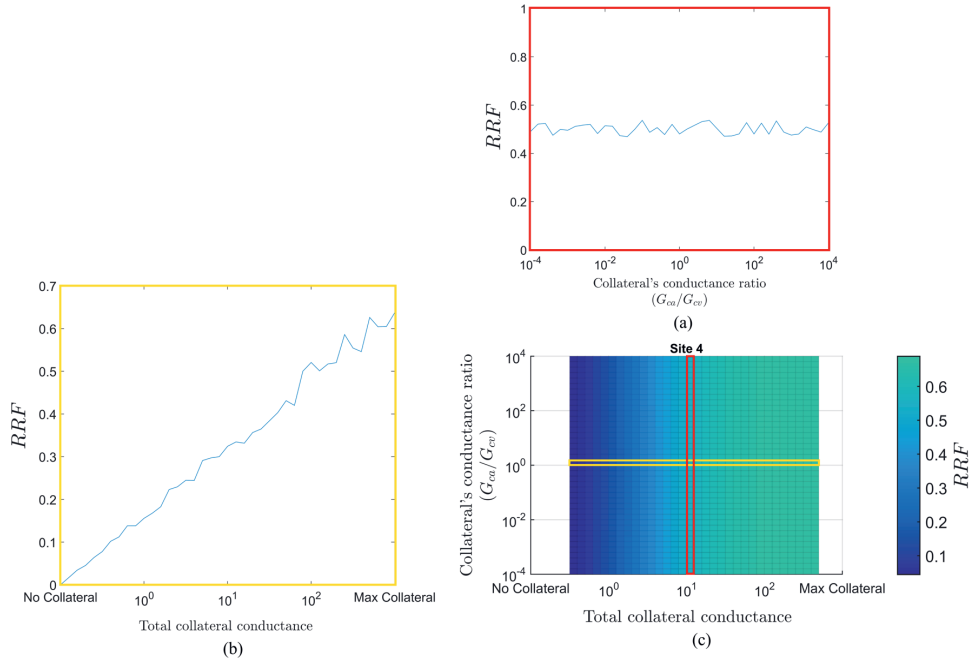

Figure 8. The effects of the balance of arterial and venous collateral conductance (a) and of the total collateral conductance (b) on the relative remaining flow(RRF) in the anastomotic site 4, demonstrating the log-linear dependence of RRF on total collateral conductance without an effect of arteriovenous balance. RRF for all levels of total collateral conductance and arteriovenous balance (c), demonstrating absence of interactive effects of both parameters.

calculated as the inverse of the sum of collateral arteries and veins resistance in a series circuit ($G_{ca} \cdot G_{cv}/(G_{ca} + G_{cv})$). **Figure 8** shows the effect of this total collateral conductance in logarithmic scale on relative remaining flow in these models. The ratio of arterial and venous conductance has a relatively minor impact on these perfusions while increasing total collateral conductances show a better perfusion of the collateral-dependent sites.

REFERENCES

1. Law S, Fok M, Chu KM, Wong J. Thoracoscopic esophagectomy for esophageal cancer. *Surgery*. 1997;122(1):8-14. doi:10.1016/S0039-6060(97)90257-9

2. Urschel JD. Esophagogastrostomy anastomotic leaks complicating esophagectomy: A review. *Am J Surg*. 1994;169(6):634-640.

3. Cassivi SD. Leaks, strictures, and necrosis: A review of anastomotic complications following esophagectomy. *Semin Thorac Cardiovasc Surg*. 2004;16(2):124-132. doi:10.1053/j.semtcvs.2004.03.011

4. Zehetner J, DeMeester SR, Alicuben ET, et al. Intraoperative Assessment of Perfusion of the Gastric Graft and Correlation With Anastomotic Leaks After Esophagectomy. *Ann Surg*. 2014;00(00):1-5. doi:10.1097/SLA.0000000000000811

5. Campbell C, Reames MK, Robinson M, Symanowski J, Salo JC. Conduit Vascular Evaluation is Associated with Reduction in Anastomotic Leak After Esophagectomy. *J Gastrointest Surg*. 2015;19(5):806-812. doi:10.1007/s11605-015-2794-3

6. Kumagai Y, Ishiguro T, Haga N, Kuwabara K, Kawano T, Ishida H. Hemodynamics of the reconstructed gastric tube during esophagectomy: Assessment of outcomes with indocyanine green fluorescence. *World J Surg*. 2014;38(1):138-143. doi:10.1007/s00268-013-2237-9

7. Rino Y, Yukawa N, Sato T, et al. Visualization of blood supply route to the reconstructed stomach by indocyanine green fluorescence imaging during esophagectomy. *BMC Med Imaging*. 2014;14(1):18. doi:10.1186/1471-2342-14-18

8. Koyanagi K, Ozawa S, Oguma J, et al. Blood flow speed of the gastric conduit assessed by indocyanine green fluorescence. *Medicine*. 2016;95(30). doi:10.1097/MD.0000000000004386

9. Chadi SA, Fingerhut A, Berho M, et al. Emerging Trends in the Etiology, Prevention, and Treatment of Gastrointestinal Anastomotic Leakage. *J*

Gastrointest Surg. 2016;20(12):2035-2051. doi:10.1007/s11605-016-3255-3

10. Bruinsma P, Arts T, Dankelman J, Spaan JAE. Model of the coronary circulation based on pressure dependence of coronary resistance and compliance. *Basic Res Cardiol*. 1988;83:510-524. doi:10.1007/BF01906680

11. Blomley MJK, Coulden R, Bufkin C, Lipton MJ, Dawson P. Contrast Bolus Dynamic Computed-Tomography for the Measurement of Solid-Organ Perfusion. *Invest Radiol*. 1993;28(5):S72-S77. doi:10.1097/00004424-199311001-00023

12. Jansen SM, de Bruin D, Strackee S, et al. PS01.186: QUANTITATIVE PERFUSION EVALUATION AFTER GASTRIC TUBE RECONSTRUCTION USING FLUORESCENCE IMAGING. *Dis Esophagus*. 2018;31(13):102-103.

13. Jacobson ED, Jerry BS. Hemodynamics of the Stomach I. Resistance-flow Relationship in the Gastric Vascular Bed. *Am J Dig Dis*. 1962;7(9):779-785.

14. Berne RM, Koeppen BM, Stanton BA. Berne & Levy Physiology. 6th ed. Mosby/Elsevier; 2008. doi:10.1002/ejoc.201200111

15. Wiedeman MP. Dimensions of Blood Vessels from Distributing Artery to Collecting Vein. *Circ Res*. 1963;12(4):375-378. doi:10.1161/01.RES.12.4.375

16. Pfitzner J. Poiseuille and his law. *Anaesthesia*. 1976;31(2):273-275. doi:10.1111/j.1365-2044.1976.tb11804.x

17. Meier P, Zierler KL. On the Theory of the Indicator-Dilution Method for Measurement of Blood Flow and Volume. *J Appl Physiol*. 1954;6(12):731-744.

18. Dormand JRR, Prince PJJ. A family of embedded Runge-Kutta formulae. *J Comput Appl Math*. 1980;6(1):19-26. doi:10.1016/0771-050X(80)90013-3

19. Schreiner W, Buxbaum PF. Computer-Optimization of Vascular Trees. *IEEE Trans Biomed Eng*. 1993;40(5):482-491.

20. Huyghe JM, Arts T, van Campen DH, Reneman RS. Porous medium finite element model of the beating left ventricle. *Am J Physiol*. 1992;262(4):H1256-H1267.

21. Biot MA. Thory of Finite Deformations of Porous Solids. *Indiana Univ Math J.* 1972;21(7):597. doi:10.1512/iumj.1972.21.21048

22. Kresh JY, Fox M, Brockman SK, Noordergraaf a. Model-based analysis of transmural vessel impedance and myocardial circulation dynamics. *Am J Physiol*. 1990;258(1 Pt 2):H262-76. http://www.ncbi.nlm.nih.gov/pubmed/2301610

23. May-newman K, Mcculloch AD. Homogenization modeling for the mechanics of perfused myocardium. *Prog Biophys Mol Biol*. 1998;69:463-481.

24. Ishiguro T, Kumagai Y, Ono T, et al. Usefulness of indocyanine green angiography for evaluation of blood supply in a reconstructed gastric tube during esophagectomy. *Int Surg*. 2012;97:340-344. doi:10.9738/cc159.1

25. Phillips BT, Lanier ST, Conkling N, et al. Intraoperative Perfusion Techniques Can Accurately Predict Mastectomy Skin Flap Necrosis in Breast Reconstruction. *Plast Reconstr Surg*. 2012;129(5):778e-788e. doi:10.1097/PRS.0b013e31824a2ae8

26. Komorowska-Timek E, Gurtner GC. Intraoperative Perfusion Mapping with Laser-AssistedIndocyanine Green Imaging Can Predict and PreventComplications in Immediate Breast Reconstruction. *Plast Reconstr Surg*. 2010;125(4):1065-1073. doi:10.1097/PRS.0b013e3181d17f80

27. Pacheco PE, Hill SM, Henriques SM, Paulsen JK, Anderson RC. The novel use of intraoperative laser-induced fluorescence of indocyanine green tissue angiography for evaluation of the gastric conduit in esophageal reconstructive surgery. *Am J Surg*. 2013;205(3):349-353. doi:10.1016/j.amjsurg.2012.11.005

28. Landau MJ, Gould DJ, Patel KM. Advances in fluorescent-image guided surgery. *Ann Transl Med*. 2016;4(20):392. doi:10.21037/atm.2016.10.70

29. Yukaya T, Saeki H, Kasagi Y, et al. Indocyanine Green Fluorescence Angiography for Quantitative Evaluation of Gastric Tube Perfusion in Patients Undergoing Esophagectomy. *J Am Coll Surg*. 2015;221(2):e37-e42. doi:10.1016/j.jamcollsurg.2015.04.022

30. Kamiya K, Unno N. Quantitative assessment of the free jejunal graft perfusion.

J Surg Res. 2015;194(2):394-399. doi:10.1016/j.jss.2014.10.049

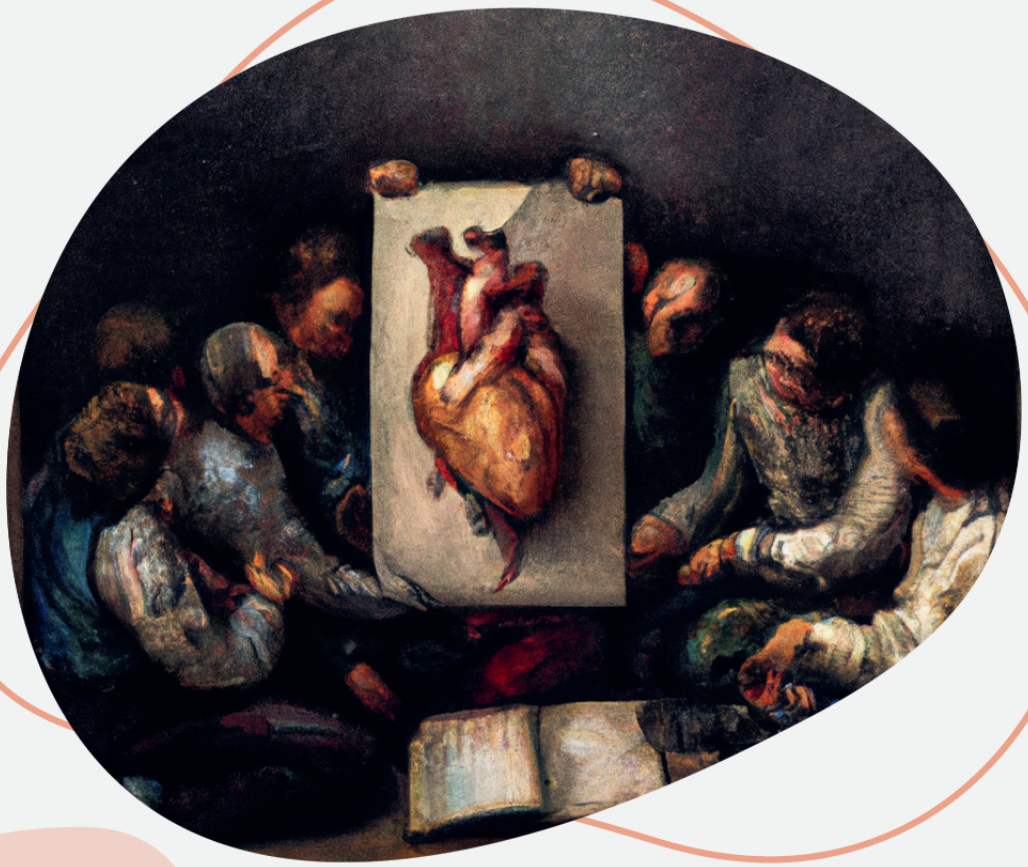

DALL·E 2: "Anatomy lesson of a heart, by Rembrandt"

Chapter 3

LIMITATIONS OF QUANTITATIVE BLUSH EVALUATOR (QUBE)

AS MYOCARDIAL PERFUSION ASSESSMENT METHOD ON DIGITAL CORONARY ANGIOGRAMS

Haryadi Prasetya, Marcel A.M. Beijk, Praneeta R. Konduri, Thabiso Epema, Alexander Hirsch, Pim van der Harst, Ed van Bavel, Bas A.J.M. de Mol, Henk A. Marquering

As published in J Clin Transl Res 2018 Jul 2;3(Suppl 2):394-400
DOI: 10.18053/jctres.03.2017S3.004

This work was supported by Indonesia Endowment Fund for Education (LPDP), Ministry of Finance, Republic of Indonesia through LPDP scholarship Program for Doctorate Students.

ABSTRACT

Background Quantitative Blush Evaluator (QuBE) is a software application that allows quantifying myocardial perfusion in coronary angiograms after a percutaneous coronary intervention. QuBE has some limitations such as the application of a crude filter to remove large scale structures and the absence of correction for cardiac motion. This study investigates the extent of these limitations and we hypothesize that enhanced image analysis methods can provide improvements.

Methods We calculated QuBE scores of 117 patients from the HEBE Trial and determined its association with the Myocardial Blush Grade (MBG) score. Accuracy of large-structure removal is qualitatively assessed for various sizes of a median filter. The influence of cardiac motion was evaluated by comparing the blush curve and QuBE score of the native QuBE with manually motion-corrected QuBE for 40 patients. The effect of different kernel sizes and motion correction to a potential improvement of the association between QuBE score and MBG was studied.

Results In our population, there was no significant association between QuBE score and MBG ($p = 0.14$). Median filters of various kernel sizes were unable to remove large structure related noise. Variations in filters and cardiac movement correction did not result in an improvement in the association with MBG scores (observer 1: $p = 0.66$; observer 2: $p = 0.72$).

Conclusions There was no significant association of QuBE with MBG scores in our population, which suggests that QuBE is not suitable for a quantitative assessment of myocardial perfusion. Alternative kernel sizes for the large structure removal filter and cardiac motion correction did not improve QuBE performance.

Relevance for patients Further improvements of QuBE to overcome its inherent limitations are necessary in order to establish QuBE as a reliable myocardial perfusion assessment method.

Keywords: myocardial perfusion; myocardial infarction; quantitative blush evaluator; coronary angiogram

INTRODUCTION

Myocardial infarction is commonly treated by primary percutaneous coronary intervention (PCI) in which various procedures such as coronary angioplasty, stent placement, or thrombus aspiration are performed. PCI aims to reestablish epicardial blood flow in the infarct-related artery and myocardial perfusion. After successful PCI, myocardial perfusion can be assessed using angiography in order to determine if the restored epicardial patency also leads to proper perfusion in the infarcted area.[1,2] The Myocardial Blush Grade (MBG) is one of the most common reperfusion scales for categorization of the quality of perfusion in this area.[1] Although MBG has been proven to be a strong predictor of mortality in patients with restored epicardial flow as indicated by Thrombolysis in Myocardial Infarction flow grade 3, it is a rather coarse scale and is also sensitive to observer dependency. This has prompted the need for an automated and quantitative approach for assessing myocardial perfusion.

Currently, quantification of myocardial perfusion is possible with Single Photon Emission Computed Tomography, Positron Emission Tomography, Cardiovascular Magnetic Resonance, and CT imaging.[3–5] However, these methods require other imaging modalities in addition to the current standard practice of using x-ray angiography during PCI. Therefore, Quantitative Blush Evaluator (QuBE) has been introduced to semi-quantitatively assess myocardial perfusion from coronary angiograms.[6]

QuBE is an open-source computer program, which has been developed by the University Medical Center Groningen, the Netherlands.[6] In general, angiographic quantification of myocardial blush poses some difficulties including cumbersome assessment because of poor blush signal to noise ratio and superimposition of irrelevant structures. Recognizing and solving these issues are important in developing a blush quantification method such as QuBE. QuBE has been validated as a good risk predictor in the TAPAS trial, which was a study that included patients with PCI and in which the MBG score was assessed on angiograms. In this study, high QuBE values were associated with high MBG scores, more ST-segment elevation resolution, smaller infarct size, and lower 1-year mortality rate.[6] Although QuBE has been shown to be reproducible, unknown effects of

different angiography hardware and techniques, median filter insufficiency as the default large structure removal method, and uncalibrated scoring remain as limitations.[7–9] These inherent limitations might obstruct accurate calculation of myocardial blush. Another possible limitation is the effect of cardiac motion on QuBE score calculation, which has not been studied before. In this study, we evaluate the accuracy of QuBE in a clinical trial data and analyze whether general difficulties of blush quantification and inherent limitations of QuBE can be resolved with enhanced image analysis methods.

METHODS

Patients

We included patients with ST-segment elevation myocardial infarction who underwent primary PCI in the HEBE trial.[10] The HEBE trial was a multi-center randomized trial with blinded evaluation of endpoints. This trial was designed to assess the effects of intracoronary infusion of bone marrow mononuclear cells and peripheral blood mononuclear cells in improving left ventricular recovery after acute myocardial infarction. Patients from the bone marrow mononuclear cells, peripheral blood, and control groups were included based on the following criteria: age 30-75 years old, successful PCI within 12h after onset of symptoms, >3 hypokinetic or akinetic left ventricular segments observed on echocardiography at least 12h after PCI, and an elevation of creatine kinase in venous blood >10 times the local upper limit of normal. In addition, patients with hemodynamic instability, upcoming additional PCI, coronary-artery bypass grafting within the next 4 months, severe comorbidity, and contraindications for MRI were excluded from this trial. We included patients from the two largest of the eight participating centers in this study. We included 58 patients from the Academic Medical Center and 87 patients from the University Medical Center Groningen.[14] Coronary angiograms made during primary PCI were collected. The inclusion criteria for accepted angiogram adhered to the guideline provided in the initial study of QuBE.[6] We included complete blush sequence and no major overlapping of other non-infarct related area in myocardial region of interest.

QuBE evaluation and Myocardial Blush Grade

In coronary angiograms, tissue perfusion appears as a blush surrounding the coronary artery. Therefore, myocardial perfusion can be observed by monitoring the dynamics of average contrast intensity within a certain region of interest (ROI), which is shown as a typical curve in **Figure 1**.

The accuracy of QuBE score calculation assumes that the blush can be isolated by removal of contributions from coronary arteries and background structures such as the diaphragm and catheter from the image using filters. This implemented removal of these structures is based on differences between the spatial frequencies of myocardial blush compared to the unwanted structures (**Figure 2**). QuBE applies a median filter, which creates an image depicting large-scale structures only.[11] Subsequently, this background image is subtracted from the original frame. This process results in an image representing myocardial blush and other high-spatial frequency noise. The noise characteristics, such as the sparsity and the intensity, depend on the kernel size of the median filter.

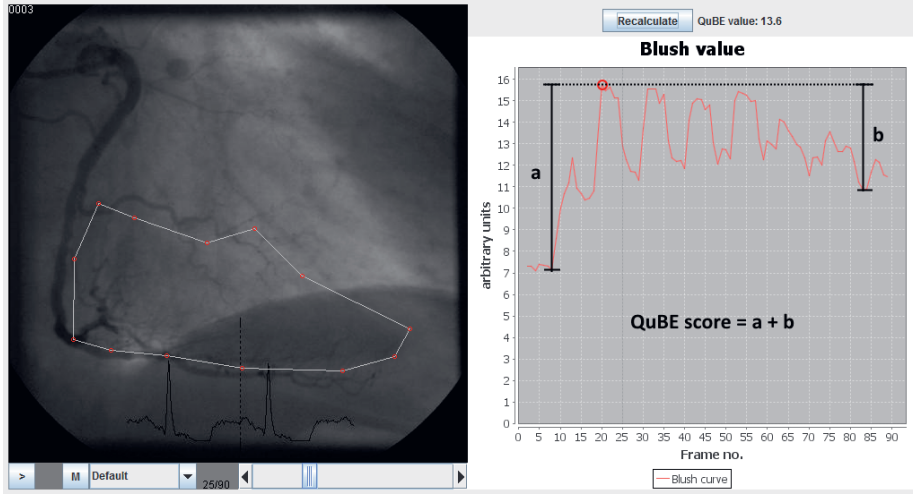

Figure 1. Left: Coronary angiogram with a ROI containing distal infarct-related area of right coronary artery. Right: Blush curve representing the average intensity of ROI for each frame. The QuBE score is defined as the sum of the maximum increase (a) and the maximum decrease (b) of intensity.

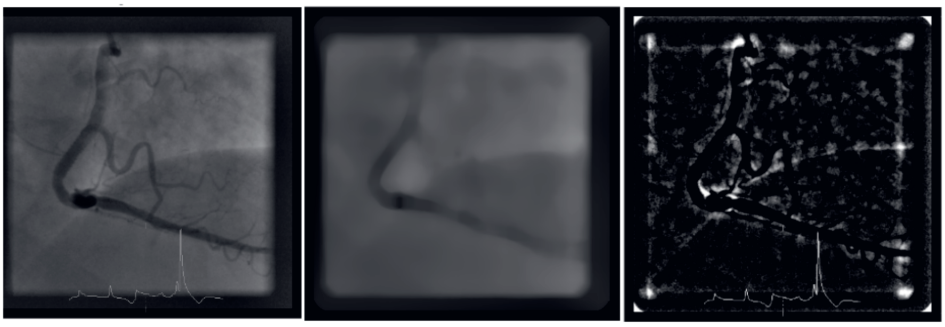

Figure 2. Large structure removal for blush extraction. The original frame of coronary angiogram (left) was filtered using median filter with kernel size of 35 pixels × 35 pixels. The resulting background (middle) was subtracted from the original image such that only blush and other smaller structures remain (right).

The native QuBE software uses a fixed kernel size of 35 pixels × 35 pixels. We evaluated the appropriateness of this kernel size for removal of large structures by comparing with results obtained from two different kernel sizes: 20 pixels × 20 pixels and 50 pixels × 50 pixels. The performance of median filters with different kernel sizes was qualitatively and quantitatively assessed.

Since QuBE uses a fixed ROI location, a bias may be introduced due to the cardiac motion. The QuBE only includes a rudimentary panning motion correction by calculating a possible translation offset of every frame, while cardiac motion is a complex combination of translation, rotation, and non-isotropic contraction and relaxation. We evaluated whether additional cardiac motion correction improves the agreement of QuBE score with MBG. The comparison was made because MBG is the most commonly used angiographic measure to assess myocardial perfusion and has moderate to good inter- and intra-observer agreement.[1,12,13] For this, a single experienced cardiologist who was blinded to clinical data first indicated the ROI on a frame of reference. Two trained observers subsequently manually adjusted the ROIs for all time frames, ensuring that the ROI indicates the same area of myocardium at all times. The cardiac motion correction was performed for 40 patients (10 of each MBG group).

The suitability of the angiographic angulation was assessed by an experienced cardiologist to avoid an overlap between infarcted and healthy myocardium. The right anterior oblique view of −30° and the left anterior oblique view of −60° to

−90° were considered to be the appropriate angulations for perfusion assessment for the left anterior descending artery. A deviation of ±10° from the two proposed projections was allowed. In appropriate angiograms, the MBG was assessed by the same cardiologist. The cardiologist delineated the ROI that contained the distal part of the perfusion area of the infarct-related artery. The MBG was scored based on the following classification: MBG 0 for no myocardial blush, MBG 1 for minimal myocardial blush, MBG 2 for moderate myocardial blush but less than that obtained during angiography of the reference artery, and MBG 3 for normal myocardial blush that is comparable to the angiographically healthy reference artery.

Statistical Analyses

QuBE scores were summarized as medians (interquartile range, IQR). Associations between QuBE scores and MBG grades were analyzed by calculating the Spearman rank correlation coefficients. Kruskal-Wallis tests were performed to analyze the differences in QuBE scores between MBG groups. Lin's concordance coefficient was calculated to quantify interobserver agreement on the QuBE scores acquired after manually correcting the cardiac motion. The significance of the difference of the QuBE scores with and without cardiac motion on QuBE score was analyzed using Wilcoxon signed-rank test. The similarity of the native and motion-corrected blush curves was analyzed using Pearson correlation where the intensities for every time frame was compared for both assessments. P-values lower than 0.05 were considered statistically significant. All statistics were performed using IBM SPSS software (version 19.0.0).

RESULTS

Out of 145 patients, 28 were excluded due to an unsuitable angulation. The remaining 117 patients (48 patients from the Academic Medical Center and 69 from the University Medical Center Groningen) were included in this analysis. The QuBE score distribution for the MBG grades are represented in **Figure 3**. The correlation between QuBE score and MBG was not significant (p = 0.14) and no significant differences were found between the grades (p = 0.22). **Table 1**

Table 1. MBG and QuBE score of 117 patients

		MBG 0	MBG 1	MBG 2	MBG 3
QuBE score	n	70	14	13	20
	Kernel Size 20×20	4.2(1.1-24)	4.0(1.4-9.4)	4.7(2.3-8.6)	4.9(2.4-9.0)
	Kernel Size 35×35 (Native)	14(3.3-31)	12(3.0-22)	15(8.5-19)	12(4.1-29)
	Kernel Size 50×50	15(4.0-35)	12(5.0-22)	15(7.9-18)	13(4.7-36)

QuBe scores are presented as median (and interquartile range); MBG, Myocardial Blush Grade; QuBE, Quantitative Blush Evaluator.

summarizes the QuBE scores stratified for MBG scores for varying kernel sizes of the median filter.

Figure 4 shows the resulting images after subtracting median filtered images for various sizes of the median filters for a single patient. For all kernel sizes the right coronary and right marginal artery were successfully removed. However, the resulting images were commonly noisy, especially around the edge of the angiogram's border, arteries, and diaphragm. This figure indicates that a kernel size of 20×20 resulted in more pronounced and higher frequency noise. On the other hand, a kernel size of 50×50 resulted in a lower noise level but in larger areas around the edges of large structures.

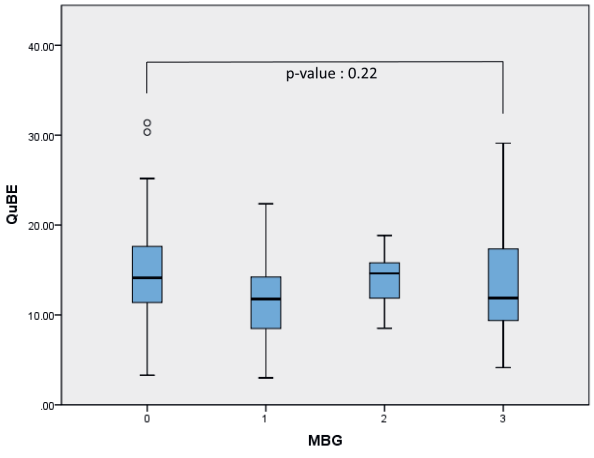

Figure 3. Association of myocardial blush grade with QuBE. MBG 0: no myocardial blush; MBG 1: minimal myocardial blush; MBG 2: moderate myocardial blush; MBG 3: normal myocardial blush.

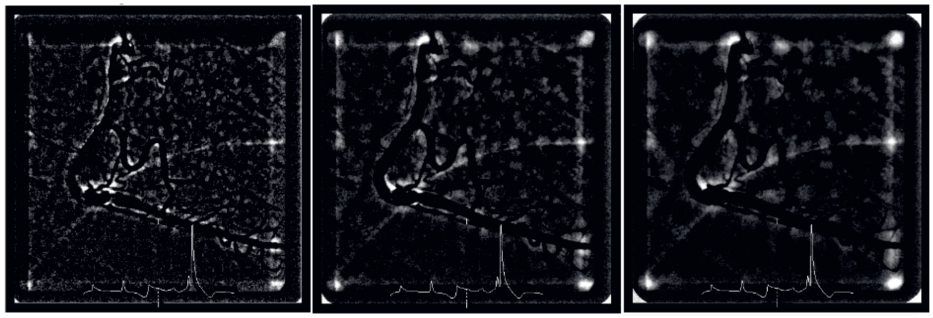

Figure 4. The remaining structure after the median-filtered frame is subtracted from the original frame. Left: kernel size of 20×20. Middle: kernel size of 35×35 (native QuBE). Right: kernel size of 50×50. Contrast is readjusted for clarity.

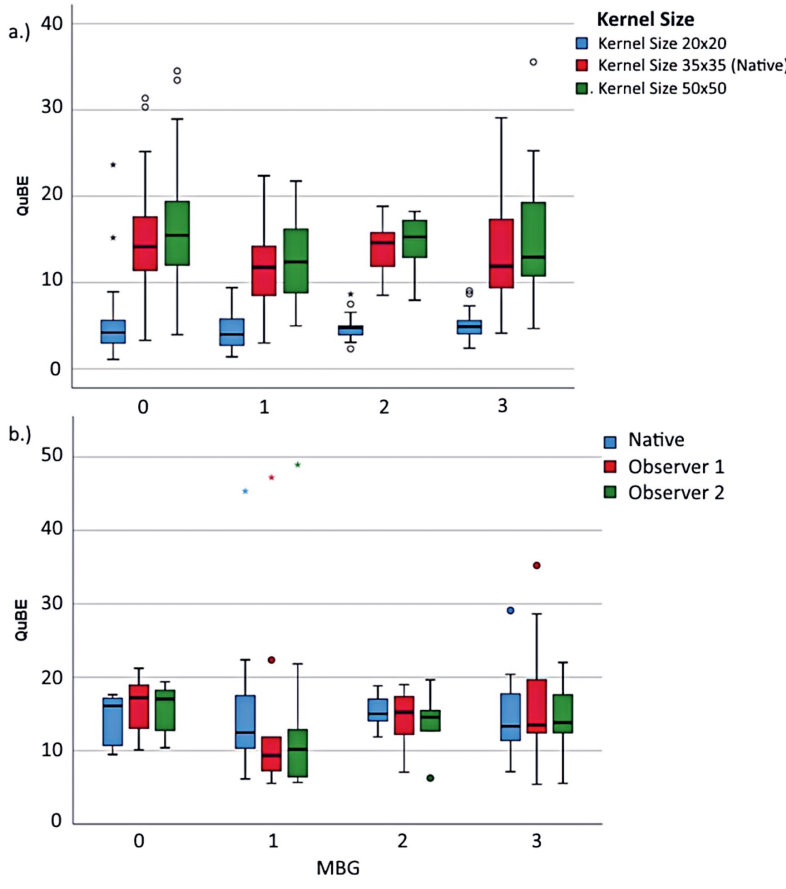

Figure 5. QuBE scores distribution per MBG: (a) for three different kernel sizes of median filter, and (b) pre- and post-motion correction in 40 patients.

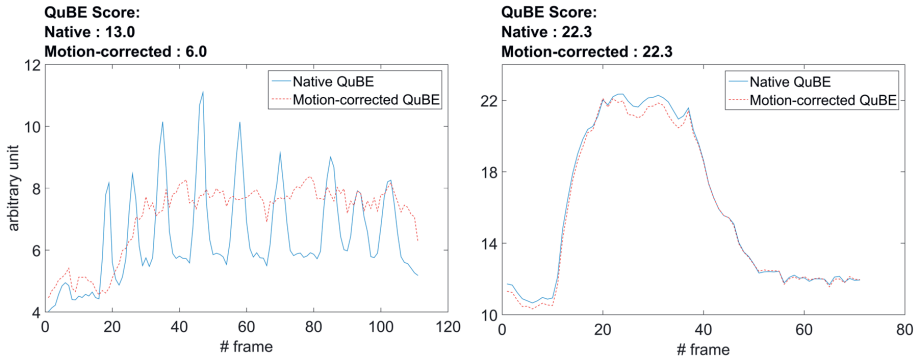

Figure 6. Comparison of the native QuBE and motion-corrected QuBE of blush curves. The frame rate is 12.5 frames per second. The largest difference in blush curves is shown in the left panel (R = 0.47). The right panel shows the best correlation between the two blush curves (R = 1.00).

Figure 5a shows the distribution of the QuBE scores for varying kernel size and MBG score. We found that there were no significant correlations between QuBE score and MBG for kernel size 20 pixels x 20 pixels (p = 0.33) and 50 pixels x 50 pixels (p = 0.16). Additionally, no significant QuBE differences were found between MBG groups for all kernel sizes (p = 0.70 and 0.28 for kernel size 20 pixels x 20 pixels and 50 pixels x 50pixels, respectively).

There were no significant differences among QuBE scores of different MBG groups of the native and motion-corrected QuBE score (p = 0.70), as can be seen in **Figure 5b**. For both observers, 38 patients demonstrated strong correlation between blush curves of native and motion-corrected QuBE and the remaining 2 patients showed moderate correlation (observer 1: median R = 0.97, range 0.47–1.00; observer 2: median R = 0.98, range 0.53–1.00). The Lin's inter-observer concordance was 90%. The native and motion corrected blush curves with the worst and the best correlation are shown in **Figure 6**. The Wilcoxon signed-rank test showed that additional manual cardiac motion correction performed by the two observers did not elicit a statistically significant change in QuBE scores (p = 0.66, 0.72).

DISCUSSION

In our population, we found no association between QuBE scores and the MBG score, suggesting that QuBE is not suitable for myocardial blush quantification.

We found that the implemented median filter is not accurate in the removal of large structures and that in the filtered images many artefacts associated with large structures remain and influence the QuBE score. We explored different sizes of filters without better results. Furthermore, cardiac motion correction did not strongly affect QuBE calculation. These findings suggest that despite the reported high reproducibility, QuBE scores may not represent the actual reperfusion state.

The feasibility of QuBE has been evaluated in a number of trials, notably the TAPAS and PREPARE trials.[8,9,14,15] These authors found that a high QuBE score significantly correlates with high MBG, ST-segment elevation resolution, smaller infarct sizes, survival at 1 year, improved functional outcome, and contrast-enhanced Cardiac Magnetic Resonance outcomes.[6,8,9] Our results do not confirm these findings.

Because QuBE is open source, it allowed for detailed inspection of the algorithms that are employed in the software. We found that the underlying cause of the lack of association between QuBE and MBG may reside within QuBE itself. We have shown that the median filter used in QuBE may not be appropriate for blush isolation. It was demonstrated that the filtered image may contain noise around the edges of removed structures that has the same spatial characteristics as the blush. QuBE calculates the local average of the intensities of the few brightest pixels as the blush value of a single frame of angiogram.[6] This calculation leads to the inclusion of the noise in the equation since there is no earlier process in QuBE that distinguishes blush from the noise.

We considered cardiac motion as a potential important limitation in the calculation of the QuBE score. Our observation, however, revealed that in most cases cardiac motion did not have a large influence on the QuBE calculation. We suspect that the limited improvement of cardiac motion correction is because the ROIs were large enough for the infarct-related artery and its perfusion area to remain inside the ROI during the cardiac cycle. On the other hand, in the cases where the ROI is close to a coronary artery bifurcation but does not include it, i.e., during reperfusion assessment of myocardium supplied by the right coronary artery, cardiac motion did have an effect. Since the most prominent cluster of noise was formed in curving arteries and bifurcations, the cardiac motion which

subsequently included and excluded this bifurcation in a cardiac cycle introduced subsequent spikes and dips in the blush curve. In these particular cases, motion correction may improve the accuracy of the QuBE score.

Describing and visualizing intermediate results in QuBE calculations set this study apart from previous QuBE studies. This allowed for careful analysis of the limitations of the specific algorithms in QuBE. Although we investigated different kernel sizes of the filter, we did not explore other large-scale structure removal methods that might provide better isolation of the myocardial blush. Several enhanced-image and segmentation methods could be employed as alternatives to median filter, i.e., digital subtraction angiography for coronary arteries or vesselness filters for better artery removal.[16,17] Since this is a retrospective analysis of trial data, no power analysis and sample size calculation were performed. Uneven distribution of samples across MBG groups may have reduced the statistical power of our findings. Additionally, the trial data used by previous studies that showed positive findings with QuBE were not available, thus, a comparison study could not be performed. However, aside from the particular limitation of the local algorithm, this discrepancy of QuBE performance may also have been caused by a number of other factors. For instance, type and volume of contrast agent, speed of injection, and the configuration of acquisition machine have not been yet standardized. Besides, the infarct location and body mass index has been known to confound QuBE value.[7] If the image acquisition protocol is standardized and the known confounders are controlled, QuBE may give a more reliable assessment. This information should be incorporated in the guidelines on the use of QuBE to assess myocardial perfusion.

In summary, QuBE may not reliably describe myocardial perfusion and extensive motion correction does not improve its performance. Alternatives for the currently used large-scale structure removal algorithms should be investigated.

REFERENCES

1. Henriques JPS, Zijlstra F, van 't Hof AWJ, et al. Angiographic assessment of reperfusion in acute myocardial infarction by myocardial blush grade. *Circulation*. 2003;107(16):2115-2119. doi:10.1161/01.CIR.0000065221.06430.ED

2. Gibson CM, Cannon CP, Murphy SA, et al. Relationship of TIMI myocardial perfusion grade to mortality after administration of thrombolytic drugs. *Circulation*. 2000;101(2):125-130. doi:10.1161/01.CIR.101.2.125

3. Wagner A, Mahrholdt H, Holly TA, et al. Contrast-enhanced MRI and routine single photon emission computed tomography (SPECT) perfusion imaging for detection of subendocardial myocardial infarcts: an imaging study. *Lancet*. 2003;361(9355):374-379. doi:10.1016/S0140-6736(03)12389-6

4. Bratis K, Mahmoud I, Chiribiri A, Nagel E. Quantitative myocardial perfusion imaging by cardiovascular magnetic resonance and positron emission tomography. *J Nucl Cardiol*. 2013;20(5):860-870. doi:10.1007/s12350-013-9762-7

5. Pelgrim GJ, Handayani A, Dijkstra H, et al. Quantitative myocardial perfusion with dynamic contrast-enhanced imaging in MRI and CT: Theoretical models and current implementation. *Biomed Res Int*. 2016;2016:1-12. doi:10.1155/2016/1734190

6. Vogelzang M, Vlaar PJ, Svilaas T, Amo D, Nijsten MWN, Zijlstra F. Computer-assisted myocardial blush quantification after percutaneous coronary angioplasty for acute myocardial infarction: A substudy from the TAPAS trial. *Eur Heart J*. 2009;30(5):594-599. doi:10.1093/eurheartj/ehn542

7. Gu YL, Haeck JDE, Vogelzang M, et al. Computer-assisted quantification of myocardial reperfusion after primary percutaneous coronary intervention predicts functional and contrast-enhanced cardiovascular magnetic resonance outcomes in patients with ST-segment elevation myocardial infarction. *Catheter Cardiovasc Interv*. 2011;77(2):174-181. doi:10.1002/ccd.22665

8. Haeck JDE, Gu YL, Vogelzang M, et al. Feasibility and applicability of

computer-assisted myocardial blush quantification after primary percutaneous coronary intervention for ST-segment elevation myocardial infarction. *Catheter Cardiovasc Interv*. 2010;75(5):701-706. doi:10.1002/ccd.22329

9. Porto I, Hamilton-Craig C, De Maria GL, et al. Quantitative Blush Evaluator accurately quantifies microvascular dysfunction in patients with ST-elevation myocardial infarction: Comparison with cardiovascular magnetic resonance. *Am Heart J*. 2011;162(2):372-381.e2. doi:10.1016/j.ahj.2011.04.014

10. Hirsch A, Nijveldt R, van der Vleuten P a, et al. Intracoronary infusion of mononuclear cells from bone marrow or peripheral blood compared with standard therapy in patients after acute myocardial infarction treated by primary percutaneous coronary intervention: results of the randomized controlled HEBE . *Eur Heart J*. 2011;32(14):1736-1747. doi:10.1093/eurheartj/ehq449

11. Huang T, Yang G, Tang G. A fast two-dimensional median filtering algorithm. *IEEE Trans Acoust*. 1979;27(1):13-18. doi:10.1109/TASSP.1979.1163188

12. van `t Hof AWJ, Liem A, Suryapranata H, Hoorntje JC a., de Boer M-J, Zijlstra F. Angiographic Assessment of Myocardial Reperfusion in Patients Treated With Primary Angioplasty for Acute Myocardial Infarction : Myocardial Blush Grade. *Circulation*. 1998;97(23):2302-2306. doi:10.1161/01.CIR.97.23.2302

13. Korosoglou G, Haars A, Michael G, et al. Quantitative evaluation of myocardial blush to assess tissue level reperfusion in patients with acute ST-elevation myocardial infarction. Incremental prognostic value compared with visual assessment. *Am Heart J*. 2007;153(4):612-620. doi:10.1016/j.ahj.2006.12.019

14. Fokkema P. J.; Vogelzang, M.; Gu, Y. L.; Kampinga, M. A.; de Smet, B. J.; Jessurun, G. A.; Anthonio, R. L.; van den Heuvel, A. F.; Tan, E. S.; Zijlstra, F. ML. V, Fokkema ML, Vlaar PJ, et al. Effect of High-Dose Intracoronary Adenosine Administration During Primary Percutaneous Coronary Intervention in Acute Myocardial Infarction A Randomized Controlled Trial. *Circ Interv*. 2009;2(4):323-329. doi:10.1161/CIRCINTERVENTIONS.109.858977.109.858977

15. Gu YL, Kampinga MA, Wieringa WG, et al. Intracoronary Versus Intravenous

Administration of Abciximab in Patients With ST-Segment Elevation Myocardial Infarction Undergoing Primary Percutaneous Coronary Intervention With Thrombus Aspiration The Comparison of Intracoronary Versus Intravenous Abci. *Circulation*. 2010;122(25):2709-2717. doi:10.1161/CIRCULATIONAHA.110.002741

16. Yamamoto M, Okura Y, Ishihara M, Kagemoto M, Harada K, Ishida T. Development of digital subtraction angiography for coronary artery. *J Digit Imaging*. 2009;22(3):319-325. doi:10.1007/s10278-008-9108-1

17. Frangi AF, Niessen WJ, Vincken KL, Viergever MA. Multiscale vessel enhancement filtering. *Int Conf Med Image Comput Comput Interv*. 1998;1496(Springer, Berlin, Heidelberg):130-137. doi:10.1016/j.media.2004.08.001

DALL·E 2: "A doctor and a humanoid inspect a holographic 3D brain scan together, digital art"

Chapter 4

qTICI

QUANTITATIVE ASSESSMENT OF BRAIN TISSUE REPERFUSION ON DIGITAL SUBTRACTION ANGIOGRAMS OF ACUTE ISCHEMIC STROKE PATIENTS

Haryadi Prasetya*, Lucas A. Ramos*, Thabiso Epema, Kilian M. Treurniet, Bart J. Emmer, Ido R. van den Wijngaard, Guang Zhang, Manon Kappelhof, Olvert A. Berkhemer, Albert J. Yoo, Yvo B.E.W.M. Roos, Robert J. van Oostenbrugge, Diederik W.J. Dippel, Wim H. van Zwam, Aad van der Lugt, Bas A.J.M de Mol, Charles B.L.M. Majoie, Ed van Bavel, Henk A. Marquering, on behalf of the MRCLEAN Registry Investigators

*contributed equally

As published in Int J Stroke 2021 Feb;16(2):207-216
DOI: 10.1177/1747493020909632

This work was supported by Indonesia Endowment Fund for Education (LPDP), Ministry of Finance, Republic of Indonesia through LPDP scholarship Program for Doctorate Students.

ABSTRACT

Background The Thrombolysis in Cerebral Infarction (TICI) scale is an important outcome measure to evaluate the quality of endovascular stroke therapy. The TICI scale is ordinal and observer-dependent, which may result in suboptimal prediction of patient outcome and inconsistent reperfusion grading.

Aims We present a semi-automated quantitative reperfusion measure (quantified TICI (qTICI)) using image processing techniques based on the TICI methodology.

Methods We included patients with an intracranial proximal large vessel occlusion with complete, good quality runs of anteroposterior and lateral digital subtraction angiography from the MR CLEAN Registry. For each vessel occlusion, we identified the target downstream territory and automatically segmented the reperfused area in the target downstream territory on final digital subtraction angiography. qTICI was defined as the percentage of reperfused area in target downstream territory. The value of qTICI and extended TICI (eTICI) in predicting favorable functional outcome (modified Rankin Scale 0-2) was compared using area under receiver operating characteristics curve and binary logistic regression analysis unadjusted and adjusted for known prognostic factors.

Results In total, 408 patients with M1 or internal carotid artery occlusion were included. The median qTICI was 78 (interquartile range 58-88) and 215 patients (53%) had an eTICI of 2C or higher. qTICI was comparable to eTICI in predicting favorable outcome with area under receiver operating characteristics curve of 0.63 vs. 0.62 (P = 0.8) and 0.87 vs. 0.86 (P = 0.87), for the unadjusted and adjusted analysis, respectively. In the adjusted regression analyses, both qTICI and eTICI were independently associated with functional outcome.

Conclusions qTICI provides a quantitative measure of reperfusion with similar prognostic value for functional outcome to eTICI score.

Keywords: Digital subtraction angiography; endovascular therapy; ischemic stroke; reperfusion.

INTRODUCTION

Various grading scales have been introduced to assess the extent of reperfusion on digital subtraction angiography (DSA) images following endovascular treatment (EVT).[1] One of the most frequently used scales is the modified Treatment in Cerebral Ischemia (mTICI) scale.[2] This scale has been recommended because of its fair interobserver agreement and clinical prognostic value.[1,3,4] mTICI assesses the proportion of brain tissue perfused in an antegrade fashion relative to the total area of the target downstream territory (TDT) distal to the target occlusion.[5] The TDT is the area of the brain that was supplied by the occluded artery prior to stroke onset.[1] The score ranges from no perfusion (mTICI = 0) to complete reperfusion (mTICI = 3). A subsequent refinement has been made to intermediate grades of reperfusion (mTICI 2B) to better define successful reperfusion.[3,4,6] Recently, the extended Thrombolysis in Cerebral Ischemia (eTICI) scale has been introduced, which includes grade 2C to account for nearly complete reperfusion with slow flow in distal cortical vessels or presence of tiny distal emboli.[7–9] This grade 2C has been retained in the expanded TICI scale, which added 67% perfusion threshold into the middle categories.[10] Recent findings suggest that eTICI 2C-3 has a stronger association with favorable functional outcome than eTICI 2B-3.[10–15]

Despite its widespread use, the eTICI score suffers from two shortcomings: it is prone to observer variance and it is an ordinal scale.[1,6,7,10,16] Moreover, a recent study showed that reperfusion is generally overestimated by the interventionalist performing EVT compared to core-lab observers.[16] An automated and quantitative reperfusion grading has the potential to provide a more clinically relevant, less observer-dependent score, and a greater ease of use. In this study, we present a quantitative reperfusion measure using semantic segmentation of DSA images. We assessed the prognostic value of the proposed quantitative reperfusion grading for predicting functional outcome in comparison with eTICI.

METHODS

Patients

This is a substudy of the Multicenter Clinical Registry of Endovascular treatment for acute ischemic stroke in the Netherlands (MR CLEAN Registry). Details of the registry, patient inclusion, baseline clinical and imaging characteristics, and interventional therapy have been described previously.[17] We included only patients with acute ischemic stroke attributable to an occlusion of the intracranial internal carotid artery (ICA) or proximal middle cerebral artery (MCA) (M1) as presented on DSA who were treated between March 2014 and June 2016. We also only included patients with good quality pre- and post-treatment DSA, with full arterial to venous anteroposterior and lateral runs, and who were eTICI graded by an independent core-lab of neuro/interventional radiologists. DSA images with motion artifacts and low contrast volume were excluded.

Image Analysis

Similar to the eTICI grading, our quantitative reperfusion measure assesses the percentage of the reperfused area within the TDT on DSA. An overview of the proposed approach is shown in **Figure 1**.

First, the reperfused area was identified by following the contrast trajectory past the initial target occlusion. The contrast trajectory can be roughly divided into three phases in the brain: the arterial, parenchymal, and venous phase. This sequence of phases occurs earlier in the proximal part of the intracranial vasculature than in the distal areas. Since perfusion is only visible during the parenchymal phase (from contrast opacification in the brain microvasculature), segmentation of the reperfused tissue can be challenging due to the lack of distinction between phases. This distinction is especially important to separate the antegrade (via recanalization) and retrograde (via pial collateral) perfusion as only the former constitutes reperfusion. Moreover, the local vessel structure, whether it is artery in earlier frames or vein in later frames, can be present during the parenchymal phase. To accurately assess the extent of reperfusion in the parenchyma, the vessel structure was removed from the images.

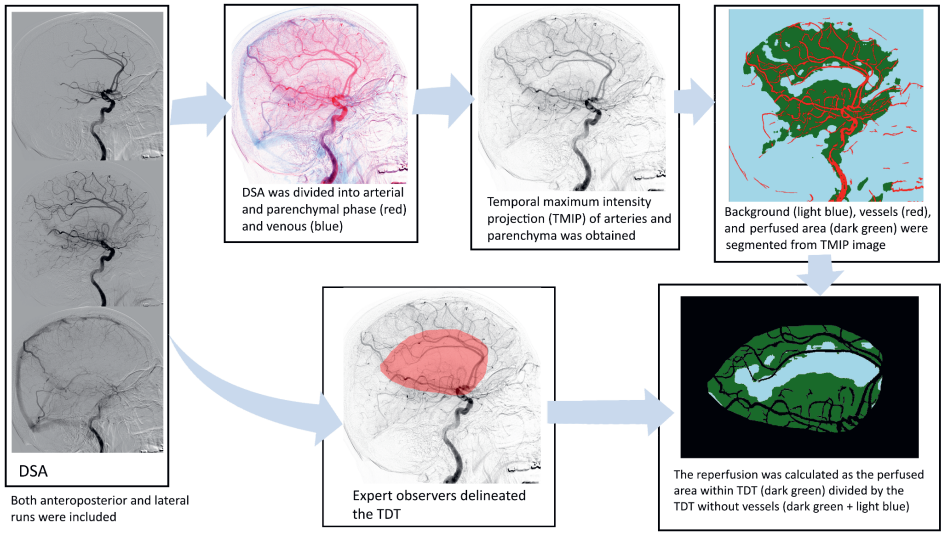

Figure 1. Overview of the image segmentation approach in a patient with M1 occlusion. There are two parallel segmentation tasks: segmentations of reperfused area and of TDT. The reperfused area was segmented from temporal maximum intensity projection of the images of the arterial and parenchymal phase. The TDT was defined as the middle cerebral artery territory and was manually delineated. The percentage of the reperfused area within the TDT was subsequently calculated

We quantified reperfusion on a temporal maximum intensity projection of the images starting at the arterial until the end of parenchymal phase. The last frame of parenchymal phase was manually determined as the immediate frame before the appearance of contrast in the superior sagittal sinus. We assumed that this frame marked the separation between antegrade and retrograde perfusion.

We adopted a multiscale vesselness filter to segment the arteries.[18] The vesselness filter detects tubular structures in images using local curvature information encoded in a Hessian matrix. Improvements were made by introducing a normalization factor to the vesselness classification to reduce blur surrounding the vessel. Details can be found in the Supplemental Materials. To obtain a parenchymal mask image that contains only the non-vessel structure, the resulting vessel mask was subtracted from the original image. This parenchymal mask comprised of reperfused area and background (which includes non-perfused areas). Finally, the reperfused area was arbitrarily determined as the area in the parenchymal mask where the pixel intensity exceeded 7% and 3% of

the maximum intensity in the original image for anteroposterior and lateral runs, respectively. These numbers reflect the minimum contrast intensity in the image that distinguishes perfusion from background area.

For TDT delineation, an expert observer blinded to all clinical data except symptomatic side visually assessed the DSA images of a subpopulation and outlined the TDTs. For this study, we included three expert observers (HP, MK, and BJE) to account for three different patient subpopulations. The M1 TDT was defined as the presumed area supplied by the MCAs including part of lenticulostriate arteries and holotemporal branch.[1] In clinical practice, the ICA TDT is dependent on the patency of the anterior communicating artery. In case the anterior communicating artery is patent, the ipsilateral anterior cerebral artery (ACA) territory is usually supplied by the contralateral anterior circulation. In this case, the ICA TDT is identical to the M1 TDT. In case of an absent or severely hypoplastic anterior communicating artery, the ICA TDT also includes the ACA territory. In practice, baseline computed tomography angiography (CTA) data can be used to inspect the patency of the anterior communicating artery. However, during the core-lab evaluations of the eTICI, this information was not available and the M1 TDT was used. Therefore, we used M1 TDT for both ICA and M1 cases in this study. The effect of using different TDTs for the ICA occlusions on the quantified TICI (qTICI) score was evaluated. We did not make a distinction in TDT between a proximal and distal ICA and M1 occlusions since there is no considerable difference in the TDT. Consensus agreement between expert observers was achieved to maintain consistency in the delineation process. An example of a TDT is shown in **Supplemental Figure S1**.

The parenchymal mask within the resulting TDT was subsequently determined. qTICI was calculated as the number of pixels of reperfused area in the TDT divided by the number of pixels in the parenchymal mask in the TDT and expressed as percentage. The average qTICI of both anteroposterior and lateral DSA was used as the final qTICI score.

Angiography Evaluation

An independent core-lab assessed all the imaging in the MR CLEAN Registry.[19] The pre- and post-treatment DSA images were used for reperfusion evaluation with target occlusion location determined from pre-treatment DSA images. The six-point eTICI grading was used to adjudicate the reperfusion of the initial target occlusion. We should clarify that we used the eTICI and not the expanded TICI definition. The eTICI is the extension of the modified TICI in which grade 2C has been added.[9] The expanded TICI further divides the scale 2B into 2B50 and 2B67.[10] At the time of the prospective patient recruitment for the registry, the expanded TICI was not yet introduced and therefore not used in the current study. In summary, eTICI 0 describes no reperfusion in TDT; eTICI 1 indicates antegrade reperfusion past the initial occlusion but minimal reperfusion of TDT, eTICI 2A is reperfusion of <50% of TDT, eTICI 2B is a reperfusion of ⩾50% of TDT, eTICI 2C reflects a near-complete perfusion with distal slow flow or presence of small cortical emboli, and eTICI 3 is a complete reperfusion.[7]

Statistical Analyses

Continuous and categorical variables were expressed as median (interquartile range (IQR)) and frequency (percentage), respectively. Kruskal–Wallis tests were performed to compare differences in qTICI scores between eTICI grades. Functional outcome was determined by assessing the modified Rankin Scale (mRS) at day 90 and dichotomized into favorable (mRS 0–2) and unfavorable outcome (mRS 3–6). Stacked bar plots were used to visually compare the ordinal mRS distribution with respect to qTICI and eTICI grades. A classification table for grouped qTICI based on the definition of the corresponding eTICI grades was provided.

The unadjusted and adjusted odds ratios for favorable outcome were estimated for qTICI and eTICI using logistic regression. Adjustments were made by including major prespecified baseline prognostic factors: age, sex, baseline stroke severity (National Institutes of Health Stroke Scale (NIHSS)), Alberta Stroke Program Early CT Score, CTA collateral score, history of hypertension, diabetes mellitus, and previous stroke, pre-treatment mRS, systolic blood pressure, administration of

intravenous thrombolytics prior to EVT, general anesthesia, time from onset-to-groin puncture, and duration of endovascular treatment. For adjusted analyses only, missing variables were imputed based on additive regression, bootstrapping, and predictive mean matching using the aforementioned variables with additional variables: glucose level, hypercholesterolemia, atrial fibrillation, history of myocardial infarction, occlusion segment, time from onset to reperfusion or last contrast bolus, and NIHSS score after 24 to 48 h.[19,20] Unadjusted and adjusted odds ratios were reported with 95% of confidence interval (CI) for statistical precision. Nagelkerke's coefficient of determination was used to compare the unadjusted and adjusted models of qTICI and eTICI in explaining the proportion of functional outcome variation. The effect of using different TDTs for ICA occlusion cases in the estimation of the odds ratio was tested in a sensitivity analysis in which the combined ACA and MCA TDTs were used instead of the MCA TDT.

The area under the receiver operating characteristic curve (AUC) was calculated to determine the prognostic value of the logistic regression models in predicting favorable outcome. P values lower than 0.05 were considered statistically significant. All statistics were performed using IBM SPSS software (version 19.0.0) and RStudio, RStudio, Inc. (version 1.2.1335).

RESULTS

A total of 524 patients met the inclusion criteria based on occlusion location and DSA availability. Based on DSA quality, 115 additional patients were excluded because of motion artifacts (N = 85) and low contrast volume (N = 30), resulting in a total of 408 patients to be included in our final analysis (**Supplemental Figure S2**). **Table 1** shows the baseline characteristics of the patients included in this study. Occlusion sites were ICA in 99 patients and M1 in 309 patients. Median age was 69 (IQR 59–78) years and 43% of patients were female. Median qTICI score was 78 (IQR 58–88). Core-lab determined eTICI was 0 in 31 patients (7%), 1 in 7 patients (2%), 2A in 64 patients (16%), 2B in 91 patients (22%), 2C in 56 patients (14%), and 3 in 159 patients (39%).

Table 1. Baseline Characteristics

N	408
Age, median (IQR)	69 (59–78)
Female sex	200 (43%)
M1 occlusion on DSA	299 (73%)
NIHSS, median (IQR)	16 (12–20)
History of ischemic stroke	67 (17%)
History of hypertension	200 (50%)
History of diabetes mellitus	65 (16%)
Prestroke mRS	
0	277 (70%)
1	48 (12%)
≥2	73 (18%)
Arterial systolic blood pressure in mmHg, median (IQR)	150 (130–165)
Treatment with IV-rtPA	318 (78%)
ASPECTS, median (IQR)	8 (7–10)
CTA collateral score	
0	36 (9%)
1	126 (33%)
2	154 (40%)
3	71 (18%)
eTICI	
0	28 (8%)
1	7 (2%)
2A	59 (16%)
2B	80 (22%)
2C	48 (13%)
3	141 (39%)
General anesthesia	170 (43%)
Onset-to-groin puncture time in min, median (IQR)	210 (163–260)
EVT time in min, median (IQR)	61 (40–86)

IQR: interquartile range; M1: M1 segment of middle cerebral artery; DSA: digital subtraction angiography; NIHSS: National Institutes of Health Stroke Scale; mRS: modified Rankin scale; IV-rtPA: intravenous recombinant tissue plasminogen activator; ASPECTS: Alberta Stroke Program Early Computed Tomography Score; CTA: computed tomography angiography; eTICI: extended thrombolysis in cerebral ischemia; EVT: endovascular treatment.

Figure 2(a) shows the distribution of qTICI values for different eTICI grades. The qTICI was significantly different between all eTICI grades ($P < 0.001$). For ICA occlusion cases only, the qTICI values were not significantly different for eTICI classifications when using the combined ACA and MCA territories ($P = 0.28$). The full result of this analysis is shown in **Supplemental Figure S3**. **Figure 2(b)** shows

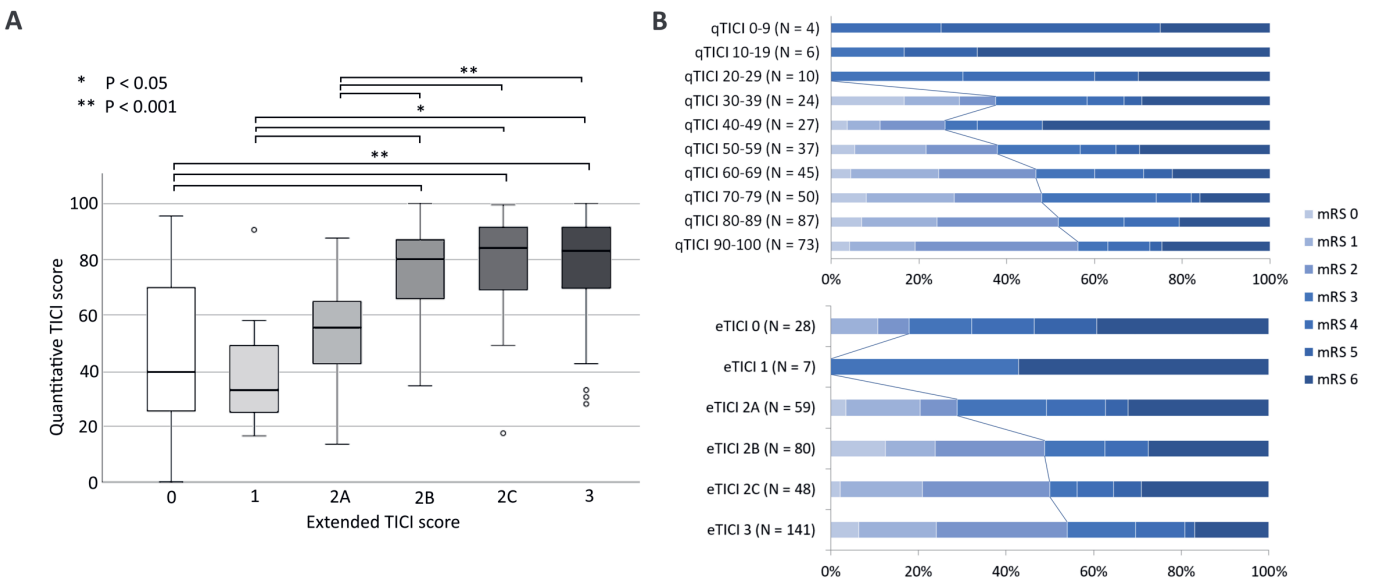

Figure 2. Comparison of qTICI and eTICI. (a) Distribution of the qTICI score for the various eTICI grades. (b) mRS at 90 days based on qTICI and eTICI. mRS: modified Ranking Scale; TICI: Thrombolysis in Cerebral Infarction; qTICI: quantified TICI; eTICI: extended TICI.

Table 2. Classification table of the grouped qTICI and the corresponding eTICI grades

	eTICI 0	eTICI 1	eTICI 2A	eTICI 2B	eTICI 2C	eTICI 3	Total
qTICI 0	**2**	0	0	0	0	0	2
	100%	0%	0%	0%	0%	0%	100%
qTICI 1-9	2	**0**	0	0	0	0	2
	100%	**0%**	0%	0%	0%	0%	100%
qTICI 10-49	14	5	**24**	12	2	11	68
	21%	7%	**35%**	18%	3%	16%	100%
qTICI 50-89	11	1	40	**65**	35	93	245
	4.5%	0.5%	16%	**27%**	14%	38%	100%
qTICI 90-99	2	1	0	12	**18**	53	86
	2%	1%	0%	14%	**21%**	62%	100%
qTICI 100	0	0	0	2	1	**2**	5
	0%	0%	0%	40%	20%	**40%**	100%
Total	31	7	64	91	56	159	408
	7%	2%	16%	22%	14%	39%	100%

TICI: Thrombolysis in Cerebral Infarction; qTICI: quantified TICI; eTICI: extended TICI. The correct classifications are in bold.

the distribution of mRS for different qTICI groups and eTICI grades. The group-wise comparison between qTICI and eTICI is shown in **Table 2**.

Ninety-five patients had missing baseline prognostic variables which were imputed for the subsequent predictive analytics.

Logistic regression analysis showed that both qTICI and eTICI were significantly associated with favorable outcome with unadjusted odds ratio of 1.25 (95% CI, 1.14–1.35, P < 0.001) for 10% qTICI increment and of 1.37 (95% CI, 1.2–1.58, P < 0.001) for one grade eTICI increment (**Table 3**). After adjustment for baseline prognostic variables, an increase in 10% point in qTICI and one grade in eTICI led to the adjusted odds ratio of 1.28 (95% CI, 1.14–1.42, P < 0.001) and 1.43 (95% CI, 1.18–1.73, P < 0.001), respectively. The models including qTICI (unadjusted: pseudo-R^2 = 0.08; adjusted: pseudo-R^2 = 0.50) outperformed the models including eTICI (unadjusted: pseudo-R^2 = 0.07; adjusted: pseudo-R^2 = 0.49) in both

Table 3. Results of unadjusted and adjusted regression analysis for the effect of reperfusion score on the dichotomized functional outcome

	Unadjusted			Adjusted[a]		
	uOR (95% CI)	p-value	Pseudo-R2	aOR (95% CI)	p-value	Pseudo-R2
qTICI per 10%	1.28 (1.14 – 1.42)	<.001	0.08	1.25 (1.14 – 1.35)	<.001	0.50
eTICI per grade	1.37 (1.2 – 1.58)	<.001	0.07	1.43 (1.18 – 1.73)	<.001	0.49

Note: Higher Pseudo-R^2 implies better models. TICI: Thrombolysis in Cerebral Infarction; qTICI: quantified TICI; eTICI: extended TICI; uOR: unadjusted odds ratio; aOR: adjusted odds ratio; CI: confidence interval; Pseudo-R^2: Nagelkerke's coefficient of determination.

[a]Adjusting for sex, age, NIHSS baseline, Alberta Stroke Program Early CT Score baseline, CTA collateral score, previous ischemic stroke, previous hypertension, previous diabetes mellitus, prestroke mRS, arterial systolic blood pressure, treatment with intravenous recombinant tissue plasminogen activator, general anesthesia, onset-to-groin puncture time, and EVT time.

unadjusted and adjusted analysis, although the differences were not statistically significant.

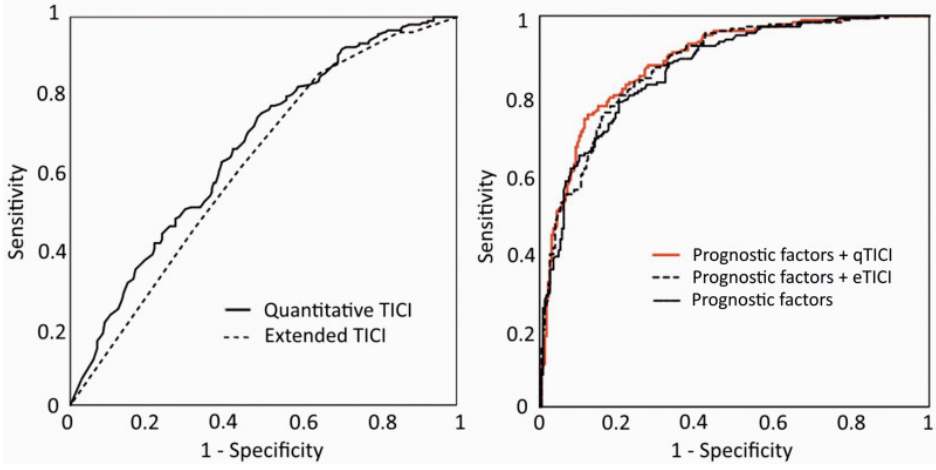

Figure 3. Receiver operating characteristic (ROC) curves for qTICI and eTICI for predicting good functional outcome (mRS 0-2). Left: The area under the curve for qTICI and eTICI as a single predictor were 0.63 and 0.62 respectively. Right: The area under the curve for the adjusted predictive model with either qTICI or eTICI were 0.87 and 0.86 respectively, a minor improvement from the area under the curve 0.85 of the model with the other prognostic factors.

As shown in **Figure 3**, receiver operator characteristics analysis showed that qTICI and eTICI were moderate predictors of favorable outcome with an AUC of 0.63 (95% CI, 0.58–0.68) vs. 0.62 (95% CI, 0.57–0.67). For the adjusted model, qTICI and eTICI were comparable with AUC 0.87 (95% CI, 0.83–0.90) and 0.86 (95% CI, 0.83–0.90), respectively. For both the adjusted and unadjusted models, the difference in AUCs of qTICI and eTICI was not significant (P = 0.87 for the adjusted model, P = 0.80 for the unadjusted model).

The sensitivity analysis showed that the unadjusted and adjusted odds ratio for 10% qTICI increment were 1.28 (95% CI, 1.16–1.4, P < 0.001) and 1.33 (95% CI, 1.18–1.49, P < 0.001) when the combination of ACA and MCA territory was used as ICA TDT. These odds ratios were higher compared to the odds ratios of qTICI using only MCA territory as the ICA TDT.

DISCUSSION

We have presented a semi-automated quantitative method to assess reperfusion on DSA images after endovascular treatment of patients with acute ischemic stroke due to large vessel occlusion. Our study shows that in our population, the qTICI is independently associated with functional outcome. We demonstrated that qTICI has a similar prognostic value compared with eTICI. This result remains consistent after the adjustment for other prognostic factors, indicating that qTICI could be a potential alternative for manual reperfusion assessment with a potentially reduced bias and interobserver variation.

Our method is the first fully quantitative scale of reperfusion assessment. There have been many iterations of angiographic reperfusion scales: starting from adopting the Thrombolysis in Myocardial Infarction scale for the brain, renaming and adjusting the score to TICI, modifying the threshold for scale 2A and 2B (from two-thirds to half of the TDT), adding scale 2C, redefining 2C (90%–99% reperfusion), and expanding scale 2B with the introduction of 2b50 and 2b67.[1,7,9,10,21] Each iteration claimed to give a better definition of successful reperfusion with a more precise threshold to determine the reperfusion result.[4–6,22,23] The inclusion of finer scales was based on evidence that this provides a better reperfusion assessment and clinical utility compared to that of coarser

scales. This underpins the potential value of our continuous quantitative measure. Additionally, qTICI has minimum source of bias as the only dependency to the observer is during the delineation of the TDT. It must be pointed out that qTICI uses a TDT estimate, which is an actual TDT with a slight extension to both cranial and caudal direction. This crude TDT may provide a less accurate assessment since the actual TDT could differ significantly per patient and per occlusion location. However, qTICI remains significantly associated with functional outcome. This is likely due to the low sensitivity of qTICI for small TDT differences. Since the TDT of ICA and M1 occlusion is large, it is expected that minor variation in TDT delineation results in small effects in the qTICI score. In addition, the crude TDT increases the ease of use as meticulous delineation of TDT is not necessary. This could be beneficial in providing a robust reperfusion assessment especially on a large data set of clinical trials and registries. It also allows for faster assessment of difficult cases because of anatomical variation or DSA overprojection.

qTICI and eTICI behave differently in cases with failure of recanalization but retrograde reperfusion via collaterals. Here, some patients have high qTICI, whereas their reperfusion were classified as eTICI 0. For these cases, the high qTICI score may have included a substantial amount of retrograde filling from collaterals in the TDT, which is not included in the eTICI grading. While this may subvert qTICI value in assessing poor reperfusion, the true utility of qTICI is at assessing moderate to high reperfusion. It has been postulated that a fast retrograde perfusion may provide sufficient sustenance to the oligemic region and thus its inclusion may be of added value, though eventual watershed infarcts have also been described in these cases.[24,25] The actual benefit of the inclusion of retrograde perfusion in the assessment was not studied. Another discrepancy between qTICI and eTICI stems from the different concern regarding vessel patency. In recanalized patients with severe stroke or a damaged blood–brain barrier, qTICI may confuse the extravasation of contrast near the artery as parenchymal blush thus exaggerating the rate of reperfusion. Further study is required to confirm the extent of this effect. Finally, **Table 2** shows that the grouped qTICI and eTICI only have a modest agreement. This could be attributed to different factors according to the degree of the reperfusion: for moderate reperfusion, a large mismatch between the

crude TDT and the actual TDT and for zero or complete reperfusion, the hypersensitivity of qTICI to TDT. Overall, grouping of qTICI based on the corresponding eTICI grades, especially qTICI 1 (eTICI 1) and qTICI 99 (eTICI 2C), was somewhat arbitrary and has minimum parallel to the clinical practice of eTICI grading. Hence, the group-wise comparison should be interpreted with caution.

It was demonstrated that the reperfusion scores by themselves have limited value in predicting functional outcome. This is illustrated by the modest predictive value of both qTICI and eTICI. Similar analyses performed on the adjusted models with either qTICI or eTICI show stronger predictive value, where these models explain about half of the variance. This suggests that in a population where most of the patients achieve successful reperfusion, the reperfusion measure becomes a non-variable and has limited effect on functional outcome prediction. However, it should be noted that in both these models, the perfusion scores are independently associated with outcome. The huge effect of endovascular treatment in recent trials has shown that the procedural outcome of endovascular treatment is important.[17,19,26,27] This confirms that although reperfusion outcome may play a substantial role, functional outcome is multifactorial.

The limitations of our study include the availability of adequate images. qTICI is sensitive to noise; motion artifacts could result in false-positive identification of reperfused tissue. A full frontal and lateral view of the affected hemisphere were required, and this was not available for all patients. Another requirement for images includes the first passage of contrast as later passages may be detrimental to the assessment accuracy. We also limited our patient inclusion to only ICA and M1 occlusions as the TDT variation was expected to be minimal.

Our method may benefit from an automatic delineation of TDT, entirely eliminating observer dependency. To complete the full spectrum of perfusion assessment, cases with more distal occlusion could be included. The high variability of TDT for distal occlusions, however, is a challenge for automated methods. Another potential improvement would be to incorporate a region-weighted score. It has been reported that infarct location, especially in the pre-central sulcus and central sulcus, is associated with functional outcome.[28]

Therefore, if implemented, qTICI may have an improved prognostic value as the perfusion is weighted based on the importance of the territory.

CONCLUSION

We developed a quantitative and semi-automated reperfusion score for endovascular treatment evaluation of patients with acute ischemic stroke due to a large vessel occlusion. We have shown that qTICI is an independent predictor of functional outcome and has similar prognostic value as the standard eTICI. The use of crude TDT in qTICI potentially minimizes observer variations and allows more robust assessment across large imaging data set, making qTICI valuable for reperfusion assessment in clinical trial or registry.

SUPPLEMENTAL MATERIALS

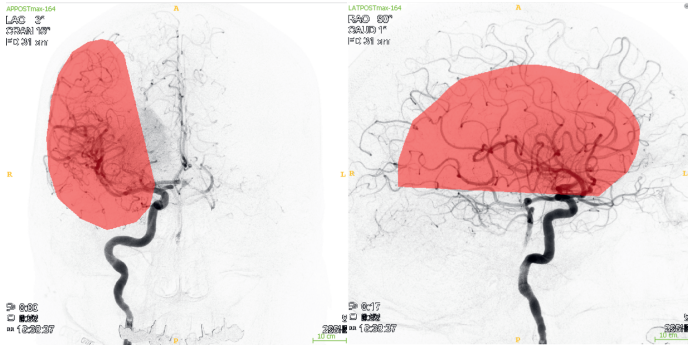

Supplemental Figure S1. The example of target downstream territory in anteroposterior and lateral runs of DSA for both M1 and ICA occlusion. The TDT is the MCA territory including basal ganglia and anterior temporal area.

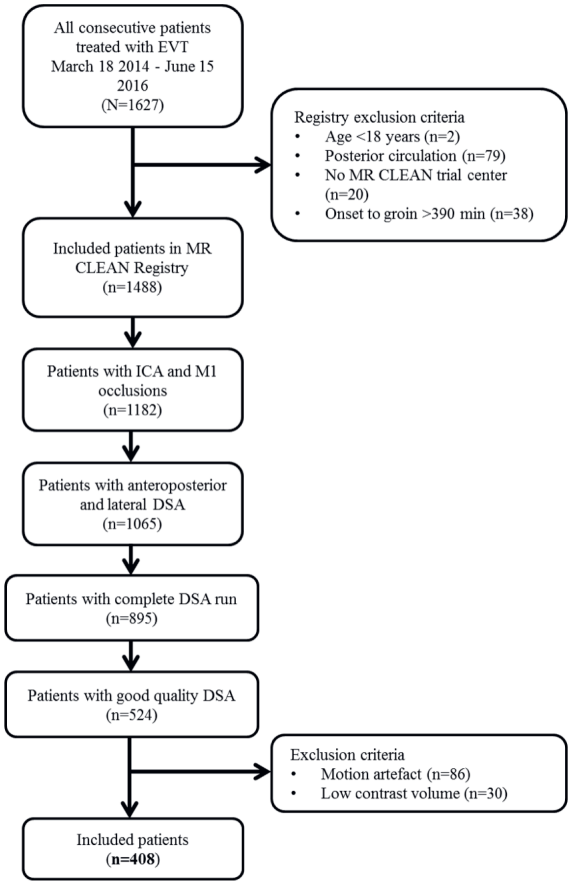

Supplemental Figure S2. Patient inclusion flow chart.

Supplemental Figure S3. The distribution of qTICI scores for various eTICI grades for ICA occlusion depending on the TDT configuration. Both measures had erroneously wide distribution on eTICI 0 and 1. For middle to high grades of eTICI, qTICI was underestimated in the combined ACA and MCA TDT. No significant differences were found between eTICI grades for qTICI scored using the combined ACA and MCA territory as TDT (P = 0.28). The differences become significant for qTICI scored using the MCA territory as TDT (P < 0.001).

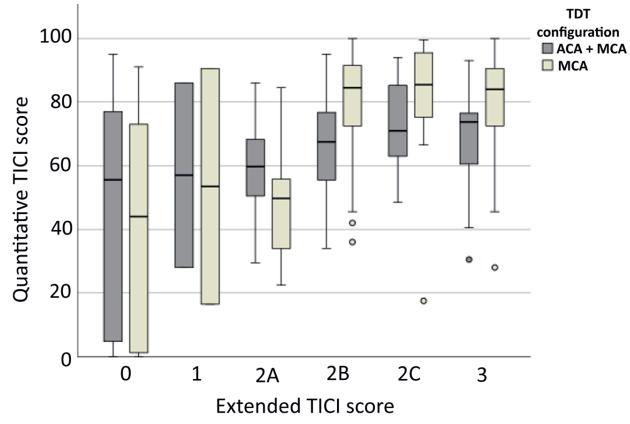

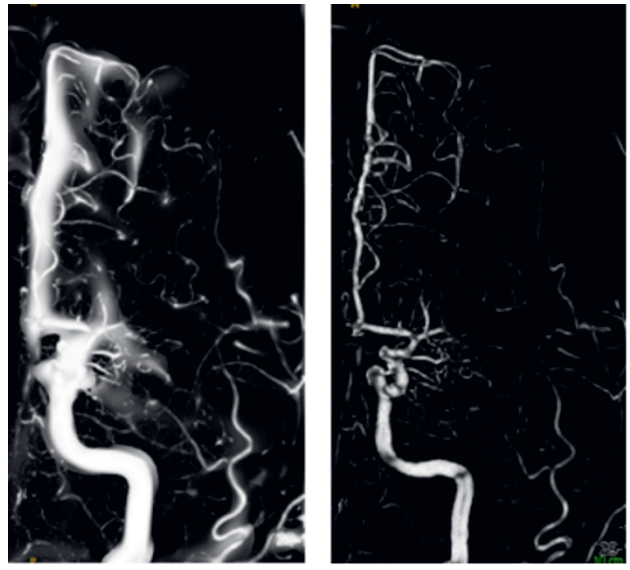

Supplemental Figure S4. The result of vessel enhancement using multiscale Frangi vesselness

Improved vesselness filter

The Frangi vesselness filter uses local structure information in the image to identify tubular shape of vessels. The detail of this method was previously described.[18] In summary, the local structure of every pixel in the image was represented by the eigenvalues (λ_1 and λ_2) and eigenvectors ($\underline{\varphi}_1$ and $\underline{\varphi}_2$) decomposed from the two-dimensional Hessian matrix of the image. This eigendecomposition is performed at multiple Gaussian scale level by applying different sizes of convolutional kernel to the image therefore ensuring the identification of a range of sizes of local structure. At every pixel and scale level, the probability-like estimates of the vessel, or Frangi response, is calculated using two criteria of eigenvalues combination,

$$F = e^{-\frac{S_1}{\beta_1}} \cdot \left(1 - e^{-\frac{S_2}{\beta_2}}\right)$$

$$S_1 = \left(\frac{\lambda_1}{\lambda_2}\right)^2$$

$$S_2 = {\lambda_1}^2 + {\lambda_2}^2$$

where F is the Frangi response, S_1 and S_2 are the factors that determine the geometrical shape of the local structure, and β_1 and β_2 are the correction constants. The final Frangi response of a pixel is the highest response at that pixel among the scale space.

In our application, the convolutional kernel is a two-dimensional array of $(6\sigma + 1)$ by $(6\sigma + 1)$ pixels, with σ representing the variance of the Gaussian filter. We used σ value ranging from 2 to 7 which yielded accurate visualization of the vessels with diameter 5 to 15 pixels. We found that the correction constants 0.5 and 15 provided better vessel enhancement. However, the multiscale approach was prone to the false enhancement of the pixels surrounding the vessel in proportion to the scale level in which the final Frangi response for that pixel was selected. To overcome this so-called blur problem, we introduced a third factor to the Frangi response equation.

$$S_3 = \frac{I - I_{min}}{I_{max} - I_{min}}$$

where I is the target pixel intensity and I_{max} and I_{min} are the maximum and the minimum pixel intensity, respectively, among the neighboring pixels including the target pixel. With this factor, the high Frangi response of the pixels close to a vessel was reduced since the intensity of these pixels were relatively low compared to the intensity of the vessel. The differences between the result of vesselness filter without and with the normalization factor is shown in **Supplemental Figure S4**.

REFERENCES

1. Zaidat OO, Yoo AJ, Khatri P, et al. Recommendations on Angiographic Revascularization Grading Standards for Acute Ischemic Stroke: A Consensus Statement. *Stroke*. 2013;44(9):2650-2663. doi:10.1161/STROKEAHA.113.001972

2. Higashida RT, Furlan AJ. Trial Design and Reporting Standards for Intra-Arterial Cerebral Thrombolysis for Acute Ischemic Stroke. *Stroke*. 2003;34(8):e109-e137. doi:10.1161/01.STR.0000082721.62796.09

3. Khatri P, Yeatts SD, Mazighi M, et al. Time to Angiographic Reperfusion and Clinical Outcome after Acute Ischemic Stroke in the Interventional Management of Stroke Phase III (IMS III) Trial: A Validation Study. *Lancet Neurol*. 2014;13(6):567-574. doi:10.1016/S1474-4422(14)70066-3.Time

4. Yoo AJ, Simonsen CZ, Prabhakaran S, et al. Refining Angiographic Biomarkers of Revascularization: Improving Outcome Prediction After Intra-arterial Therapy. *Stroke*. 2013;44(9):2509-2512. doi:10.1161/STROKEAHA.113.001990

5. Tomsick T, Broderick J, Carrozella J, et al. Revascularization results in the interventional management of stroke II trial. *Am J Neuroradiol*. 2008;29:582-587. doi:10.3174/ajnr.A0843

6. Marks MP, Lansberg MG, Mlynash M, et al. Correlation of AOL Recanalization, TIMI Reperfusion and TICI Reperfusion with Infarct Growth and Clinical Outcome. *J Neurointerv Surg*. 2014;6(10):724-728. doi:10.1109/TMI.2012.2196707.Separate

7. Goyal M, Fargen KM, Turk AS, et al. 2C or not 2C: defining an improved revascularization grading scale and the need for standardization of angiography outcomes in stroke trials. *J Neurointerv Surg*. 2014;6(2):83-86. doi:10.1136/neurintsurg-2013-010665

8. Noser EA, Shaltoni HM, Hall CE, et al. Aggressive mechanical clot disruption: A safe adjunct to thrombolytic therapy in acute stroke? *Stroke*. 2005;36(2):292-296. doi:10.1161/01.STR.0000152331.93770.18

9. Mulder MJHL, Jansen IGH, Goldhoorn RJB, et al. Time to Endovascular Treatment and Outcome in Acute Ischemic Stroke: MR CLEAN Registry Results. *Circulation*. 2018;138(3):232-240. doi:10.1161/CIRCULATIONAHA.117.032600

10. Liebeskind DS, Bracard S, Guillemin F, et al. eTICI reperfusion: defining success in endovascular stroke therapy. *J Neurointerv Surg*. 2019;11:433-438. doi:10.1136/neurintsurg-2018-014127

11. Almekhlafi MA, Mishra S, Desai JA, et al. Not all "successful" angiographic reperfusion patients are an equal validation of a modified TICI scoring system. *Interv Neuroradiol*. 2014;20(1):21-27. doi:10.15274/INR-2014-10004

12. Tung EL, McTaggart RA, Baird GL, et al. Rethinking Thrombolysis in Cerebral Infarction 2b: Which Thrombolysis in Cerebral Infarction Scales Best Define Near Complete Recanalization in the Modern Thrombectomy Era? *Stroke*. 2017;48(9):2488-2493. doi:10.1161/STROKEAHA.117.017182

13. Kaesmacher J, Maegerlein C, Zibold F, Wunderlich S, Zimmer C, Friedrich B. Improving mTICI2b reperfusion to mTICI2c/3 reperfusions: A retrospective observational study assessing technical feasibility, safety and clinical efficacy. *Eur Radiol*. 2018;28(1):274-282. doi:10.1007/s00330-017-4928-3

14. Dekker L, Geraedts VJ, Hund H, et al. Importance of Reperfusion Status after Intra-Arterial Thrombectomy for Prediction of Outcome in Anterior Circulation Large Vessel Stroke. *Interv Neurol*. 2018;7(3-4):137-147. doi:10.1159/000486246

15. Carvalho A, Rocha M, Rodrigues M, et al. Time to Reset the Definition of Successful Revascularization in Endovascular Treatment of Acute Ischemic Stroke. *Cerebrovasc Dis*. 2018;46(1-2):40-45. doi:10.1159/000491553

16. Zhang G, Treurniet KM, Jansen IGH, et al. Operator Versus Core Lab Adjudication of Reperfusion After Endovascular Treatment of Acute Ischemic Stroke. *Stroke*. 2018;49(10):2376-2382. doi:10.1161/STROKEAHA.118.022031

17. Berkhemer OA, Fransen PSS, Beumer D, et al. A Randomized Trial of Intraarterial Treatment for Acute Ischemic Stroke. *N Engl J Med*. 2015;372(1):11-20. doi:10.1056/NEJMoa1411587

18. Frangi AF, Niessen WJ, Vincken KL, Viergever MA. Multiscale vessel enhancement filtering. *Int Conf Med Image Comput Comput Interv*. 1998;1496:130-137. doi:10.1016/j.media.2004.08.001

19. Jansen IGH, Mulder MJHL, Goldhoorn RJB. Endovascular treatment for acute ischaemic stroke in routine clinical practice: Prospective, observational cohort study (MR CLEAN Registry). *BMJ*. 2018;360. doi:10.1136/bmj.k949

20. Donders ART, van der Heijden GJMG, Stijnen T, Moons KGM. Review: A gentle introduction to imputation of missing values. *J Clin Epidemiol*. 2006;59(10):1087-1091. doi:10.1016/j.jclinepi.2006.01.014

21. Chesebro JH, Knatterud G, Roberts R, et al. Thrombolysis in Myocardial Infarction (TIMI) Trial , Phase I : a comparison between intravenous tissue plasminogen activator and intravenous streptokinase. *Circulation*. 1987;76(1):142-154.

22. Khatri P, Neff J, Broderick JP, Khoury JC, Carrozzella J, Tomsick T. Revascularization end points in stroke interventional trials: Recanalization versus reperfusion in IMS-I. *Stroke*. 2005;36(11):2400-2403. doi:10.1161/01.STR.0000185698.45720.58

23. Suh SH, Cloft HJ, Fugate JE, Rabinstein AA, Liebeskind DS, Kallmes DF. Clarifying Differences Among Thrombolysis in Cerebral Infarction Scale Variants: Is the Artery Half Open or Half Closed? *Stroke*. 2013;44(4):1166-1168. doi:10.1109/TMI.2012.2196707.Separate

24. Liebeskind DS. Collaterals in acute stroke: Beyond the clot. *Neuroimaging Clin N Am*. 2005;15(3):553-573. doi:10.1016/j.nic.2005.08.012

25. Van Den Wijngaard IR, Boiten J, Holswilder G, et al. Impact of collateral status evaluated by dynamic computed tomographic angiography on clinical outcome in patients with ischemic stroke. *Stroke*. 2015;46(12):3398-3404. doi:10.1161/STROKEAHA.115.010354

26. Saver JL, Goyal M, Bonafe A, et al. Stent-Retriever Thrombectomy after Intravenous t-PA vs. t-PA Alone in Stroke. *N Engl J Med*. 2015;372(24):2285-2295. doi:10.1056/NEJMoa1415061

27. Zaidat OO, Bozorgchami H, Ribó M, et al. Primary Results of the Multicenter ARISE II Study (Analysis of Revascularization in Ischemic Stroke With EmboTrap). *Stroke*. 2018;49:1107-1115. doi:10.1161/STROKEAHA.117.020125

28. Ernst M, Boers AMM, Aigner A, et al. Association of Computed Tomography Ischemic Lesion Location with Functional Outcome in Acute Large Vessel Occlusion Ischemic Stroke. *Stroke*. 2017;48(9):2426-2433. doi:10.1161/STROKEAHA.117.017513

DALL·E 2: "A colorful picture of a brain breaking down into a pile of numbers, digital art"

Chapter 5

VALUE OF CT PERFUSION FOR COLLATERAL STATUS ASSESSMENT

IN PATIENTS WITH ACUTE ISCHEMIC STROKE

Haryadi Prasetya, Manon Tolhuisen, Miou Koopman, Manon Kappelhof, Frederick JA Meijer, Lonneke SF Yo, Geert J Lycklama à Nijeholt, Wim H van Zwam, Aad van der Lugt, Yvo BWEM Roos, Charles BLM Majoie, Ed van Bavel, Henk A. Marquering, on behalf of the MR CLEAN Registry Investigators

As published in Diagnostics 2022, 12(12):3014
DOI: 10.3390/diagnostics12123014

This work was supported by Indonesia Endowment Fund for Education (LPDP), Ministry of Finance, Republic of Indonesia through LPDP scholarship Program for Doctorate Students.

ABSTRACT

Good collateral status in acute ischemic stroke patients is an important indicator for good outcomes. Perfusion imaging potentially allows for the simultaneous assessment of local perfusion and collateral status. We combined multiple CTP parameters to evaluate a CTP-based collateral score. We included 85 patients with a baseline CTP and single-phase CTA images from the MR CLEAN Registry. We evaluated patients' CTP parameters, including relative CBVs and tissue volumes with several time-to-maximum ranges, to be candidates for a CTP-based collateral score. The score candidate with the strongest association with CTA-based collateral score and a 90-day mRS was included for further analyses. We assessed the association of the CTP-based collateral score with the functional outcome (mRS 0–2) by analyzing three regression models: baseline prognostic factors (model 1), model 1 including the CTA-based collateral score (model 2), and model 1 including the CTP-based collateral score (model 3). The model performance was evaluated using C-statistic. Among the CTP-based collateral score candidates, relative CBVs with a time-to-maximum of 6–10 s showed a significant association with CTA-based collateral scores ($p = 0.02$) and mRS ($p = 0.05$) and was therefore selected for further analysis. Model 3 most accurately predicted favorable outcomes (C-statistic = 0.86, 95% CI: 0.77–0.94) although differences between regression models were not statistically significant. We introduced a CTP-based collateral score, which is significantly associated with functional outcome and may serve as an alternative collateral measure in settings where MR imaging is not feasible.

Keywords: perfusion, CTP, collaterals, ischemic stroke

INTRODUCTION

In patients with acute ischemic stroke, leptomeningeal collateral blood flow potentially maintains blood supply to the ischemic region until the occluded vessel is revascularized.[1] Good collateral status is associated with favorable outcomes, smaller infarct volumes, and lower incidences of hemorrhagic transformation following endovascular therapy.[2–10]

Collateral capacity can be assessed using several imaging modalities, including DSA, CTA, and MRA.[11–14] MRA and CTA have been used to indirectly assess collateral status based on contrast filling in the arteries distal to the clot. In those studies, the collateral status is graded by classifying the extent, the intensity, the speed, or combinations of these contrast filling variables in arteries downstream of the thrombus.

These collateral grading systems have coarse qualitative grading scales and their own limitations. For example, CTA is sensitive to inaccurate scan timing and may miss slower retrograde contrast enhancement of the pial arteries because of the lack of temporal resolution.[6] Collateral grading based on (single vessel) DSA allows only a limited assessment of the MCA territory and is only available after a patient has been selected for treatment.[15] Although these approaches provide an indication of collateral capacity, they do not offer information on the local perfusion of the affected tissue. Perfusion-based imaging acquisitions may provide improved estimates of collateral status in addition to their value in the assessment of stroke pathophysiology and penumbra volume.[16]

A recent study suggested that MR perfusion allows for the quantitative assessment of collateral status with a high agreement with a DSA-based collateral score.[17] In that study, perfusion parameters, such as the time delay of the tissue residue function and the corresponding blood volume, were combined to determine a perfusion collateral index. Because the arterial time delay and relative CBV (rCBV) are generated automatically by MR perfusion imaging software, the perfusion collateral index can be calculated quickly and independent of expert readers. In the time-critical setting of acute stroke care,

such rapid assessment of collateral status may provide added clinical value and factor into therapeutic decision-making.

Compared to CT, MRI has a number of limitations in the acute setting, including its limited availability and longer acquisition times.[18] CT is more widely available in acute stroke care settings. Moreover, CTP is increasingly performed in clinical practice. We hypothesize that, next to MR perfusion, CTP also allows for the assessment of the collateral capacity. We aimed to evaluate various baseline CTP parameters to select a CTP-based collateral score (CTP-CS). We subsequently aimed to assess the association of this CTP-CS with functional outcome after endovascular treatment for acute ischemic stroke.

MATERIALS AND METHODS

Patients

The MR CLEAN Registry (A Multicenter Clinical Registry of Endovascular Treatment for Acute Ischemic Stroke in the Netherlands) is a prospective, multicenter registry collecting data of patients treated with endovascular treatment for ischemic stroke from all stroke intervention centers in the Netherlands. In this study, we selected patients from the MR CLEAN Registry who were treated between June 2016 and November 2017 and for whom baseline CTP and CTA data were available. We further included patients with an occlusion of the M1- or M2-segment of the middle cerebral artery. We excluded patients with poor scan quality due to motion artefact, insufficient contrast or noise, and low temporal imaging resolution. Collateral scores based on baseline single-phase CTA images (CTA-CS) and functional outcomes at 90 days (assessed with mRS) were collected.[19]

CT Perfusion Analysis

CTP data were analyzed using a commercially available software package (Syngo.via; Siemens Healthineers, Erlangen, Germany) to generate perfusion parameters, i.e., CBF, CBV, MTT, and the time to the maximum of residue function (Tmax). For each dataset, the software automatically stripped the skull by finding the bone contour and removed both cerebrospinal fluid and calcifications by

intensity thresholding. The locations to assess the global arterial input function and venous output function were automatically determined at the internal carotid artery and superior sagittal sinus, respectively. Thresholding was performed to remove peripheral and perforating vessels, as their inclusion could lead to the overestimation of microvascular flow. Subsequently, the software generated time attenuation curves of contrast enhancement in Hounsfield Units at the arterial input function and venous output function locations, and in each voxel in the brain area. CBV, CBF, MTT, and Tmax for every voxel of brain tissue were then calculated from the time attenuation curve-derived residue function.[20]

A moderately hypoperfused area is indicative of penumbra, which is sustained by collaterals.[21,22] We chose two CTP parameters to represent the delay and dispersion components of collaterals in moderately hypoperfused areas: Tmax and rCBV. [17] rCBV is defined as the volume of intravascular blood in mL per 100 mL of the brain, compared to that in the contralateral hemisphere.

Additional Imaging Assessments

We chose two measures each for six different ranges of Tmax as candidates for CTP-CS. The two measures were the mean rCBV of the volume defined by Tmax ($rCBV_{Tmax(t1)-(t2)}$) and this rCBV multiplied by total volume of brain tissue defined by the Tmax ($Vol_{Tmax(t1)-(t2)}$). To calculate the measures, we first created Tmax masks, which included all voxels within the predefined Tmax ranges. The contralateral mask was created by mirroring the ipsilateral mask in the midplane. rCBV was calculated as the mean CBV of the ipsilateral masked volume divided by the mean CBV of the contralateral masked volume. The total volume of grey and white matter was calculated by multiplying the voxel volume with the number of voxels that had Tmax values within the given range. The six predefined ranges of Tmax, which depicted the different degrees of hypoperfusion, were 2–4 s, 4–6 s, 2–6 s, 6–10 s, 4–10 s, and 10–14 s. In total we evaluated 12 CTP-CS candidates and subsequently selected one measure as the CTP-CS for further analysis. **Figure 1** shows how the rCBV multiplied by the Tmax-based tissue volume was calculated. An example for the mask of Tmax 6–10 s is also shown.

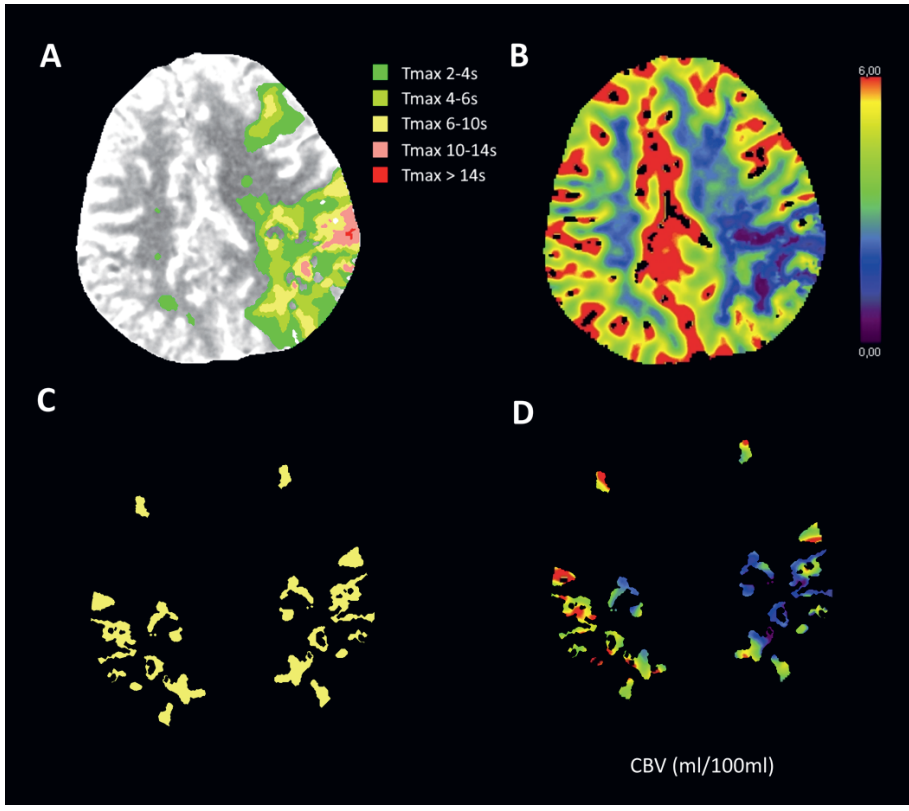

Figure 1. Illustration of one measure as a candidate for baseline CTP-based collateral score: relative CBV multiplied by the total volume of brain tissue defined by time-to-maximum (Tmax). (**A**): Areas with various Tmax value ranges; (**B**): The corresponding CBV values of A (mL/100 mL); (**C**): Mask for Tmax 6–10 s. The contralateral mask is acquired by mirroring the ipsilateral mask using the midline; (**D**): CBV within mask C. The score is the mean CBV of the ipsilateral masked volume relative to the mean CBV of the contralateral masked volume multiplied by the total volume of all the voxels with Tmax value of 6–10 s.

We used data on CTA occlusion locations and collateral scores assessed by an independent core laboratory of neuroradiologists.[19] CTA-CS was based on a 4-point scale: 0 for absent collaterals (no filling of the territory distal to the occlusion), 1 for poor collaterals (less than half filling of the territory), 2 for moderate collaterals (more than half filling of the territory), and 3 for good collaterals (complete filling of the territory).[23] The unaffected contralateral hemisphere was used as reference to evaluate the contrast filling.

Statistical Analysis

Continuous and categorical variables were summarized as median (interquartile range, IQR) and frequency (percentage), respectively. We used the Jonckheere-Terpstra test to determine which CTP-CS candidate had a significant association with CTA-CS and a 90-day mRS. The associations of CTA-CS and the optimal CTP-CS measure with functional independence (mRS 0–2) were assessed using multivariable logistic regression models. For this analysis, we evaluated three models. In the base model (model 1), baseline prognostic factors including age, NIHSS, time from onset to groin puncture, history of hypertension, diabetes mellitus, and previous strokes were included. In model 2, we added the CTA-CS to model 1. In model 3, the CTP-CS was added to model 1. The adjusted OR for statistically significant predictors were reported with 95% CI to indicate statistical precision. Receivers operating characteristics were subsequently determined to compare the predictive power of the models in distinguishing favorable from unfavorable functional outcomes. We compared the C-statistics between models using likelihood ratio tests. We used the Akaike information criterion to compare the relative quality of the regression models. Lower Akaike information criterion implies a more parsimonious model. p-values smaller than 0.05 were considered statistically significant. All statistics were performed using IBM SPSS software (version 19.0.0).

RESULTS

A total of 85 patients were included in our analysis (**Figure 2**). **Table 1** shows the baseline characteristics of the patients included in the study. The median age of the patients was 75 years (IQR 63–81); 41 patients (48%) were female, and the median NIHSS was 16 (IQR 11–20). Core-lab determined that the CTA collateral score was 0 in 4 patients (5%), 1 in 37 patients (43%), 2 in 37 patients (43%), and 3 in 7 patients (9%).

Table 1. Baseline Characteristics

N	85
Age, median (IQR)	75 (63 - 81)
Female sex	41 (48%)
M1 occlusion on CT	66 (78%)
NIHSS, median (IQR)	16 (11 - 20)
History of ischemic stroke	18 (21%)
History of hypertension	42 (50%)
History of diabetes mellitus	8 (9%)
Prestroke mRS	
0	60 (70%)
1	11 (13%)
⩾2	14 (17%)
RR systolic in mmHg, median (IQR)	144 (130 - 160)
Treatment with IV-rtPA	62 (73%)
ASPECTS, median (IQR)	9 (9 - 10)
CTA collateral score	
0	4 (5%)
1	37 (43%)
2	37 (43%)
3	7 (9%)
eTICI	
0	13 (15%)
1	4 (5%)
2A	16 (19%)
2B	14 (16%)
2C	13 (15%)
3	25 (30%)
General anesthesia	7 (8%)
Onset-to-groin puncture time in min, median (IQR)	150 (118 - 211)
EVT time in min, median (IQR)	52 (31 - 81)

IQR indicates interquartile range; M1, M1 segment of middle cerebral artery; eTICI, extended treatment in cerebral ischemia; and EVT, endovascular treatment.

The Jonckheere-Terpstra test showed that among the 12 candidates we evaluated, only the mean rCBV of the Tmax between 6 and 10 s area ($rCBV_{Tmax6-10}$) was significantly associated with the change of both CTA-CS and ordinal mRS (**Table 2**). We therefore selected $rCBV_{Tmax6-10}$ as CTP-CS for further analysis.

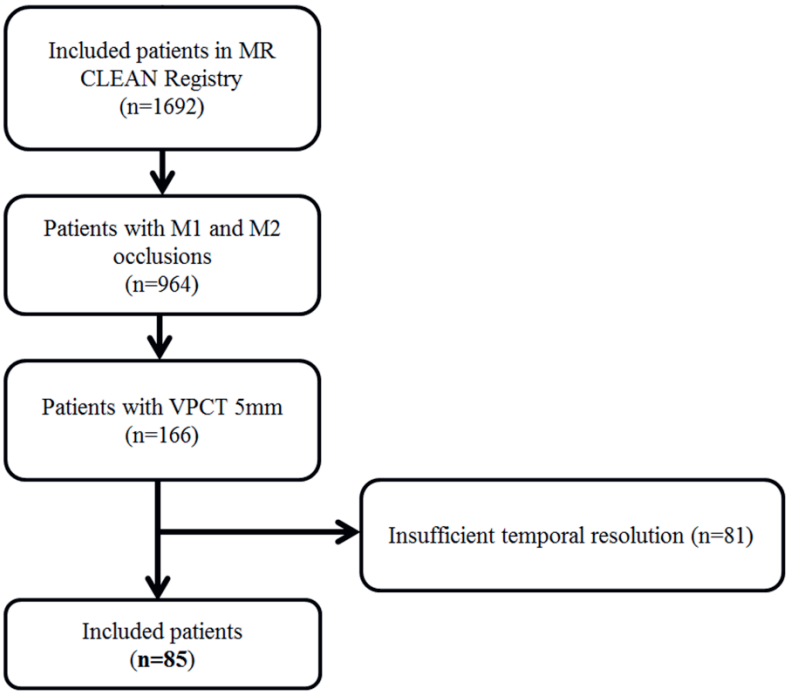

Figure 2. Flowchart of patient inclusion in the study.

Six patients with missing outcome variables were excluded from the multivariable regression analyses. We found that in our patient population, CTA-CS was not significantly associated with a favorable outcome (p = 0.26), as shown in **Table 3**. On the other hand, CTP-CS was significantly associated with favorable outcomes with adjusted OR 1.04 (95% CI, 1.002–1.068, p = 0.036) per 1% increase of CTP-CS. Regression model analysis showed that the C-statistic for model 1 was 0.83 (95% CI, 0.74–0.92; **Table 4**). With the addition of CTA-CS, model 2 had a C-statistic of 0.84 (95% CI, 0.75–0.93). Finally, favorable outcomes were most accurately predicted by model 3 with a C-statistic of 0.86 (95% CI, 0.77–0.94). This model also had the lowest Akaike information criterion. The differences between the C-statistics of the regression models were not statistically significant (model 1 vs. model 2, p = 0.88; model 2 vs. model 3, p = 0.75; model 1 vs. model 3, p = 0.63). **Figure 3** shows the receiver operating characteristics curves of the three regression models.

Table 2. Result of Jonckheere-Terpstra tests of the associations of the baseline CTP-based collateral score (CTP-CS) candidates with baseline single-phase CTA-based collateral score (CTA-CS) and ordinal 90-day mRS.

CTP-CS candidates	P-value	
	Association with CTA-CS	Association with mRS
$rCBV_{Tmax2-4} \times Vol_{Tmax2-4}$ (ml)	0.028[a]	0.19
$rCBV_{Tmax4-6} \times Vol_{Tmax4-6}$ (ml)	0.99	0.91
$rCBV_{Tmax6-10} \times Vol_{Tmax6-10}$ (ml)	0.036[a]	0.35
$rCBV_{Tmax2-6} \times Vol_{Tmax2-6}$ (ml)	0.13	0.39
$rCBV_{Tmax4-10} \times Vol_{Tmax4-10}$ (ml)	0.16	0.56
$rCBV_{Tmax10-14} \times Vol_{Tmax10-14}$ (ml)	<0.001[a]	0.12
$rCBV_{Tmax2-4}$	0.18	0.89
$rCBV_{Tmax4-6}$	0.049[a]	0.59
$rCBV_{Tmax6-10}$	0.020[a]	0.045[b]
$rCBV_{Tmax2-6}$	0.16	0.80
$rCBV_{Tmax4-10}$	0.038[a]	0.23
$rCBV_{Tmax10-14}$	0.036[a]	0.09

Tmax: time to maximum of residue function; $Vol_{Tmaxa-b}$: tissue volume as indicated by Tmax a–b seconds; $rCBV_{Tmaxa-b}$: mean relative CBV of the brain tissue as indicated by Tmax a–b seconds.

[a] Significantly different between groups defined by CTA collateral score (P<0.05)

[b] Significantly different between groups defined by mRS (P<0.05)

Table 3. Adjusted Odds Ratio of logistic regression models of CS-CTA and CS-CTP for favorable outcome

	Adjusted OR	95% CI	p-value
CS-CTA per grade	1.62	0.70-3.73	0.26
CS-CTP per 1%	1.04	1.002-1.068	0.036

OR: odds ratio; CI: confidence interval; CTA-CS: baseline single phase CTA-based collateral score; CTP-CS: baseline CTP-based collateral score.

Table 4. Logistic regression models for favorable functional outcome with C-statistic and Akaike information criterion

Model	C-statistic	AIC
Baseline prognostic factors	0.83	93.5
Baseline prognostic factors + CTA-CS	0.84	94.2
Baseline prognostic factors + CTP-CS	0.86	90.7

AIC: Akaike Information Criterion; CTA-CS: baseline single phase CTA-based collateral score; CTP-CS: baseline CTP-based collateral score.

Higher C-statistic and lower AIC imply better models

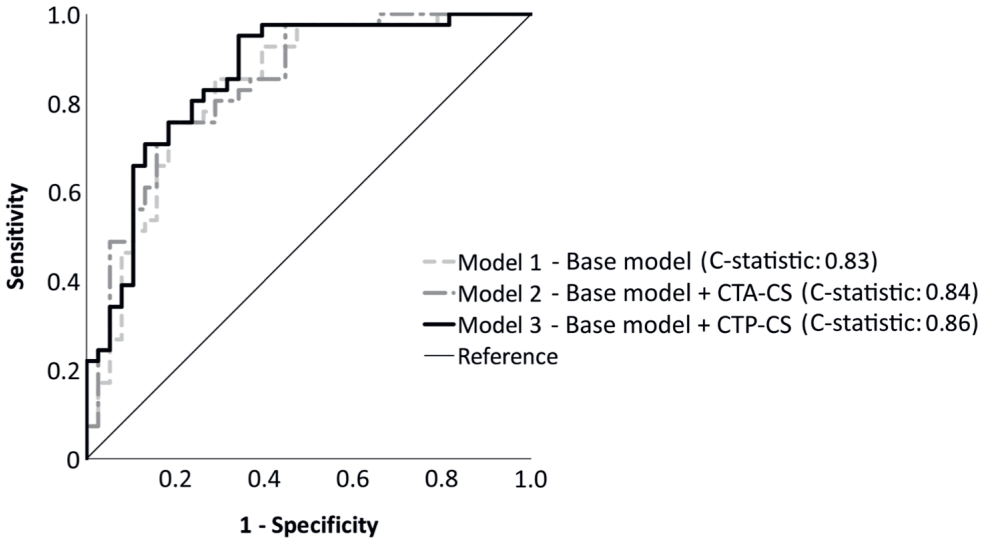

Figure 3. Receiver-operating characteristics curves for three different models for predicting favorable functional outcomes (mRS 0–2). Model 1 is the base model with baseline prognostic factors as the independent variables: age, stroke severity (NIHSS), time from onset to groin puncture, history of hypertension, diabetes mellitus, and previous strokes. Model 2 and model 3 are model 1 with the addition of collateral scores as assessed by CTA and CTP, respectively. The C-statistic for model 1, model 2, and model 3 respectively are 0.83 (95% CI, 0.74–0.92), 0.84 (95% CI, 0.75–0.93), and 0.86 (95% CI, 0.77–0.94). There are no significant differences between the C-statistics of the models.

DISCUSSION

We showed that the CTP parameters Tmax and rCBV can be used to automatically assess collateral capacity in patients who received endovascular treatment for acute ischemic stroke due to a proximal anterior circulation occlusion.

We consider the rCBV of moderately hypoperfused volumes to be a proxy for collaterals; it is an estimate of how much a collateralized microvascular volume is reduced from its healthy volume. The hypoperfused volume represents penumbra which is likely sustained by collaterals.[24–27] Therefore, the delayed perfusion time may be indicative of collateral status.[28] This was confirmed in multiple MR perfusion studies that associated delayed perfusion time with collateral status.[17,28–32] In addition to the delay, the microvascular blood volume of the hypoperfused area may be indicative of the dispersion of collateral flow.[33–35] Delay and dispersion are two important features for the accurate determination

of collateral status.[34] For example, the late arrival time (delay), the speed of vessel filling, and the amount of contrast (dispersion) in pial arteries provide insights into leptomeningeal collateral status.[36] The use of rCBV as CS-CTP relies on having a substantial amount of moderately hypoperfused volume at the time of measurement. This constraint avoids possible mirroring errors during contralateral mask creation. Additionally, sufficient volume suppresses noise which otherwise could negatively impact the reading accuracy. Consequently, the CTP-CS may not be suitable for patients with an insufficient penumbra volume.

We expected that blood volume would be lower on the affected side compared with the unaffected side, resulting in an rCBV ranging from 0 to 1, with a higher rCBV indicating better collaterals.[35,37] Interestingly, this did not seem to be the case as most rCBV medians were larger than 1. One possible explanation is the loss of vascular tone and the recruitment of capillaries in the penumbral microcirculation as a response to hypoxia.[38]

A study on MR perfusion-based collateral assessment suggests that an arterial time delay of 2–6 s best describes the moderately hypoperfused volume.[17] The follow-up study with CTP confirmed that an arterial time delay of 2–6 s was indicative of collateralization.[39] We could not reproduce this finding in our CTP-based study as the volume of brain tissue with a Tmax of 2–6 s, although showing the expected trend, was not significantly associated with either the CTA collateral score nor the ordinal mRS in our patient population. This discrepancy may stem from a bias selection in the population and the inherent differences between the hemodynamical parameters estimation methods employed between their study and ours: the arterial time delay parameter is a Bayesian-estimated Tmax as opposed to the Tmax derived from a singular value decomposition model.[40] The 6 s threshold for determining hypoperfused tissue is consistent with other studies which use MR perfusion-weighted imaging on the DEFUSE study population.[29,31,41] The volume of this hypoperfused tissue had been used to categorize the collateral extent in the infarcted hemisphere.[31,42] The hypoperfusion intensity ratio, the volume of the tissue with a Tmax > 10 s divided by the volume of the tissue with a Tmax > 6 s, has shown to be significantly associated with a persistent perfusion profile for more than 38 h which may indicate favorable collaterals.[43] A recent study on the CTP-based hypoperfusion

intensity ratio of 22 patients demonstrated significant associations between the ratio, using Tmax > 10 s and Tmax> 4 s, and a dynamic CTA-based collateral score and functional outcomes.[44] The evaluation of such thresholds in our collateral formulation did not show an association between the CTA collateral score and the functional outcome.

Most collateral grading methods require extensive assessment from experienced neuroradiologists, which might introduce bias.[45] Inter-observer agreements for collateral grading in various imaging modalities were insufficiently investigated, although some studies reported fair to good agreements.[36,46] The observer dependency is alleviated in our method because the entire process, from reading the CTP source images to generating the collateral score, is fully automated.

We acknowledge several limitations in this study. We included only cases with a middle cerebral artery occlusion. The CTP-based collateral score could be generalized to more proximal or distal occlusion cases, although the perfusion characteristics of the tissue sustained by different types of collaterals may not share the same properties with the tissue supplied by leptomeningeal collaterals. Furthermore, the high threshold of Tmax for our CTP-CS may exclude benign oligemia, which is within the domain of collaterals. We did not investigate the potential contributions of slow flow from pervious thrombus or incomplete occlusions into the moderately hypoperfused tissue, thus confounding the collateral assessment. We also recognize that a considerable amount of penumbra volume is necessary to ensure that the signal to noise ratio is large enough to limit an inaccurate estimation of collateral capacity. Moreover, we found no significant association between CTA-based collateral scores and functional outcomes.[47] This may be caused by imbalanced data due to the lack of samples in extreme grades, i.e., 4 patients with CTA-CS 0 and 9 patients of CTA-CS 3. In addition, some difficult cases in intermediate grades may have complicated the reading. Finally, the prominent discrepancy between CTP software packages may require a fine-tuning of the perfusion parameters to achieve similar results.[48,49] Further studies are warranted to evaluate the robustness of the CTP-based collateral score on different patient populations with a proximal anterior circulation occlusion.

CONCLUSION

This study demonstrates that the CTP parameters Tmax and rCBV can be used to automatically assess collateral capacity in patients who underwent endovascular treatment for acute ischemic stroke due to a proximal anterior circulation occlusion. We selected the mean of relative CBVs of the area with a Tmax of 6–10 s as the CTP collateral score because of its associations with both CTA collateral score and functional outcome. In addition, we showed that the multivariable prognostic model with the CTP-collateral score outperforms models without a collateral score or with the CTA-based collateral score, although these differences were not statistically significant. Because the perfusion parameters are automatically generated by CTP software, CTP-CS is quickly available and does not require an expert reader, potentially increasing its clinical utility in acute stroke settings.

REFERENCES

1. Shuaib A, Butcher K, Mohammad AA, Saqqur M, Liebeskind DS. Collateral blood vessels in acute ischaemic stroke: A potential therapeutic target. *Lancet Neurol*. 2011;10(10):909-921. doi:10.1016/S1474-4422(11)70195-8

2. Singer OC, Berkefeld J, Nolte CH, et al. Collateral Vessels in Proximal Middle cerebral artery Occlusion: The ENDOSTROKE Study 1. *Radiology*. 2015;274(3):851-858. doi:10.1148/radiol.14140951

3. Bang OY, Saver JL, Buck BH, et al. Impact of collateral flow on tissue fate in acute ischaemic stroke. *J Neurol Neurosurg Psychiatry*. 2008;79(6):625-629. doi:10.1136/jnnp.2007.132100

4. Menon BK, O'Brien B, Bivard A, et al. Assessment of leptomeningeal collaterals using dynamic CT angiography in patients with acute ischemic stroke. *J Cereb Blood Flow Metab*. 2013;33(3):365-371. doi:10.1038/jcbfm.2012.171

5. Berkhemer OA, Jansen IGH, Beumer D, et al. Collateral Status on Baseline Computed Tomographic Angiography and Intra-Arterial Treatment Effect in Patients with Proximal Anterior Circulation Stroke. *Stroke*. 2016;47(3):768-776. doi:10.1161/STROKEAHA.115.011788

6. Menon BK, Smith EE, Modi J, et al. Regional leptomeningeal score on CT angiography predicts clinical and imaging outcomes in patients with acute anterior circulation occlusions. *Am J Neuroradiol*. 2011;32(9):1640-1645. doi:10.3174/ajnr.A2564

7. Kucinski T, Koch C, Eckert B, et al. Collateral circulation is an independent radiological predictor of outcome after thrombolysis in acute ischaemic stroke. *Neuroradiology*. 2003;45(1):11-18. doi:10.1007/s00234-002-0881-0

8. Sheth SA, Sanossian N, Hao Q, et al. Collateral flow as causative of good outcomes in endovascular stroke therapy. *J Neurointerv Surg*. 2016;8(1):2-7. doi:10.1136/neurintsurg-2014-011438

9. Seyman E, Shaim H, Shenhar-Tsarfaty S, Jonash-Kimchi T, Bornstein NM, Hallevi H. The collateral circulation determines cortical infarct volume in

anterior circulation ischemic stroke. *BMC Neurol*. 2016;16(1):1-9. doi:10.1186/s12883-016-0722-0

10. Elijovich L, Goyal N, Mainali S, et al. CTA collateral score predicts infarct volume and clinical outcome after endovascular therapy for acute ischemic stroke: A retrospective chart review. *J Neurointerv Surg*. 2016;8(6):559-562. doi:10.1136/neurintsurg-2015-011731

11. Higashida RT, Furlan AJ. Trial Design and Reporting Standards for Intra-Arterial Cerebral Thrombolysis for Acute Ischemic Stroke. *Stroke*. 2003;34(8):e109-e137. doi:10.1161/01.STR.0000082721.62796.09

12. Miteff F, Levi CR, Bateman GA, Spratt N, McElduff P, Parsons MW. The independent predictive utility of computed tomography angiographic collateral status in acute ischaemic stroke. *Brain*. 2009;132(8):2231-2238. doi:10.1093/brain/awp155

13. Lee KY, Latour LL, Luby M, Hsia AW, Merino JG, Warach MpS. Distal hyperintense vessels on FLAIR: An MRI marker for collateral circulation in acute stroke? *Neurology*. 2009;72(13):1134-1139. doi:10.1212/01.wnl.0000345360.80382.69

14. Silvestrini M, Altamura C, Cerqua R, et al. Early activation of intracranial collateral vessels influences the outcome of spontaneous internal carotid artery dissection. *Stroke*. 2011;42(1):139-143. doi:10.1161/STROKEAHA.110.595843

15. Jansen IGH, Berkhemer OA, Yoo AJ, et al. Comparison of CTA- and DSA-Based Collateral Flow Assessment in Patients with Anterior Circulation Stroke. *Am J Neuroradiol*. 2016;37(11):2037-2042. doi:10.3174/ajnr.A4878

16. Parsons MW. Perfusion CT: Is it clinically useful? *Int J Stroke*. 2008;3(1):41-50. doi:10.1111/j.1747-4949.2008.00175.x

17. Nael K, Doshi A, Leacy R De, et al. MR Perfusion to Determine the Status of Collaterals in Patients with Acute Ischemic Stroke : A Look Beyond Time Maps. *Am J Neuroradiol*. 2018;39(2):219-225. doi:10.3174/ajnr.A5454

18. Jauch EC, Saver JL, Adams HP, et al. Guidelines for the early management of

patients with acute ischemic stroke: A guideline for healthcare professionals from the American Heart Association/American Stroke Association. *Stroke*. 2013;44(3):870-947. doi:10.1161/STR.0b013e318284056a

19. Jansen IGH, Mulder MJHL, Goldhoorn RJB. Endovascular treatment for acute ischaemic stroke in routine clinical practice: Prospective, observational cohort study (MR CLEAN Registry). *BMJ*. 2018;360. doi:10.1136/bmj.k949

20. Abels B, Klotz E, Tomandl BF, Kloska SP, Lell MM. Perfusion CT in acute ischemic stroke: A qualitative and quantitative comparison of deconvolution and maximum slope approach. *Am J Neuroradiol*. 2010;31(9):1690-1698. doi:10.3174/ajnr.A2151

21. Bivard A, Levi C, Spratt N, Parsons M. Perfusion CT in Acute Stroke: A Comprehensive Analysis of Infarct and Penumbra. *Radiology*. 2013;267(2):543-550. doi:10.1148/radiol.12120971

22. Pallesen L-P, Lambrou D, Eskandari A, et al. Perfusion computed tomography in posterior circulation stroke: predictors and prognostic implications of focal hypoperfusion. *Eur J Neurol*. 2018;25(5):725-731. doi:10.1111/ene.13578

23. Tan IYL, Demchuk AM, Hopyan J, et al. CT Angiography Clot Burden Score and Collateral Score: Correlation with Clinical and Radiologic Outcomes in Acute Middle Cerebral Artery Infarct. *Am J Neuroradiol*. 2009;30(3):525-531. doi:10.3174/ajnr.A1408

24. Beretta S, Cuccione E, Versace A, et al. Cerebral collateral flow defines topography and evolution of molecular penumbra in experimental ischemic stroke. *Neurobiol Dis*. 2015;74:305-313. doi:10.1016/j.nbd.2014.11.019

25. Kawano H, Bivard A, Lin L, et al. Relationship between Collateral Status, Contrast Transit, and Contrast Density in Acute Ischemic Stroke. *Stroke*. 2016;47(3):742-749. doi:10.1161/STROKEAHA.115.011320

26. Rusanen H, Saarinen JT, Sillanpää N. Collateral circulation predicts the size of the infarct core and the proportion of salvageable penumbra in hyperacute ischemic stroke patients treated with intravenous thrombolysis. *Cerebrovasc Dis*. 2015;40(3-4):182-190. doi:10.1159/000439064

27. Santos EMM, Marquering HA, den Blanken MD, et al. Thrombus Permeability Is Associated With Improved Functional Outcome and Recanalization in Patients With Ischemic Stroke. *Stroke*. 2016;47(3):732-741. doi:10.1161/STROKEAHA.115.011187

28. Campbell BC, Christensen S, Tress BM, et al. Failure of collateral blood flow is associated with infarct growth in ischemic stroke. *J Cereb Blood Flow Metab*. 2013;33(8):1168-1172. doi:10.1038/jcbfm.2013.77

29. Lansberg MG, Lee J, Christensen S, et al. RAPID automated patient selection for reperfusion therapy: A pooled analysis of the echoplanar imaging thrombolytic evaluation trial (EPITHET) and the diffusion and perfusion imaging evaluation for understanding stroke evolution (DEFUSE) study. *Stroke*. 2011;42(6):1608-1614. doi:10.1161/STROKEAHA.110.609008

30. Olivot JM, Mlynash M, Inoue M, et al. Hypoperfusion intensity ratio predicts infarct progression and functional outcome in the DEFUSE 2 cohort. *Stroke*. 2014;45(4):1018-1023. doi:10.1161/STROKEAHA.113.003857

31. Marks MP, Lansberg MG, Mlynash M, et al. Effect of Collateral Blood Flow on Patients Undergoing Endovascular Therapy for Acute Ischemic Stroke. *Stroke*. 2014;45(4):1035-1039. doi:10.1161/STROKEAHA.113.004085

32. Nicoli F, Scalzo F, Saver JL, et al. The combination of baseline magnetic resonance perfusion-weighted imaging-derived tissue volume with severely prolonged arterial-tissue delay and diffusion-weighted imaging lesion volume is predictive of MCA-M1 recanalization in patients treated with endo. *Neuroradiology*. 2014;56(2):117-127. doi:10.1007/s00234-013-1310-2

33. Liebeskind DS. Collateral circulation. *Stroke*. 2003;34(9):2279-2284. doi:10.1161/01.STR.0000086465.41263.06

34. Liebeskind DS. Collaterals in acute stroke: Beyond the clot. *Neuroimaging Clin N Am*. 2005;15(3):553-573. doi:10.1016/j.nic.2005.08.012

35. Cortijo E, Calleja AI, García-Bermejo P, et al. Relative Cerebral Blood Volume as a Marker of Durable Tissue-at-Risk Viability in Hyperacute Ischemic Stroke. *Stroke*. 2014;45(1):113-118. doi:10.1161/STROKEAHA.113.003340

36. McVerry F, Liebeskind DS, Muir KW, McVerry F, Liebeskind DS, Muir KW. Systematic Review of Methods for Assessing Leptomeningeal Collateral Flow. *AJNR Am J Neuroradiol*. Published online 2012:1-7. doi:10.3174/ajnr.A2794

37. Arenillas JF, Cortijo E, García-Bermejo P, et al. Relative cerebral blood volume is associated with collateral status and infarct growth in stroke patients in SWIFT PRIME. *J Cereb Blood Flow Metab*. 2018;38(10):1839-1847. doi:10.1177/0271678X17740293

38. Jordan JD, Powers WJ. Cerebral autoregulation and acute ischemic stroke. *Am J Hypertens*. 2012;25(9):946-950. doi:10.1038/ajh.2012.53

39. Nael K, Sakai Y, Larson J, et al. CT Perfusion collateral index in assessment of collaterals in acute ischemic stroke with delayed presentation: Comparison to single phase CTA. *J Neuroradiol*. 2022;49(2):198-204. doi:10.1016/j.neurad.2021.11.002

40. Boutelier T, Kudo K, Pautot F, Sasaki M. Bayesian hemodynamic parameter estimation by bolus tracking perfusion weighted imaging. *IEEE Trans Med Imaging*. 2012;31(7):1381-1395. doi:10.1109/TMI.2012.2189890

41. Olivot JM, Mlynash M, Thijs VN, et al. Optimal Tmax Threshold for Predicting Penumbral Tissue in Acute Stroke. *Stroke*. 2009;40(2):469-475. doi:10.1161/STROKEAHA.108.526954

42. Son JP, Lee MJ, Kim SJ, et al. Impact of Slow Blood Filling via Collaterals on Infarct Growth: Comparison of Mismatch and Collateral Status. *J Stroke*. 2017;19(1):88-96. doi:10.5853/jos.2016.00955

43. Christensen S, Mlynash M, Kemp S, et al. Persistent target mismatch profile >24 hours after stroke onset in DEFUSE 3. *Stroke*. 2019;50(3):754-757. doi:10.1161/STROKEAHA.118.023392

44. Lin L, Chen C, Tian H, et al. Perfusion computed tomography accurately quantifies collateral flow after acute ischemic stroke. *Stroke*. 2020;51:1006-1009. doi:10.1161/STROKEAHA.119.028284

45. Zhang G, Treurniet KM, Jansen IGH, et al. Operator Versus Core Lab

Adjudication of Reperfusion After Endovascular Treatment of Acute Ischemic Stroke. *Stroke*. 2018;49(10):2376-2382. doi:10.1161/STROKEAHA.118.022031

46. Kauw F, Dankbaar JW, Martin BW, et al. Collateral Status in Ischemic Stroke: A Comparison of Computed Tomography Angiography, Computed Tomography Perfusion, and Digital Subtraction Angiography. *J Comput Assist Tomogr*. 2020;44(6):984-992. doi:10.1097/RCT.0000000000001090

47. Jansen IGH, Mulder MJHL, Goldhoorn RJB, et al. Impact of single phase CT angiography collateral status on functional outcome over time: Results from the MR CLEAN Registry. *J Neurointerv Surg*. 2019;11(9):866-873. doi:10.1136/neurintsurg-2018-014619

48. Bathla G, Limaye K, Policeni B, Klotz E, Juergens M, Derdeyn C. Achieving comparable perfusion results across vendors. The next step in standardizing stroke care: a technical report. *J Neurointerv Surg*. 2019:11(12):1257-1260. doi:10.1136/neurintsurg-2019-014810

49. Fahmi F, Marquering HA, Streekstra GJ, et al. Differences in CT perfusion summary maps for patients with acute ischemic stroke generated by 2 software packages. *Am J Neuroradiol*. 2012;33(11):2074-2080. doi:10.3174/ajnr.A3110

DALL·E 2: "A photograph of a humanoid and a human doctor walking into a sunset"

Chapter 6

GENERAL DISCUSSION

Adequate tissue-level oxygenation through microvascular perfusion is crucial in maintaining physiological functions. Various medical imaging technologies allow visual inspection of perfusion by contrast injection.[1] In addition to its direct objective to evaluate disease severity, periprocedural perfusion assessment can be used to assess therapeutic responses and adjust revascularization strategy. For example, in the brain, the perfusion score TICI 2b or better has been widely used as an indicator of successful revascularization in acute stroke management.[2] In a patient with myocardial infarction, successful percutaneous coronary intervention is indicated by two criteria: stenosis diameter reduction of < 50% and grade 3 TIMI flow.[3] As another example, fluorescence-based microvascular perfusion assessment of post-esophagectomy gastric conduits may guide surgery, thereby potentially reducing anastomotic leaks.[4] In addition, perfusion measures have also been demonstrated to be good predictors of functional outcome.[2,5]

Objective assessment of perfusion is important to optimize clinical workflow and improve clinical decision-making. In this thesis, we report advancements toward reducing observer dependency by automating assessment and developing alternative quantitative measures for crude visual scales in several organs and imaging modalities.

Generally, there are clear benefits in automating and quantifying visual perfusion scales. A fully automated method removes observer bias from the assessment as only objective information is used. Additionally, it may reduce the workload of the clinician and improve disease management workflow. This is particularly important in acute settings where swift care is of importance. The quantitative aspect may add more resolution to the perfusion grading, which may improve accuracy in clinical decision-making. We discuss these automation and quantitative components further in the next sections.

AUTOMATION OF IMAGING-BASED PERFUSION ASSESSMENT

Rule-based vs data-driven

Automation of imaging-based perfusion assessment essentially reduces and eventually removes the role of human judgment in perfusion grading based on medical images while maintaining similar or better performance compared to

assessment by radiologists. In chapter 3, the Quantitative Blush Evaluator (QuBE) method is addressed. QuBE automates myocardial perfusion assessment on coronary angiograms and, as such, reduces the manual activities down to drawing an area of interest. The Quantitative Treatment in Cerebral Ischemia (qTICI) scale achieved a similar degree of automation for brain perfusion assessment on DSA, as described in chapter 4. In chapter 5, a CTP-based collateral score (CTP-CS) was introduced as a method to automate collateral assessment using CTP images. These automations were achieved heuristically by employing a rule-based system. A rule-based system is developed by translating domain experts' knowledge and activities into a series of computer logics or algorithms to achieve the desired outcome. A sequence of image processing techniques such as image enhancement, semantic segmentation, and pixel-wise quantification resulting in a perfusion score is an example of this approach. On the opposite end of the spectrum, data-driven approaches, i.e., machine learning, are gaining traction in clinical research because of their potential and versatility. Supervised learning, especially using convolutional neural networks, is a branch of machine learning currently often used to process imaging data. With supervised learning, relationship patterns between imaging data (input) and expert-annotated labels (output) are learned based on extensive data of input-output pairs. Such a resulting model can subsequently be used to, for example, prospectively assess perfusion based on new imaging data. Data-driven models, however, are commonly difficult to interpret and are therefore often regarded as black-box solutions. **Figure 1** illustrates the difference between rule-based systems and machine learning approaches.

In Chapter 3, the limitations of QuBE algorithms were analyzed. The algorithm-level examination was possible because QuBE is a rule-based system. The success of the automation is measured from the match of the QuBE score with the Myocardial Blush Grade and by assessing the association with functional outcome. It is easy to presume that all the automated processes work appropriately in case of a good match. Yet, we found that the large-scale structure removal algorithm, which supposedly subtracts coronary arteries, the diaphragm, and the catheter from angiograms, did not adequately yield the intended result. This inaccurate pre-processing step indicates a potentially

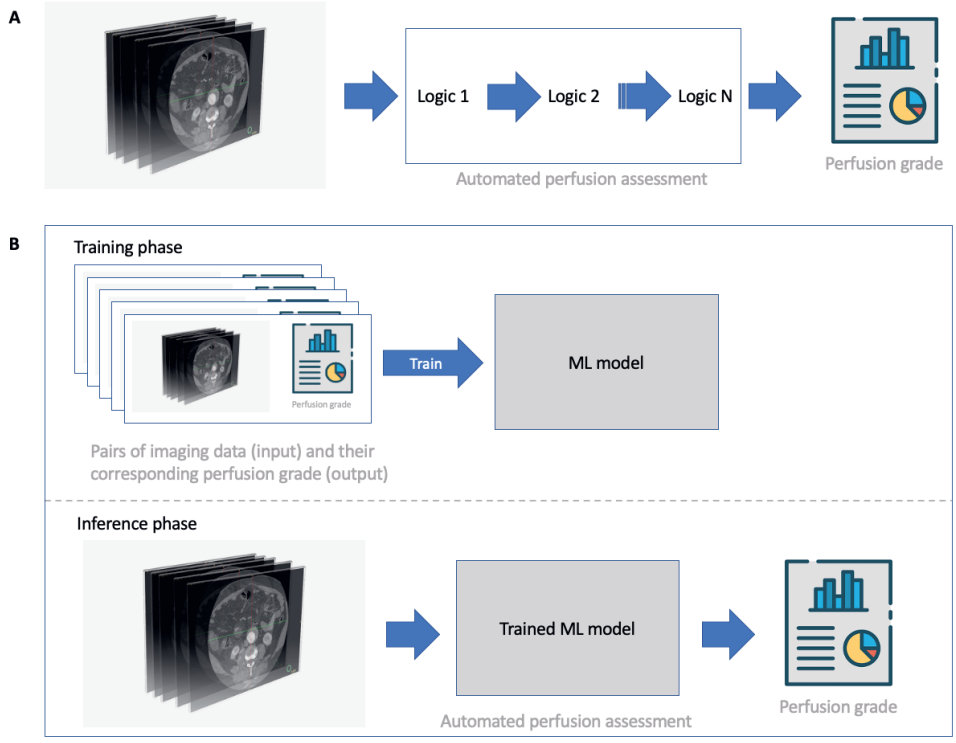

Figure 1. (A) Rule-based systems vs (B) machine learning approaches (supervised learning) in automating perfusion assessment. Rule-based systems require decomposing clinical insights into a programmable sequence of logics. This design allows inspection of each process, providing meaningful information and a clear workflow from processing medical images to generating perfusion grades. Supervised learning approaches learn the "sequence of logics" by modeling the complex interactions between a considerable amount of imaging features and the corresponding perfusion grade. The trained model is then used to provide the perfusion grading of the "unseen" medical images. Such a model, in most cases, is inscrutable.

compromised blush quantification. While this was a limitation of this approach, at least the rule-based design provides the level of transparency and explainability that is preferred for clinical end use.[6]

TOWARDS A FULLY AUTOMATED PERFUSION ASSESSMENT

A fully automated method of perfusion assessment is achieved when the imaging data can be processed to generate perfusion grades without any human inputs. QuBE provides partial automation because some human input is still required: An

observer needs to draw an area of interest, the target downstream territory (TDT). Also, qTICI (chapter 4) is considered partial automation since TDT delineation is required.

Why is TDT delineation difficult to automate?

In brain perfusion, the TDT is the region of the brain that was previously supplied by the occluded vessel causing an acute ischemic stroke.[7] Naturally, the boundary of this territory is dependent on multiple factors. First, the occlusion location affects the size and shape of the territory; the more distal the occlusion, the smaller the territory and the more sensitive it is to anatomical variation. QuBE and qTICI are performed on two-dimensional imaging modalities (coronary angiogram and DSA, respectively), complicating the three-dimensional TDT delineation. Such delineation is even more difficult in coronary angiograms, as the heart motion is a confounding factor. Also, the additional variability of the image acquisition projection affects the delineation.

Besides QuBE and qTICI, there are several other perfusion assessment automation studies that performed a manual delineation of the region of interest. In a study that evaluated angiographic parametric imaging to automatically locate infarct core in DSA, the downstream territory was indicated manually to prevent extension into the extracranial space.[8] A study evaluating the DSA of foot perfusion following infrapopliteal angioplasty utilized user-specified regions of interest.[9] A study on automatic flow analysis suggested a different approach to avoid manual selection of regions of interest by analyzing flow according to the imaging phase.[10] Another effort on automating TICI redefined TDT to simplify the delineation of the downstream area.[11] In that study, the TDT was defined as only the non- or under-perfused area regardless the supply origin. With this definition, TDT is severely underestimated, especially when it includes large areas of overlapping vessels from different arterial circulations. **Figure 2** shows such TDT compared to the recommended definition of TDT.

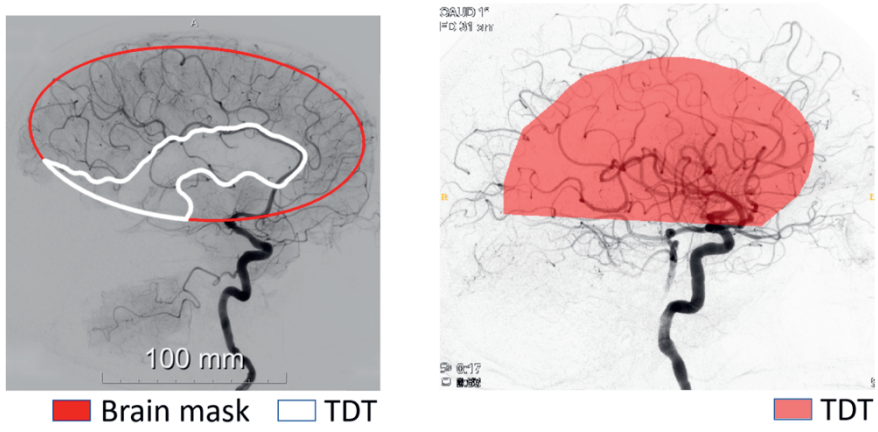

Figure 2. TDT according to Su et.al[11](left) and the recommended definition of TDT (right) of M1 occlusion in lateral view. The M1 segment supplies the entire middle cerebral artery region. Therefore the TDT is the full middle cerebral artery downstream region. In the lateral view, the middle cerebral artery superior division superpositions with parts of the anterior cerebral artery region, and this should be included in the TDT, as shown on the right. The TDT delineation on the right requires domain knowledge of vascular anatomy and is considerably more difficult to achieve compared to the TDT on the left, which is obtainable by simple intensity thresholding. The left image is reprinted with permission from IEEE Transactions of Medical Imaging © 2021, IEEE.

Leveraging machine learning for full automation

With machine learning approach, the delineation of TDT is irrelevant, as demonstrated by a recent study that automated the TICI scoring using a deep learning model.[12]

Various machine learning models trained on medical images and their derivatives have been quite successful in automating perfusion assessment for different organs.[13–15] A study addressing myocardial CTP shows that deep learning techniques can automatically distinguish well-perfused myocardium from perfusion defects.[13] A similar success was found in an angiographic optical coherence tomography study. Here, automated segmentation of the nonperfusion area, an important biomarker for diabetic retinopathy, by a convolutional neural network exhibited higher performance than human experts.[14] In another study, a convolutional neural network trained using diffusion-weighted and perfusion-weighted imaging maps to predict lesions in an acute stroke setting

outperformed other lesion prediction methods.[15] Moreover, neural network models can be repurposed for other tasks through a process called transfer learning. In transfer learning, the existing model is used as a base to train another model; the trained parameters in each neuron are preserved before re-training the neural network with the new data. This feature overcomes training data scarcity, supports mutual collaboration among studies and encourages gradual improvements by building upon the progress of other studies. For instance, a recent OCT study leveraged transfer learning and developed a convolutional neural network to automatically segment the microvasculature and intercapillary area in deep vascular complexes by fine-tuning an existing model for vessel segmentation in the foveal avascular zone.[16]

QUANTIFICATION OF PERFUSION ASSESSMENT

Visual perfusion scales are often coarse. Their definition is based on providing the most useful set of perfusion grades for supporting clinical decision-making. However, such scales may be adapted to maintain robustness despite the limited capacity of human eyes. The grade 2 in the original TICI was redefined in the modified TICI because it is more difficult for humans to accurately estimate two third of TDT as compared to half of TDT.[7] The meaningful distinction between grades is usually identified by statistically analyzing the differences with respect to functional improvement. However, higher resolution does not always translate to higher clinical value. The expanded TICI 2b67 scale, for instance, introduced a higher resolution to the TICI grading scale (see **Table 1**).[17] It was found that this additional step in the resolution improves the accuracy of the procedural outcome and provides evidence that higher perfusion results in better functional outcome.[18] However, this grading scale led to a higher grading discrepancy between observers.[17] Furthermore, this grade is not indicative of treatment success. Therefore, despite the better resolution, the current grading scale has limited clinical value.

Automated perfusion assessment can provide continuous, quantitative values, with the number of possible outcomes frequently only limited by image discretization. Such pseudo-precision should be interpreted with caution because of the diminutive covariance between meaningful physiological information and

Table 1. Comparison of the existing TICI grading scale criteria

TICI Grade	Original TICI[19]	Modified TICI[7]	Modified TICI with 2c[20]	Expanded TICI[17]
0/1	No/minimal reperfusion	No/minimal reperfusion	No/minimal reperfusion	No/minimal reperfusion
2a	*Partial filling <2/3 territory	Partial filling < 50% territory	Partial filling < 50% territory	Partial filling < 50% territory
2b	Partial filling ≥ 2/3 territory	*Partial filling ≥ 50% territory	*Partial filling ≥ 50% territory	Partial filling (50%–66%)
2b67	n/a	n/a	n/a	Partial filling (67%–89%)
2c	n/a	n/a	Near complete perfusion except slow flow or few distal cortical emboli	*Near complete filling (90%–99%)
3	Complete perfusion	Complete perfusion	Complete perfusion	Complete perfusion

*Recommended angiographic target for endovascular treatment in ischemic stroke

perfusion score.[21] This continuous value, however, provides a basis for new stratification of potentially more accurate and clinically relevant perfusion grades, unconstrained by human visual acumen.

Quantitative estimation of perfusion parameters can also be extracted from bolus tracking derived from time-series medical images, e.g., cine-angiogram, near-infrared fluorescent images, or CTP source images. In chapter 2, we developed a new perfusion estimator derived from time-intensity curves of simulated contrast flow in four demarcated areas of the gastric conduit model. We found that a low relative time-to-intensity threshold is predictive of perfusion deterioration. This finding is consistent with the theoretical basis of CTP, where high contrast delay, represented by a long time to the maximum of the residue function (also known as Tmax), indicates perfusion impairment.[22] Moreover, the effect of various vessel configurations to contrast dynamics confirmed that similar to the time-to-peak of CTP, the time-to-intensity threshold is affected by arterial dispersion.[23] This quantitative perfusion data allows such observation, which is difficult to achieve by visual inspection of the images alone.

In a more complex approach, modular quantification, in which multiple perfusion parameters are combined, can be used. This allows the inclusion of numerous quantifiable measures pertaining to perfusion into a single metric. In chapter 5, we investigated a multi-parametric approach of CTP to calculate collateral perfusion (CS-CTP) by multiplying the volume of interest derived from Tmax of 6-10 seconds and its relative cerebral blood volume. The interpretation of this score is not so trivial, as collateral status is inferred through cerebral blood volume of hypoperfused tissue with delayed contrast arrival, indicating the extent of retrograde flux from the collateral network. Many CTP studies leveraged multi-parametric approaches because several perfusion parameters are readily available from the standard package of CTP analysis.[24–26]

FUTURE DIRECTIONS AND OPPORTUNITIES

This thesis has shown several automated quantification alternatives to visual assessment of perfusion in various imaging modalities. Although the potential clinical value of these automated scores compared to the manual counterparts was demonstrated, further studies are warranted to ascertain the robustness of the methods. Validation studies, i.e., the agreement of these scores with the consensus of expert observers' assessment, should be performed to supplement the findings. In addition, the effect of variation in imaging modality vendors, scan quality, and patient population on the scoring result should be analyzed to measure the generalizability of the method. Perfusion quantification methods outlined in this thesis may especially be advantageous in clinical trials or registries of reperfusion treatment. In clinical trial, for example, an automated quantitative perfusion score can be employed as a surrogate endpoint to measure treatment success.[27] In a typical clinical registry with a large dataset, automated perfusion assessment potentially allows for robust and rapid assessment, even for difficult cases.

In general, the automation of medical image analysis is progressing rapidly alongside the increased computing power and the abundance of data. This trend directly ushered the deep learning era in computer-aided diagnosis fields.[28] Due to the demonstrated versatility and performance, deep learning may become, if not already is, the state-of-the-art technology in automating medical image

analysis including perfusion assessment. Therefore, the following factors that improve deep learning overall performance in the future may support the advancement of such computer-aided perfusion assessment into clinical practice:

- Advancement in computational architecture. More efficient and powerful processing units allow the development of larger and more sophisticated deep learning models. Historical trend on state-of-the-art models suggests that model size often corresponds with performance.[29]

- Increasing collective effort of standardizing imaging data across different trials. This may substantially increase the number of high-quality imaging data available that can potentially be used for training deep learning models to solve clinical problems.

- Advancements in imaging modalities and post-processing techniques. The progress in this domain may improve the quality of medical images, which is beneficial for both rule-based and data-driven approaches. For example, less noisy medical images simplify post-processing steps in the rule-based system. For a data-driven approach, better image quality often translates to the better overall performance of the predictive model.

- Overcoming the shortage of annotated data. Despite the influx of imaging data, deep supervised learning is unusable without annotation. Rigorous data annotation is unfortunately expensive and time-consuming. This is the main bottleneck in many medical image segmentation studies using, but not limited to, deep learning solutions. There have been many efforts to overcome this bottleneck. One approach is to develop more data-efficient models. Some studies eased the burden of annotation by automatically generating the annotation throughout the training process with a "human-in-the-loop" framework.[30,31] Future progresses related to the efficiency improvement of the annotation digestion tract in supervised learning frameworks may reduce the reliance to annotated data. Another approach to tackle the scarcity of annotated data is the wide adoption of open data policy, for example by providing indexed and curated imaging datasets. There have been

distributed endeavors to collect annotated, anonymized medical images and to make them publicly available, including several segmentation challenges.[32–37] Maintaining and expanding these databases will help accelerate AI-powered medical image segmentation studies across domains.

- The emergence of new AI technologies:
    - Advancements of explainable models. For instance, the introduction of a new deep learning architecture: transformer architecture.[38] This new architecture can process sequential data more efficiently by utilizing the attention mechanism while overcoming recurrent neural network limitations. In short, rather than committing all information into memory, the transformer includes context analysis to determine which information is the most significant and deserves more attention. In the context of medical image segmentation, this approach provides an attention map. This map can be overlaid with the input scan, thus indicating which region in the scan contributes the most to the outcome. A recent study, for example, successfully developed a transformer model to grade diabetic retinopathy.[39] Debunking the black-box stigma of deep learning may increase its adoptability by clinicians with apprehension toward unexplainable technology.
    - Progressing towards unsupervised learning. As we discussed, decreasing the reliance on annotated data is of key importance. Reinforcement learning is one of the machine learning branches where the amount of annotated data becomes less important.[40] With this learning type, image segmentation is perceived as a sequential problem in which the model tries to predict the trajectory of the segmentation. The model gets rewarded when it finds the correct path and gets penalized otherwise. A recent study on left ventricle segmentation showed the efficacy of deep

reinforcement learning by using 10% of the annotated data with comparable results to the fully supervised method.[41]

Although the rule-based approach is seemingly pale in comparison with the data-driven approach, it is still valuable to solve simple medical image processing challenges in a perfusion assessment automation pipeline, e.g., image noise removal or motion correction. In this function, rule-based approaches can be coupled with deep learning models as pre-processing modules of raw data. These pre-processing modules may increase the quality and robustness of the input data, which may eventually improve the model performance. Such hybrid systems are continued to be used in some AI-powered medical applications.[42,43] Further research in finding the best configuration between both approaches may build a foundation for future state-of-the-art automated perfusion assessment systems.

CONCLUSION

In this thesis, we introduce quantitative assessments of brain perfusion and collaterals on DSA and CTP, respectively, and a quantitative model of fluorescence imaging to identify perfusion deficiency after esophagectomy. We also show limitations of the existing quantitative assessment of myocardial perfusion on coronary angiograms. We demonstrate that both quantitative perfusion and CTP-based collateral scores have significant associations with functional outcome. In the gastric model study, quantitative parameters derived from fluorescence dynamics are predictive of impaired perfusion. Additionally, the technical assessment of QuBE revealed that its image pre-processing algorithm might be inappropriate and ultimately lead to inaccurate perfusion reading. This thesis highlights the feasibility of automated and quantitative perfusion scores as an alternative to their corresponding visual grading methods. It also increases our understanding of the inner working of computer-assisted perfusion quantification.

REFERENCES

1. Blomley MJK, Coulden R, Bufkin C, Lipton MJ, Dawson P. Contrast Bolus Dynamic Computed-Tomography for the Measurement of Solid-Organ Perfusion. *Invest Radiol*. 1993;28(5):S72-S77. doi:10.1097/00004424-199311001-00023

2. Yoo AJ, Simonsen CZ, Prabhakaran S, et al. Refining Angiographic Biomarkers of Revascularization: Improving Outcome Prediction After Intra-arterial Therapy. *Stroke*. 2013;44(9):2509-2512. doi:10.1161/STROKEAHA.113.001990

3. Smith J, Dove JT, Jacobs AK, et al. ACC/AHA guidelines for percutaneous coronary intervention (revision of the 1993 PTCA guidelines) - Executive summary: A report of the American College of Cardiology/American Heart Association Task Force on Practice Guidelines (Committee to Revise the 1993 guidelines for percutaneous transluminal coronary angioplasty) endorsed by the Society for Cardiac Angiography and Interventions. *Circulation*. 2001;103(24):3019-3041. doi:10.1161/01.cir.103.24.3019

4. Jansen SM, de Bruin DM, van Berge Henegouwen MI, et al. Quantitative change of perfusion in gastric tube reconstruction by sidestream dark field microscopy (SDF) after esophagectomy, a prospective in-vivo cohort study. *Eur J Surg Oncol*. 2021;47(5):1034-1041. doi:10.1016/j.ejso.2020.09.006

5. Marks MP, Lansberg MG, Mlynash M, et al. Angiographic outcome of endovascular stroke therapy correlated with MR findings, infarct growth, and clinical outcome in the DEFUSE 2 trial. *Int J Stroke*. 2014;9(7):860-865. doi:10.1111/ijs.12271

6. Tonekaboni S, Joshi S, McCradden MD, Goldenberg A. What Clinicians Want: Contextualizing Explainable Machine Learning for Clinical End Use. 2019;(Ml):1-21. doi:10.48550/arXiv.1905.05134

7. Zaidat OO, Yoo AJ, Khatri P, et al. Recommendations on Angiographic Revascularization Grading Standards for Acute Ischemic Stroke: A Consensus Statement. *Stroke*. 2013;44(9):2650-2663. doi:10.1161/STROKEAHA.113.001972

8. Rava RA, Mokin M, Snyder K V., et al. Performance of angiographic parametric imaging in locating infarct core in large vessel occlusion acute ischemic stroke patients. *J Med Imaging*. 2020;7(01):1. doi:10.1117/1.jmi.7.1.016001

9. Kagadis GC, Tsantis S, Gatos I, Spiliopoulos S, Katsanos K, Karnabatidis D. 2D perfusion DSA with an open-source, semi-automated, color-coded software for the quantification of foot perfusion following infrapopliteal angioplasty: a feasibility study. *Eur Radiol Exp*. 2020;4(1). doi:10.1186/s41747-020-00176-z

10. Lee HJ, Hong JS, Lin CJ, et al. Automatic flow analysis of digital subtraction angiography using independent component analysis in patients with carotid stenosis. *PLoS One*. 2017;12(9):1-13. doi:10.1371/journal.pone.0185330

11. Su R, Cornelissen SAP, van der Sluijs M, et al. autoTICI: Automatic Brain Tissue Reperfusion Scoring on 2D DSA Images of Acute Ischemic Stroke Patients. *IEEE Trans Med Imaging*. 2021;40(9):2380-2391. doi:10.1109/TMI.2021.3077113

12. Nielsen M, Waldmann M, Frölich AM, et al. Deep learning-based automated thrombolysis in cerebral infarction scoring: A timely proof-of-principle study. *Stroke*. 2021;52(11):3497-3504. doi:10.1161/STROKEAHA.120.033807

13. Monti CB, Codari M, van Assen M, De Cecco CN, Vliegenthart R. Machine Learning and Deep Neural Networks Applications in Computed Tomography for Coronary Artery Disease and Myocardial Perfusion. *J Thorac Imaging*. 2020;35:S58-S65. doi:10.1097/RTI.0000000000000490

14. Guo Y, Hormel TT, Xiong H, et al. Development and validation of a deep learning algorithm for distinguishing the nonperfusion area from signal reduction artifacts on OCT angiography. *Biomed Opt Express*. 2019;10(7):3257. doi:10.1364/boe.10.003257

15. Nielsen A, Hansen MB, Tietze A, Mouridsen K. Prediction of tissue outcome and assessment of treatment effect in acute ischemic stroke using deep learning. *Stroke*. 2018;49(6):1394-1401. doi:10.1161/STROKEAHA.117.019740

16. Lo J, Heisler M, Vanzan V, et al. Microvasculature segmentation and intercapillary area quantification of the deep vascular complex using transfer

learning. *Transl Vis Sci Technol*. 2020;9(2):1-12. doi:10.1167/tvst.9.2.38

17. Liebeskind DS, Bracard S, Guillemin F, et al. eTICI reperfusion: defining success in endovascular stroke therapy. *J Neurointerv Surg*. 2019;11:433-438. doi:10.1136/neurintsurg-2018-014127

18. Lecouffe NE, Kappelhof M, Treurniet KM, et al. 2B, 2C, or 3: What Should Be the Angiographic Target for Endovascular Treatment in Ischemic Stroke? *Stroke*. 2020;51:1790-1796. doi:10.1161/STROKEAHA.119.028891

19. Higashida RT, Furlan AJ. Trial Design and Reporting Standards for Intra-Arterial Cerebral Thrombolysis for Acute Ischemic Stroke. *Stroke*. 2003;34(8):e109-e137. doi:10.1161/01.STR.0000082721.62796.09

20. Goyal M, Fargen KM, Turk AS, et al. 2C or not 2C: defining an improved revascularization grading scale and the need for standardization of angiography outcomes in stroke trials. *J Neurointerv Surg*. 2014;6(2):83-86. doi:10.1136/neurintsurg-2013-010665

21. Wilcox AJ. On precision. *Epidemiology*. 2004;15(1):1. doi:10.1097/01.ede.0000101026.08873.14

22. Olivot JM, Mlynash M, Thijs VN, et al. Optimal Tmax Threshold for Predicting Penumbral Tissue in Acute Stroke. *Stroke*. 2009;40(2):469-475. doi:10.1161/STROKEAHA.108.526954

23. Wouters A, Christensen S, Straka M, et al. A comparison of relative time to peak and tmax for mismatch-based patient selection. *Front Neurol*. 2017;8:1-7. doi:10.3389/fneur.2017.00539

24. Peretz S, Orion D, Last D, et al. Incorporation of relative cerebral blood flow into CT perfusion maps reduces false “at risk” penumbra. *J Neurointerv Surg*. 2018;10(7):659-665. doi:10.1136/neurintsurg-2017-013268

25. Wang CM, Chang YM, Sung PS, Chen CH. Hypoperfusion index ratio as a surrogate of collateral scoring on ct angiogram in large vessel stroke. *J Clin Med*. 2021;10(6):1-10. doi:10.3390/jcm10061296

26. Fainardi E, Borrelli M, Saletti A, et al. CT perfusion mapping of hemodynamic

disturbances associated to acute spontaneous intracerebral hemorrhage. *Neuroradiology*. 2008;50(8):729-740. doi:10.1007/s00234-008-0402-x

27. Vogelzang M, Vlaar PJ, Svilaas T, Amo D, Nijsten MWN, Zijlstra F. Computer-assisted myocardial blush quantification after percutaneous coronary angioplasty for acute myocardial infarction: A substudy from the TAPAS trial. *Eur Heart J*. 2009;30(5):594-599. doi:10.1093/eurheartj/ehn542

28. Chan HP, Hadjiiski LM, Samala RK. Computer-aided diagnosis in the era of deep learning. In: *Medical Physics*. Vol 47. John Wiley and Sons Ltd; 2020:e218-e227. doi:10.1002/mp.13764

29. Hestness J, Narang S, Ardalani N, et al. Deep Learning Scaling is Predictable, Empirically. *arXiv*. 2017. doi:10.48550/arXiv.1712.00409

30. Lu Y, Zheng K, Li W, et al. Contour Transformer Network for One-Shot Segmentation of Anatomical Structures. *IEEE Trans Med Imaging*. 2021;40(10):2672-2684. doi:10.1109/TMI.2020.3043375

31. Lutnick B, Ginley B, Govind D, et al. An integrated iterative annotation technique for easing neural network training in medical image analysis. *Nat Mach Intell*. 2020;1(2):112-119. doi:10.1038/s42256-019-0018-3.An

32. van Ginneken B, Stegmann MB, Loog M. Segmentation of anatomical structures in chest radiographs using supervised methods: A comparative study on a public database. *Med Image Anal*. 2006;10(1):19-40. doi:10.1016/j.media.2005.02.002

33. Reeves AP, Biancardi AM, Yankelevitz D, et al. A public image database to support research in computer aided diagnosis. *Proc 31st Annu Int Conf IEEE Eng Med Biol Soc Eng Futur Biomed EMBC*. 2009:3715-3718. doi:10.1109/IEMBS.2009.5334807

34. Yan K, Wang X, Lu L, Summers RM. DeepLesion: automated mining of large-scale lesion annotations and universal lesion detection with deep learning. *J Med Imaging*. 2018;5(03):1. doi:10.1117/1.jmi.5.3.036501

35. Menze BH, Jakab A, Bauer S, et al. The Multimodal Brain Tumor Image Segmentation Benchmark (BRATS). *IEEE Trans Med Imaging*. 2015;34(10):1993-

2024. doi:10.1109/TMI.2014.2377694

36. Bakas S, Akbari H, Sotiras A, et al. Advancing The Cancer Genome Atlas glioma MRI collections with expert segmentation labels and radiomic features. *Sci Data*. 2017;4:1-13. doi:10.1038/sdata.2017.117

37. Bakas S, Reyes M, Jakab A, et al. Identifying the Best Machine Learning Algorithms for Brain Tumor Segmentation, Progression Assessment, and Overall Survival Prediction in the BRATS Challenge. *arXiv*. 2018. doi:10.48550/arXiv.1811.02629

38. Vaswani A, Shazeer N, Parmar N, et al. Attention Is All You Need. In: *31st of International Conference of Neural Information Processing Systems*. Curran Associates Inc.; 2017:6000-6010. doi:10.1109/2943.974352

39. Wu J, Hu R, Xiao Z, Chen J, Liu J. Vision Transformer-based recognition of diabetic retinopathy grade. *Med Phys*. 2021;48(12):7850-7863. doi:10.1002/mp.15312

40. Lillicrap TP, Hunt JJ, Pritzel A, et al. Continuous control with deep reinforcement learning. *4th Int Conf Learn Represent ICLR 2016 - Conf Track Proc*. Published online 2016.

41. Xiong J, Po LM, Cheung KW, et al. Edge-sensitive left ventricle segmentation using deep reinforcement learning. *Sensors*. 2021;21(7):1-19. doi:10.3390/s21072375

42. Fasen BACM, Berendsen RCM, Kwee RM. Artificial intelligence software for diagnosing intracranial arterial occlusion in patients with acute ischemic stroke. *Neuroradiology*. 2022;64(8):1579–83. doi:10.1007/s00234-022-02912-1

43. Barragán-Montero A, Javaid U, Valdés G, Nguyen D, Desbordes P, Macq B, et al. Artificial intelligence and machine learning for medical imaging: A technology review. *Phys Medica*. 2021;83(May):242–56. doi: 10.1016/j.ejmp.2021.04.016

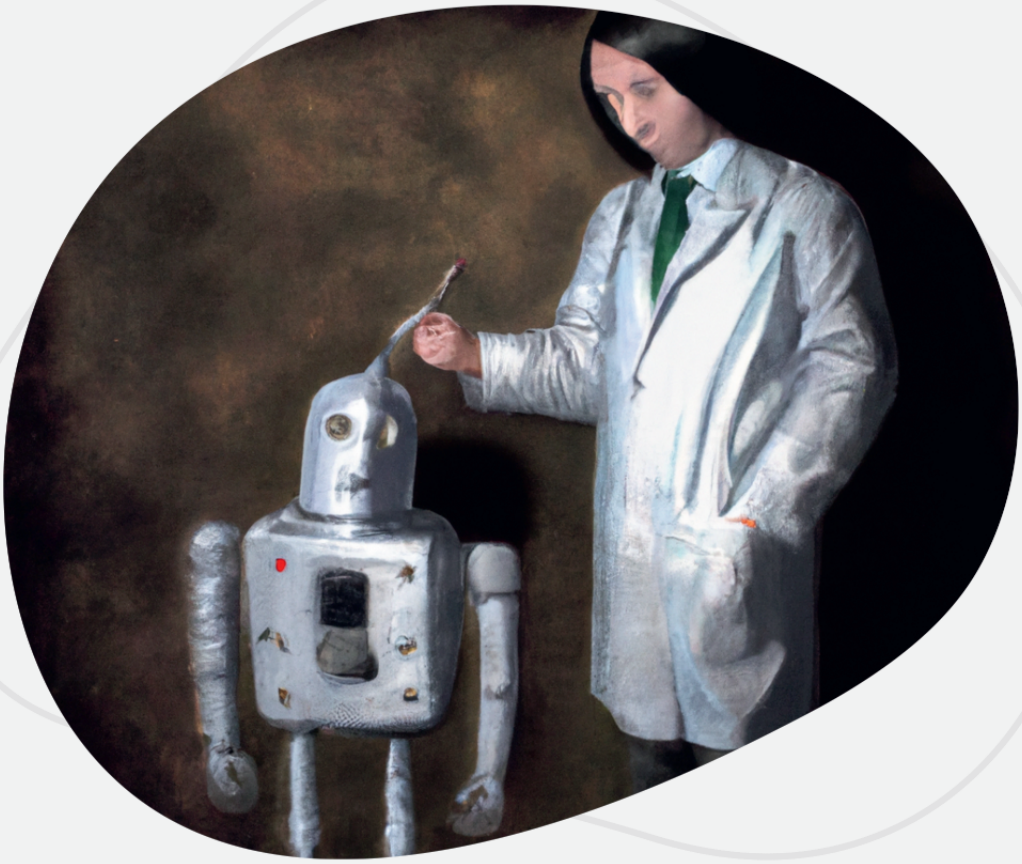

DALL·E 2: "A painting of a doctor in a white coat and a robot on a dark background, by Da Vinci"

APPENDICES

SUMMARY

Perfusion assessment can be used to determine disease severity, provide intraoperative guidance, indicate treatment success, and predict functional outcome. Physicians commonly visually evaluate perfusion on medical images according to a perfusion grading scale which often is ordinal and in low resolution. This crude classification may not precisely measure the actual tissue perfusion. Moreover, visual assessment is very subjective and prone to observer bias. Therefore, automating and quantifying this assessment is necessary to decrease such bias and increase the robustness and accuracy of the assessment. The aim of this thesis is to analyze medical images and their corresponding perfusion grading to form a base for new automated and quantitative alternatives to the qualitative perfusion scores.

One of the emerging technologies that allow intraoperative evaluation of tissue perfusion is fluorescence imaging. Quantitative assessment of fluorescent dynamics may be valuable in detecting impaired perfusion. In **chapter 2**, we developed a perfusion model of the gastric tube after esophagectomy to analyze fluorescent dynamics in relation to impaired perfusion. A lumped-parameter model was used to represent the fundus and the distal regions of the gastric tube. We derived and evaluated a quantitative parameter from fluorescent dynamics, relative time-to-threshold (RTT), as a predictor of relative remaining flow (RRF). RTT of the fundus regions was expressed relative to that in the distal regions. RRF expresses the flow to each ROI post-ligation relative to pre-ligation. We evaluated thresholds for RTT ranging from 20% to 50% of the maximum intensity of the distal regions. Additionally, the effects of model parameters such as vascular conductance and volume on the RTT-RRF relation were evaluated over a large variation of parameter combinations. Our model showed a strong and complex dependency of the RTT-RRF relation on collateral conductance, large vessel conductance, and vascular volume. We demonstrated that vessel conductance positively related to RTT and RRF. Furthermore, the absolute volume of a vessel compartment was inconsequential to the RTT-RRF relation, while the volume ratio of the arterial compartment and venous compartment affected RTT-RRF for high flows. We found that RTT is predictive of flow deterioration. The threshold of 20% was the best estimate of reduced perfusion in the anastomotic

ROIs. As this study was based on hypothetical data, the validity of the presented model remains a limitation. Further research using actual fluorescent imaging data is required to establish the clinical value of RTT as a predictor of perfusion deficiency.

In the heart, the Myocardial Blush Grade (MBG) is a commonly used visual grading system for myocardial perfusion assessment. In **chapter 3**, we evaluated an alternative method to this scale: the quantitative blush evaluator (QuBE). QuBE is a computer-assisted method that quantifies myocardial perfusion based on coronary angiography images. We have identified insufficiencies in the pre-processing methods of QuBE and proposed improvements through enhanced image analysis. We used coronary angiography images of 117 patients enrolled in the HEBE trial, in which the effects of intracoronary infusion of bone marrow mononuclear cells after primary percutaneous coronary intervention were evaluated. Within this patient population, we demonstrated that there was no significant association between MBG and QuBE scores. Furthermore, we found through qualitative assessment that the median filter that was used by QuBE to remove large structure related noise on the images was not sufficient. Various median filters and cardiac motion correction methods were evaluated but proved to be unable to improve the association between MBG and QuBE significantly. It was concluded that further improvements on QuBE are required to overcome such limitations in order for this score to become the standard for myocardial perfusion assessment.

In **chapter 4**, we developed a semi-automated quantitative brain perfusion assessment for acute ischemic stroke patients as an alternative to the visual grading of perfusion using the treatment in cerebral ischemia (TICI) scale. We included patients with intracranial proximal large vessel occlusion with complete DSA runs in lateral and anteroposterior views. The so-called quantified TICI scale (qTICI) was developed using semantic segmentation techniques, including vessel removal and perfusion segmentation on a maximum intensity projection image. The target downstream territory was delineated by expert observers and was the only user input in this process. qTICI was defined as the reperfused area divided by the total target downstream territory. After evaluating qTICI using patients from the MR CLEAN Registry, we showed that qTICI is significantly associated

with the expanded TICI (eTICI) score and has a comparable discriminatory capacity of functional outcome. The results suggest that qTICI can be used as an alternative to the visual eTICI score during treatment. Moreover, qTICI can also be used to provide perfusion assessment in clinical trials or registries as a robust and objective cerebral perfusion grading across different patient populations.

Ischemic tissue can be retrogradely perfused by collaterals. Collaterals may supply blood flow to tissue when the direct flow is obstructed and potentially diminish infarct progression. In **chapter 5**, we developed a cerebral collateral score based on multiple CT perfusion parameters (CTP-CS). We established collateral score candidates by first selecting moderately hypoperfused tissue, presumably collateral-supplied tissue, as determined by the time-to-maximum of the residue function (Tmax) value. Subsequently, we created a mask to cover tissue with Tmax values within various ranges. The mask included the contralateral side which was acquired by mirroring the ipsilateral mask using the midline. The total tissue volume covered by the mask was calculated. Pixel-wise cerebral blood volume (CBV) and their average per hemisphere side were calculated. Relative CBV was defined as the average of CBV in the ipsilateral side divided by the average of CBV in the contralateral side. We found that the mean relative CBV in the area with Tmax 6 to 10 seconds is indicative of collateral capacity and significantly associated with both CTA collateral score and functional outcome. Furthermore, a multivariable prognostic model with CTP-CS outperformed other prognostic models, with and without CTA collateral score, although the differences were not statistically significant.

Finally, the main findings were further discussed in **chapter 6**. We provided a future outlook with an emphasis on deep learning and hybrid systems, which combine rule-based and data-driven approaches as the potential state-of-the-art technology towards fully automated quantitative perfusion assessment.

NEDERLANDSE SAMENVATTING

Perfusiebeoordeling kan gebruikt worden voor het vaststellen van de ernst van de aandoening, het voorzien van intra-operatieve begeleiding, de bepaling van het behandelsucces en voor het voorspellen van de functionele uitkomst. Artsen evalueren de perfusie gewoonlijk door middel van visuele inspectie van medische beeldvorming, waarbij vaak een ordinale beoordelingsschaal met een lage resolutie gebruikt wordt. Deze grove classificatie geeft mogelijk geen nauwkeurig beeld van de daadwerkelijke weefselperfusie. Daarnaast is visuele beoordeling erg subjectief en gevoelig voor waarnemersbias. Het is daarom noodzakelijk om perfusiebeoordeling te automatiseren en kwantificeren om bias te verminderen en robuustheid en betrouwbaarheid te verhogen. Het doel van dit proefschrift is om medische beeldvorming en de daarbij horende perfusiebeoordeling te analyseren om een basis te leggen voor nieuwe geautomatiseerde en kwantitatieve alternatieven voor huidige kwalitatieve perfusiebeoordelingen.

Een van de opkomende technologieën die intra-operatieve evaluatie van weefselperfusie mogelijk maakt is fluorescente beeldvorming. Kwantitatieve beoordeling van fluorescente dynamica is mogelijk waardevol voor het detecteren van verminderde perfusie. In **hoofdstuk 2** ontwikkelden we een perfusiemodel van de buismaag na slokdarmresectie, om fluorescente dynamica te analyseren in relatie tot verminderde perfusie. Een model op basis van vaste elementen is gebruikt om de fundus en de distale gebieden van de maagbuis weer te geven. We hebben een kwantitatieve parameter van de fluorescente dynamiek, de relatieve tijd-tot-drempelwaarde (RTT), afgeleid en geëvalueerd als een voorspeller voor de relatieve resterende stroming (RRF). De RTT van de fundus is relatief bepaald ten opzichte van de distale gebieden. De RRF drukt de post-ligatie stroming naar de gebieden van interesse relatief uit ten opzichte van de pre-ligatie situatie. We evalueerden drempelwaarden voor RTT variërend tussen 20% en 50% van de maximale intensiteit van de distale regio's. Aanvullend hebben we geëvalueerd wat de effecten zijn van variaties in model-parameters zoals vasculaire geleiding en volume op de RTT-RRF relatie. Ons model liet zien dat de RTT-RRF relatie een sterke en complexe afhankelijkheid heeft van de collaterale geleiding, grote vaten geleiding en het vasculaire volume. We demonstreerden dat vaatgeleiding positief gerelateerd is aan RTT en

RRF. Bovendien was het absolute volume van een vatcompartiment niet van invloed op de RTT-RRF-relatie, terwijl de volumeverhouding van het arteriële en het veneuze compartiment de RTT-RRF beïnvloedde voor hoge stromingen. We ontdekten dat RTT voorspellend is voor verslechtering van de bloedstroming. De drempel van 20% gaf de beste schatting van verminderde perfusie in de gebieden van anastomose. De validiteit van het gepresenteerde model is mogelijk beperkt, aangezien deze studie is gebaseerd op hypothetische data. Aanvullend onderzoek met behulp van werkelijke fluorescerende beeldvormingsgegevens is noodzakelijk om de klinische waarde van RTT als voorspeller van perfusiedeficiëntie vast te stellen.

In het hart is de Myocardial Blush Grade (MBG) een veelgebruikt visueel graderingssysteem voor de beoordeling van de myocardperfusie. In **hoofdstuk 3** evalueerden we een alternatieve methode voor deze schaal: de Quantitative Blush Evaluator (QuBE). QuBE is een computerondersteunde methode voor de kwantificatie van de myocardperfusie gebaseerd op coronaire angiografiebeelden. We hebben tekortkomingen in de voorbereidende methoden van QuBE geïdentificeerd en verbeteringen voorgesteld door middel van verbeterde beeldanalyse. We gebruikten coronaire angiografiebeelden van 117 patiënten die deelnamen aan de HEBE-studie, waarin de effecten van intracoronaire infusie van mononucleaire beenmergcellen na primaire percutane coronaire interventie werden geëvalueerd. Binnen deze patiëntenpopulatie hebben we aangetoond dat er geen significant verband was tussen MBG- en QuBE-scores. Daarnaast ontdekten we door middel van kwalitatieve beoordeling dat het mediaanfilter dat door QuBE werd gebruikt om ruis van grote structuren te verwijderen niet voldoende werkt. Verschillende mediaanfilters en correctiemethoden voor cardiale bewegingen werden geëvalueerd, maar bleken niet in staat om de associatie tussen MBG en QuBE significant te verbeteren. Verdere verbeteringen aan QuBE zijn nodig zijn om dergelijke beperkingen te overkomen, voordat deze score de standaard kan worden voor de beoordeling van myocardperfusie.

In **hoofdstuk 4** hebben we een semi-automatische kwantitatieve bepaling van de hersenperfusie ontwikkeld voor patiënten met een acute ischemische beroerte, als alternatief voor de visuele beoordeling van perfusie met behulp van de Treatment In Cerebral Ischemia (TICI)-schaal. We includeerden patiënten met

intracraniële proximale occlusies van grote vaten met volledige digitale substractie-angiografie beeldvorming (DSA) in laterale en anteroposterieure richtingen. De zogenaamde gekwantificeerde TICI-schaal (qTICI) is ontwikkeld met behulp van semantische segmentatietechnieken, waaronder verwijdering van bloedvaten en perfusiesegmentatie op maximale intensiteit projecties. Het stroomafwaartse doelgebied werd omlijnd door expert waarnemers en was de enige benodigde gebruikersinput in dit proces. qTICI werd gedefinieerd als het gereperfundeerde gebied gedeeld door het totale stroomafwaartse doelgebied. Na evaluatie van qTICI voor patiënten uit de MR CLEAN Registry, toonden we aan dat qTICI significant geassocieerd is met de uitgebreide TICI-score (eTICI) en een vergelijkbaar discriminerend vermogen heeft voor functionele uitkomst. De resultaten suggereren dat qTICI kan worden gebruikt als alternatief voor de visueel eTICI-score tijdens de behandeling. Bovendien kan qTICI worden gebruikt om perfusie te beoordelen in klinische onderzoeken of registers als een robuuste en objectieve cerebrale perfusie gradatie voor verschillende patiëntenpopulaties.

Ischemische weefsels kunnen retrograad worden geperfuseerd door collateralen. Collateralen kunnen de bloedstroom naar het weefsel leveren wanneer de directe stroom wordt belemmerd, waardoor mogelijk de progressie van het infarct afneemt. In **hoofdstuk 5** hebben we een cerebrale collaterale score ontwikkeld op basis van meerdere CT-perfusieparameters (CTP-CS). We hebben kandidaten voor collaterale scores vastgesteld door eerst matig onder-geperfundeerde weefsels te selecteren, vermoedelijk weefsels gevoed vanuit collateralen, bepaald door middel van de tijd-tot-maximale restfunctie (Tmax) waarde. Vervolgens hebben we een masker gemaakt voor weefsels met Tmax-waarden binnen een bepaald bereik. Het masker omvatte de contralaterale zijde die werd verkregen door het ipsilaterale masker te spiegelen met behulp van de middellijn. Het totale weefselvolume bedekt door het masker werd berekend. Het pixel-gewijze cerebraal bloedvolume (CBV) en gemiddelden per hersenhelft werden berekend. Relatieve CBV werd gedefinieerd als het gemiddelde van CBV in de ipsilaterale zijde gedeeld door het gemiddelde van CBV in de contralaterale zijde. We ontdekten dat de gemiddelde relatieve CBV in het gebied met Tmax 6 tot 10 seconden indicatief is voor de collaterale capaciteit en significant geassocieerd is met zowel de CTA collaterale score als de functionele uitkomst. Daarnaast

presteerde een multivariabel prognostisch model met CTP-CS beter dan andere prognostische modellen, met en zonder CTA collaterale score, hoewel de verschillen niet statistisch significant waren.

Tot slot werden de belangrijkste bevindingen verder besproken in **hoofdstuk 6**. We hebben een toekomstperspectief gegeven met de nadruk op deep learning en hybride systemen, die regels-gebaseerde en datagedreven benaderingen combineren als de potentiële state-of-the-art technologie voor volledig geautomatiseerde kwantitatieve perfusiebeoordeling.

RINGKASAN

Pengukuran perfusi dapat digunakan untuk mengestimasi tingkat keparahan penyakit, memandu operasi, mengindikasikan keberhasilan pengobatan, dan memprediksi hasil akhir fungsional paska operasi. Dokter, pada umumnya, mengukur perfusi melalui pengamatan citra medis secara visual berdasarkan skala penilaian perfusi yang biasanya ordinal dan memiliki tingkat resolusi yang rendah. Klasifikasi yang kasar ini berpotensi menghasilkan pengukuran perfusi yang tidak presisi. Selain itu, penilaian secara visual sangat subjektif dan rentan akan bias observasi. Karena itu, otomatisasi dan kuantifikasi pengukuran perfusi diperlukan untuk mengurangi bias tersebut serta meningkatkan konsistensi dan akurasi pengukuran perfusi. Tujuan dari tesis ini adalah untuk menganalisa citra medis dan penilaian perfusi yang sesuai untuk membentuk landasan dalam mengembangkan kuantifikasi perfusi secara otomatis.

Salah satu teknologi baru dalam pengukuran perfusi jaringan intraoperatif adalah pencitraan fluorosensi. Pengukuran kuantitatif dinamika sinyal fluoresen dapat digunakan dalam mendeteksi gangguan perfusi. Di **bab 2**, kami mengembangkan model perfusi dari tabung lambung yang direkonstruksi paska esofagektomi untuk menganalisa sinyal fluoresen dan hubungannya dengan gangguan perfusi. Model dengan parameter tunggal digunakan untuk merepresentasikan area fundus dan area distal dari tabung lambung. Parameter kuantitatif, waktu tempuh relatif ke batas atas (RTT), diperoleh dan dievaluasi dari sinyal fluoresen sebagai prediktor dari sisa aliran relatif (RRF). RTT dari area fundus adalah waktu tempuh sinyal ke batas atas area fundus dibandingkan dengan waktu tempuh sinyal ke batas atas area distal. RRF adalah aliran fluoresen di area tertentu di tabung lambung paska ligasi dibandingkan dengan aliran tersebut sebelum ligasi. Kami mengevaluasi beberapa batas atas untuk RTT dimulai dari 20% intensitas fluoresen maksimal dari area distal hingga 50%. Selain itu, efek dari parameter model seperti konduktansi dan volume vaskular dievaluasi dalam banyak variasi dari kombinasi parameter-parameter model untuk menyelidiki hubungan parameter tersebut dengan RTT dan RFF. Model kami menunjukkan adanya hubungan dependensi yang kuat dan kompleks antara RTT-RFF dengan konduktansi kolateral, konduktansi pembuluh darah besar, dan volume vaskular. Kami memperlihatkan bahwa konduktansi pembuluh darah memiliki hubungan

positif dengan RTT dan RRF. Selain itu, volume absolut dari kompartemen pembuluh darah tidak mempengaruhi hubungan RTT dan RRF. Rasio volume dari kompartemen arteri dan vena mempengaruhi RTT dan RRF untuk aliran yang tinggi. Kami menemukan bahwa RTT dapat memprediksi penurunan aliran. Batas atas 20% menghasilkan estimasi penurunan perfusi terbaik di area anastomosis. Karena studi ini berdasarkan data hipotetikal, validitas model dianggap sebagai limitasi studi. Penelitian lanjut menggunakan data aktual pencitraan fluoresensi dibutuhkan untuk membuktikan nilai klinis RTT sebagai prediktor penurunan perfusi.

Di jantung, skala pengukuran perfusi miokardium (MBG) merupakan sistem skala visual yang umum digunakan dalam mengukur perfusi miokardium. Di **bab 3**, kami mengevaluasi metode alternatif dari skala ini: evaluator kuantitatif perfusi (QuBE). QuBE adalah metode dengan bantuan komputer yang dapat mengkuantifikasi perfusi miokardium berdasarkan citra angiografi koroner. Kami berhasil mengidentifikasi kekurangan dari metode pra-pengolahan citra QuBE dan merekomendasikan koreksi melalui analisis perbaikan citra. Kami menggunakan citra angiografi koroner dari 117 pasien yang terdaftar di uji coba klinis HEBE, di mana efek dari infusi intrakoroner sel mononuklear sum-sum tulang paska intervensi koroner perkutan primer dievaluasi. Dalam populasi pasien tersebut, kami menunjukkan bahwa tidak terdapat asosiasi signifikan antara MBG dan skor QuBE. Kami menyimpulkan bahwa diperlukan perbaikan lebih lanjut pada QuBE sebelum QuBE bisa menjadi standar pengukuran perfusi miokardium.

Di **bab 4**, kami mengembangkan metode kuantitatif pengukuran perfusi otak semi-otomatis untuk pasien stroke iskemik akut sebagai alternatif dari penilaian perfusi secara visual menggunakan skala pengobatan iskemia serebral (TICI). Kami melibatkan pasien dengan oklusi pembuluh darah besar proksimal intrakranial yang memiliki citra DSA lateral dan anteroposterior. Skala TICI kuantitatif (qTICI) dikembangkan menggunakan teknik segmentasi semantik yang meliputi subtraksi pembuluh darah dan segmentasi perfusi pada citra proyeksi intensitas maksimum. Batas area hilir target diindikasikan oleh pengamat ahli dan merupakan satu-satunya input manual dalam proses ini. qTICI didefinisikan sebagai area reperfusi dibagi dengan total area hilir target. Setelah mengevaluasi

qTICI menggunakan pasien dari MR CLEAN Registry, kami menunjukkan bahwa qTICI berasosiasi signifikan dengan skor TICI ekspansif dan memiliki kapasitas diskriminatif hasil akhir fungsional yang sebanding dengan skor TICI ekspansif. Hasil ini menunjukkan bahwa qTICI dapat digunakan sebagai alternatif untuk skor visual TICI ekspansif di dalam masa pengobatan. Selain itu, qTICI juga dapat digunakan dalam uji klinis atau registri data sebagai metode pengukuran perfusi otak yang konsisten dan objektif lintas populasi pasien.

Jaringan iskemik dapat mengalami perfusi mundur dari pembuluh darah kolateral. Pembuluh darah kolateral dapat menyalurkan aliran darah ke jaringan ketika aliran utama terhambat sehingga perkembangan infark dapat dikurangi. Di **bab 5**, kami mengembangkan skor kolateral otak berdasarkan sejumlah parameter CT perfusi (CTP-CS). Kami menetapkan kandidat skor kolateral dengan pertama-tama menyeleksi jaringan hipoperfusi sedang, dengan asumsi bahwa jaringan ini disuplai oleh kolateral, sebagaimana terindikasikan oleh nilai Tmax di citra CT perfusi. Selanjutnya, kami membuat citra layar berdasarkan berbagai rentang nilai Tmax. Citra layar ini meliputi sisi kontralateral yang diperoleh dengan mencerminkan citra layar sisi ipsilateral terhadap garis tengah citra CT perfusi. Volume jaringan total yang diliputi citra layar ini dihitung. Volume darah otak (CBV) setiap pixel dan nilai rata-ratanya per belahan otak juga dihitung. CBV relatif didefinisikan sebagai rata-rata CBV di sisi ipsilateral dibagi dengan rata-rata CBV di sisi kontralateral. Kami menemukan bahwa rata-rata CBV relatif di area dengan Tmax antara 6 hingga 10 detik mengindikasikan kapasitas kolateral dan berasosiasi signfikan dengan skor kolateral CTA dan hasil akhir fungsional. Selain itu, model prognostik multivariabel dengan CTP-CS mengungguli model prognostik lain dengan dan tanpa skor kolateral CTA, walaupun perbedaannya tidak signifikan secara statistik.

Akhir kata, temuan utama didiskusikan lebih lanjut di bab 6. Prediksi pengukuran perfusi otomatis di masa depan terutama dalam hubungannya dengan *deep learning* dan sistem hybrid juga didiskusikan, di mana kombinasi pendekatan berdasarkan aturan dan data berpotensi menjadi teknologi utama menuju otomatisasi penuh pengukuran perfusi kuantitatif.

LIST OF CONTRIBUTORS AND AFFILIATIONS

MR CLEAN Registry Investigators

Executive committee: Diederik W.J. Dippel[1]; Aad van der Lugt[2]; Charles B.L.M. Majoie[3]; Yvo B.W.E.M. Roos[4]; Robert J. van Oostenbrugge[5]; Wim H. van Zwam[6]; Jelis Boiten[14]; Jan Albert Vos[8]

Study coordinators: Ivo G.H. Jansen[3]; Maxim J.H.L. Mulder[1,2]; Robert- Jan B. Goldhoorn[5,6]; Kars C.J. Compagne[2]; Manon Kappelhof[3]; Josje Brouwer[4]; Sanne J. den Hartog[1,2,40]; Wouter H. Hinsenveld[5,6]

Local principal investigators: Diederik W.J. Dippel[1]; Bob Roozenbeek[1]; Aad van der Lugt[2]; Adriaan C.G.M. van Es[2]; Charles B.L.M. Majoie[3]; Yvo B.W.E.M. Roos[4]; Bart J. Emmer[3]; Jonathan M. Coutinho[4]; Wouter J. Schonewille[7]; Jan Albert Vos[8]; Marieke J.H. Wermer[9]; Marianne A.A. van Walderveen[10]; Julie Staals[5]; Robert J. van Oostenbrugge[5]; Wim H. van Zwam[6]; Jeannette Hofmeijer[11]; Jasper M. Martens[12]; Geert J. Lycklama à Nijeholt[13]; Jelis Boiten[14]; Sebastiaan F. de Bruijn[15]; Lukas C. van Dijk[16]; H. Bart van der Worp[17]; Rob H. Lo[18]; Ewoud J. van Dijk[19]; Hieronymus D. Boogaarts[20]; J. de Vries[22]; Paul L.M. de Kort[21]; Julia van Tuijl[21]; Jo P. Peluso[26]; Puck Fransen[22]; Jan S.P. van den Berg[22]; Boudewijn A.A.M. van Hasselt[23]; Leo A.M. Aerden[24]; René J. Dallinga[25]; Maarten Uyttenboogaart[28]; Omid Eschgi[29]; Reinoud P.H. Bokkers[29]; Tobien H.C.M.L. Schreuder[30]; Roel J.J. Heijboer[31]; Koos Keizer[32]; Lonneke S.F. Yo[33]; Heleen M. den Hertog[22]; Tomas Bulut[35]; Paul J.A.M. Brouwers[34]

Imaging assessment committee: Charles B.L.M. Majoie[3] (chair); Wim H. van Zwam[6]; Aad van der Lugt[2]; Geert J. Lycklama à Nijeholt[13]; Marianne A.A. van Walderveen[10]; Marieke E.S. Sprengers[3]; Sjoerd F.M. Jenniskens[27]; René van den Berg[3]; Albert J. Yoo[38]; Ludo F.M. Beenen[3]; Alida A. Postma[6]; Stefan D. Roosendaal[3]; Bas F.W. van der Kallen[13]; Ido R. van den Wijngaard[13]; Adriaan C.G.M. van Es[2]; Bart J. Emmer[3]; Jasper M. Martens[12]; Lonneke S.F. Yo[33]; Jan Albert Vos[8]; Joost Bot[36]; Pieter-Jan van Doormaal[2]; Anton Meijer[27]; Elyas Ghariq[13]; Reinoud P.H. Bokkers[29]; Marc P. van Proosdij[37]; G. Menno Krietemeijer[33]; Jo P. Peluso[26]; Hieronymus D. Boogaarts[20]; Rob Lo[18]; Dick Gerrits[35]; Wouter Dinkelaar[2]; Auke P.A. Appelman[29]; Bas Hammer[16]; Sjoert Pegge[27]; Anouk van der Hoorn[29]; Saman Vinke[20]

Writing committee: Diederik W.J. Dippel[1] (chair); Aad van der Lugt[2]; Charles B.L.M. Majoie[3]; Yvo B.W.E.M. Roos[4]; Robert J. van Oostenbrugge[5]; Wim H. van Zwam[6]; Geert J. Lycklama à Nijeholt[13]; Jelis Boiten[14]; Jan Albert Vos[8]; Wouter J. Schonewille[7]; Jeannette Hofmeijer[11]; Jasper M. Martens[12]; H. Bart van der Worp[17]; Rob H. Lo[18]

Adverse event committee: Robert J. van Oostenbrugge[5] (chair); Jeannette Hofmeijer[11]; H. Zwenneke Flach[23]

Trial methodologist: Hester F. Lingsma[40]

Research nurses / local trial coordinators: Naziha el Ghannouti[1]; Martin Sterrenberg[1]; Wilma Pellikaan[7]; Rita Sprengers[4]; Marjan Elfrink[11]; Michelle Simons[11]; Marjolein Vossers[12]; Joke de Meris[14]; Tamara Vermeulen[14]; Annet Geerlings[19]; Gina van Vemde[22]; Tiny Simons[30]; Gert Messchendorp[28]; Nynke Nicolaij[28]; Hester Bongenaar[32]; Karin Bodde[24]; Sandra Kleijn[34]; Jasmijn Lodico[34]; Hanneke Droste[34]; Maureen Wollaert[5]; Sabrina Verheesen[5]; D. Jeurrissen[5]; Erna Bos[9]; Yvonne Drabbe[15]; Michelle Sandiman[15]; Nicoline Aaldering[11]; Berber Zweedijk[17]; Jocova Vervoort[21]; Eva Ponjee[22]; Sharon Romviel[19]; Karin Kanselaar[19]; Denn Barning[10]

PhD / Medical students: Esmee Venema[40]; Vicky Chalos[1,40]; Ralph R. Geuskens[3]; Tim van Straaten[19]; Saliha Ergezen[1]; Roger R.M. Harmsma[1]; Daan Muijres[1]; Anouk de Jong[1]; Olvert A. Berkhemer[1,3,6]; Anna M.M. Boers[3,39]; J. Huguet[3]; P.F.C. Groot[3]; Marieke A. Mens[3]; Katinka R. van Kranendonk[3]; Kilian M. Treurniet[3]; Manon L. Tolhuisen[3,39]; Heitor Alves[3]; Annick J. Weterings[3], Eleonora L.F. Kirkels[3], Eva J.H.F. Voogd[11]; Lieve M. Schupp[3]; Sabine L. Collette[28,29]; Adrien E.D. Groot[4]; Natalie E. LeCouffe[4]; Praneeta R. Konduri[39]; Haryadi Prasetya[39]; Nerea Arrarte-Terreros[39]; Lucas A. Ramos[39]

Affiliations

Department of Neurology[1], Radiology[2], Public Health[40], Erasmus MC University Medical Center;
Department of Radiology and Nuclear Medicine[3], Neurology[4], Biomedical Engineering & Physics[39], Amsterdam UMC, University of Amsterdam, Amsterdam;

Department of Neurology[5], Radiology[6], Maastricht University Medical Center and Cardiovascular Research Institute Maastricht (CARIM);
Department of Neurology[7], Radiology[8], Sint Antonius Hospital, Nieuwegein;
Department of Neurology[9], Radiology[10], Leiden University Medical Center;
Department of Neurology[11], Radiology[12], Rijnstate Hospital, Arnhem;
Department of Radiology[13], Neurology[14], Haaglanden MC, the Hague;
Department of Neurology[15], Radiology[16], HAGA Hospital, the Hague;
Department of Neurology[17], Radiology[18], University Medical Center Utrecht;
Department of Neurology[19], Neurosurgery[20], Radiology[27], Radboud University Medical Center, Nijmegen;
Department of Neurology[21], Radiology[26], Elisabeth-TweeSteden ziekenhuis, Tilburg;
Department of Neurology[22], Radiology[23], Isala Klinieken, Zwolle;
Department of Neurology[24], Radiology[25], Reinier de Graaf Gasthuis, Delft;
Department of Neurology[28], Radiology[29], University Medical Center Groningen;
Department of Neurology[30], Radiology[31], Atrium Medical Center, Heerlen;
Department of Neurology[32], Radiology[33], Catharina Hospital, Eindhoven;
Department of Neurology[34], Radiology[35], Medical Spectrum Twente, Enschede;
Department of Radiology[36], Amsterdam UMC, Vrije Universiteit van Amsterdam, Amsterdam;
Department of Radiology[37], Noordwest Ziekenhuisgroep, Alkmaar;
Department of Radiology[38], Texas Stroke Institute, Texas, United States of America

PHD PORTFOLIO

Name PhD candidate: Haryadi Prasetya
PhD period: July 2015 – November 2022
Name PhD supervisor: prof. dr. H.A. Marquering
prof. dr. E.T. van Bavel
Name PhD co-supervisor: prof. dr. B.A.J.M. de Mol

PhD Training	Year	ECTS
General Courses (7.2 ECTS)		
AMC World of Science	2015	0.7
Medical Literature: Searching for a Systematic Review	2015	0.1
Practical Biostatistics	2015	1.1
Medical Literature: Embase-Medline via OvidSP	2016	0.1
Citation Analysis and Impact Factors	2016	0.1
Entrepreneurship in Health and Life Sciences	2016	1.5
E-Science	2018	0.7
Scientific Writing in English for Publication	2018	1.5
Project Management	2018	0.6
Oral Presentation in English	2019	0.8
Specific courses (3.8 ECTS)		
Front-end vision and multi-scale image analysis, TU/e	2015	2.5
Time Management	2018	0.3
Medical Imaging Summer School	2018	1
Seminars, workshops and master classes (7.5 ECTS)		
Cardiovascular Engineering Meeting	2015-2019	4.0
Plenary Stroke Meeting	2016-2019	2.0
Machine learning Meeting	2017-2019	1.0
APROVE Science Nights	2015-2019	0.5
(Inter)national conferences (3.5 ECTS)		
Fall Meeting of the NVPHBV (the Dutch Society of Pattern Recognition and Image processing)	2015	0.25
MICCAI	2017	0.75

Institute QuantiVision conference	2017	0.25
International Conference on Medical Imaging with Deep Learning (MIDL)	2018	0.75
Medical Imaging Symposium (MISP)	2018	0.25
World AI Summit	2018	0.5
International Stroke Conference	2019	0.75

Teaching	**Year**	**ECTS**
Lecturing and Tutoring (2.5 ECTS)		
MIK – Advanced Medical Imaging Processing	2015	1.5
Practicum Physics/Astronomy	2017	1.0
Supervising (12 ECTS)		
Aude Maurel	2016	1.0
Mariaconcetta Mele	2016	2.0
Emeric Barrier	2017	2.0
Dronika Debisarun	2017	0.25
Stephen Broeils	2017	0.25
Hugo Hoving	2017	0.25
Maarten Both	2017	0.25
Thabiso Epema	2017-2018	2.0
Merel van der Stelt	2018	2.0
Lisa MH Vermeulen	2018	1.0
Marc T Visser	2018	1.0

Parameters of Esteem	**Year**
Grants	
Research Grant, the Indonesian Endowment Fund for Education	2015-2019

ABOUT THE AUTHOR

Haryadi Prasetya is an Indonesian born on 4 March 1988 in Laxou, France. After his parents earned their doctorate degrees there, he relocated to Palembang, Indonesia, and had his primary education there. He was raised in an academic family and learned early on that pursuing the highest level of education is his family's hill to die on. At the ripe age of 14, Haryadi was sent 1000 kilometers away from home to forge his mind and body in a renowned military high school in Tidar Valley, Magelang, for three years. In 2005, he went to a high-standing engineering institute in Indonesia, Bandung Institute of Technology, for his undergraduate program majoring in Electrical Engineering. He was introduced to biomedical engineering and unwittingly fell into a deep fascination with the topic. He wrote his first paper then, presenting a method to detect cerebral aneurysms on CT Angiogram images based on curvature analysis.

Fresh off obtaining his engineering degree, Haryadi worked as a system engineer in the Home Theater System Division of Samsung Electronics Indonesia for one year. In 2011, he was awarded a full scholarship, a joint program between the Ministry of Communication and Information Technology of Indonesia and Korea University, to attend a Master's program at Korea University, Seoul, South Korea. In two years (2012-2014), Haryadi labored in the Digital Media Lab of Korea University, working on a Moiré pattern elimination project sponsored by Samsung on which his Master's thesis was based. During the program, he studied Computer Vision and strengthened his fundamentals in machine learning, pattern recognition, and K-Pop culture. Some of his research endeavors included indoor-outdoor scene classification using local and global descriptors, SIFT descriptor vocabulary construction using k-means clustering, and proof of concept of pedestrian tracking using a Support Vector Machine. Haryadi obtained his Master of Engineering degree with a GPA of 97.8 out of 100, which to his family's standard, was somewhat a slightly lamentable result.

In 2014, he returned to Indonesia to become a research assistant in the Biomedical Engineering department of Bandung Institute of Technology. For a year, Haryadi worked on developing a new medical device prototype of a non-invasive vascular analyzer before he was granted a doctoral scholarship from the Indonesia Endowment Fund for Education (LPDP) from the Ministry of Finance of Indonesia. He came to the Netherlands in 2015 for his PhD trajectory in the Biomedical Engineering & Physics Department of Amsterdam University Medical Centers, location AMC. In 2019, he started working as a Machine Learning Engineer in GlobalOrange, where he utilized natural language processing to summarize reports of elderly care nurses and developed an anomaly detection method to recognize fraudulent financial transactions in a general ledger. In 2021, Haryadi pivoted to become a quality engineer in the medical device domain, his current role in Nicolab.

In his spare time, Haryadi likes to read books, play basketball, strum his acoustic guitar, sing broken lyrics, argue with his 4-year-old daughter, and pretend to host a thought-provoking podcast.

ACKNOWLEDGMENTS

I would like to preface this by saying that if this is the first chapter that you read, then you know you helped shape my PhD journey. The lack of mention here, if any, does not take that away but does mean that I owe you a drink. Please come collect should an opportunity arise; a Prasetya always pays his debt.

I have dreamt about writing this acknowledgment. In that dream, I could not feel my limbs and my fingers were jelly, the so-called nonreciprocal flaccid paralysis. But I could remember that my chest was swelling with gratitude, elation was spilling over, and the anticipation of freedom began to crescendo. Of course, then, I woke up.

Now, a couple years and one pandemic later, my limbs are perfectly intact and in solid-state, my fingers are not viscous, and the crescendo continues as I recollect names to which my appreciation is abundant.

First, I would like to convey my earnest gratitude to the Indonesian Endowment Fund for Education, Ministry of Education, Indonesia for granting me the opportunity to be in this wonderful academic journey.

I will never obtain my degree without my promotion team, **Henk**, **Ed**, and **Bas**. **Henk**, your prayer has been answered, we made it! Your persistence that pulled me back in after the long hiatus has, quite frankly, resurrected this PhD, for which I am forever grateful. I learned many things from you: the value of hard work, saying "no", the joy of writing, and many more. Your no-nonsense attitude pulled myself up by the bootstrap and slapped my passive, hesitant old self out of existence. **Ed**, thank you for your boundless patience and constant support during my PhD. I always enjoy our theoretical discussion. The way you untangle esoteric concepts into digestible knowledge speaks volume to your fundamental understanding of the topic at hand. You spark curiosity and I will miss our discussions dearly. **Bas**, you have been very kind since our first interaction, as you warmly welcomed me into AMC. Thank you for extending the olive branch and turning my wish to pursue higher education in Europe into reality. Your valuable insights, relentless life and career advice, and words of encouragement have helped me tremendously.

I would like to extend my deep appreciation to my doctoral committee members, **Prof. Reekers**, **Prof. de Jong**, **Prof. de Winter**, **Prof. Hoekstra**, **Prof. Reneman**, and **Prof. Rajab**, for their invaluable contributions to the critical review of my thesis and their participation in my defense.

I would also like to express my sincerest gratitude to **Dara**. Your unwavering support have been crucial in helping me navigate the challenges of transitioning from Indonesia to the Netherlands. I am not sure if you are aware, but your generosity has left a lasting impact on me and my family. It meant the world, Mbak.

My Indonesian friends whom I met in Netherlands, **Edward**, **Viqa**, **Tezar**, **Intan**, **Rusydi**, **Fajran**, **Kania**, dan **Olivia**. Mas **Edo** dan Mbak **Viqa**, asimilasi hidup di Belanda di tahun-tahun pertama terasa mudah karena diisi hangatnya ramah-tamah Mas Edo sekeluarga. Nggak salah kalau kita bilang Mas Edo, Mbak Viqa, dan Raiden saat itu adalah hal terdekat yang bisa kita panggil keluarga di Amsterdam. Mas **Tezar**, Mbak **Intan**, **Rusydi**, Mbak **Kania**, dan Mas **Fajran**, terima kasih sudah menginspirasi akhir minggu kita dengan obrolan-obrolan santai, life hacks, masakan Indonesia ternikmat di Amsterdam, dan memberi bukti bahwa bapak-bapak pun masih bisa bermain game. **Olivia**, you have no idea how happy I was when I met you. You kept me sane, bailed me out of tough situations, and made work a bit more bearable. Akhirnya terjawab sudah pertanyaan favoritmu: “kapan PhD selesai?”.

Rekan-rekan seperjuangan, kandidat PhD di Amsterdam dari Indonesia, Mbak **Tiwi**, Mas **Eko**, Mas **Joko**, **Waway**, **Karis**, **Qalby**, Mbak **Indri**, Mbak **Meli**, Mbak **Amy**, Mbak **Mia**, Mbak **Meta**, Mbak **Dilfa**, Mas **Insan**, **Zulfan**, Mbak **Harmil**, Mas **Faqi**, Mbak **Widya**, dan banyak lagi, maaf kalau tidak semuanya tersebut (refer ke paragraf 1). Terima kasih buat semua makan siang barengnya, keluh kesah beasiswa dan PhD di belanda, dan saling menyemangati satu sama lain. Senang akhirnya saya bisa menyusul jejak langkah teman-teman semua dengan menyelesaikan studi saya di sini.

Ikastara family in Netherlands, **Hanif**, **Lydia**, kak **Myra**, Bang **Yosep**, Bang **Wibi**, Kak **Puri**, Bang **Okky**, dan lainnya yang tidak bisa saya sebut satu persatu, terima kasih

buat wisata kulinernya, sharing pengalaman dan nostalgia, canda tawa, dan obrolan tentang masa depannya.

Semuanya, terima kasih banyak sudah menjadi "little Indonesia" saya di Amsterdam.

My mentors in Institut Teknologi Bandung, Bu **Tati** dan Pak **Hasballah**. Terima kasih untuk inspirasinya dan kesempatan untuk melakukan riset di Teknik Biomedika ITB. Saya mungkin tidak akan putar arah kembali ke bidang biomedika tanpa anjuran dan bimbingan dari Ibu dan Bapak. Terima kasih juga untuk kolega-kolega di jurusan: **Siddiq**, **Eko**, Mas **Doni**, Mas **Agung**, Mbak **Astri**, **Nedya**, **Sari** dan Mas **Sandra**.

Old and long-distance friends who stayed in touch, **Arie**, **Kiki**, **Cheppy**, **Tyaz**, **Dahsi**, **Riza**, **Haris**, **Agung**, **Sakti**, **Affan**, **Catur**, **Muthya**, **Andhika**, and **Janar**. Exchanging stories with you kept me grounded and my mind centered. Thanks for making the time to check in and looking forward to our reunion.

My colleagues in BMEP and Radiology departments: **Mustafa**, **Jorrit**, **Emilie**, **Ralph**, **Merel**, **Renan**, **Wessel**, **Ilaria**, **Marit**, **Eva**, **ManonT**, **Lucas**, **Bruce**, **Henkie**, **Nerea**, **Ricardo**, **Marcela**, **Nils**, **Kilian**, **Ivo**, **ManonK**, and **Raquel**. Right from the get-go, I knew I was in a good company: beautiful minds, work-hard-play-harder attitude, shower of puns and sarcasm and inappropriate jokes, just about anything you need to be productive in your PhD. Thanks for all the coffee breaks, lunches, nerf gunning, darts throwing, basketball scrimmages, occasional dinners and drinks, sailings, escape rooms, Casablanca karaoke, fun conferences and summer schools, and the unforgettable getaways to Majorca/Malaga. **Mustafa**, thanks for the instant brotherhood, brother. Talking with you was always uplifting, you made sure that I felt that I belonged whenever I was drowning in impostor syndrome. **Merel**, boss lady! You are such an inspiration, except for maybe the jaywalking, or the occasional self-induced face planting. If every time I face a problem I ask myself "what would Merel do?", I think I'd be set for life. Thanks for the friendship and singing AC/DC with me back in Quebec City. **Renan**, my boy from Ipanema. I don't know if you have any idea how much you have shaped my life here, intentionally or not. You believed in me even when I didn't even believe in

myself. You pulled me out of a slump twice, and for that, I will always be doubly grateful. **Wessel**, thanks for all the movie nights, offhand quips, screaming "livin' on a prayer" to the mic, and simply being a great friend. I don't think I'll ever thank you enough for that phone call we had during the challenging time when my dad had a stroke. **Ilaria**, you had been so kind to me, popping in for a quick catch-up whenever you passed by our office. I miss chatting on the parenthood journey with you. Mama **Marit**, thanks for always looking out for me. Your tough exterior, earth-shattering sneezes, and unfiltered comments could not disguise how warm-hearted and compassionate of a person that you are to me. **Eva**, thanks for the small talk, positive attitude, and your unlimited tolerance dealing with noisy office mates like me, Bart, and especially Praneeta. **Manon T**, your tenacity to ensure non-Dutch speaking colleagues to always feel included and welcomed is an inspiration. I will always feel grateful to you for taking care of me when I had a dreadful toothache during our long flight from Canada. **Lucas**, the certified AI guru in my time, but I wasted your time talking about anime and manga instead. Thanks for all the fun conversations and good vibe. Your lego Luffy still stands tall on my office desk. **Henkie**, thanks for allowing me to pick your brain now and then. You have always been full of insights and well-informed on a lot of things. I really enjoy learning something new from our seemingly mundane conversations. Also, thanks for being so cool whenever I invaded your office to play darts. **Nerea**, in a bleak Dutch weather, you carried with you the Basque's sun. Your warm personality, fast-talking and proclivity to switch to Spanish mid-conversation, sprinkled with animated hand gestures and shoulder shrugs never failed to brighten my days. I'm very happy to call you one of my closest friends. **Kilian**, thanks for the short collaboration we had. I valued your opinion so much so whenever you agreed with my point my self-confidence shot through the roof. **Ivo**, the coolest dude in the radiology department, and now in the office. Always with the LA vibe and that majestic hair flip. I missed giving you flowers for your contribution to my work so let me officially redeem myself here: without you, chapter 4 would never materialize into existence. Thank you for your amazing work with MRCLEAN Registry that allows me and many more like-minded people to keep the momentum in stroke research going. If you still have some concern about this, let's settle it on the basketball court ☺. **Manon K**, your dedication to work is un-be-liev-a-ble. I was hoping to catch some of your hard-working virus

by being close to you but unfortunately, I think I was immune to it. Anyway, Hawaii was legendary indeed and I am happy I got to share it with you. Also, being interviewed in a Stroke podcast with you was a very cool experience as well. **Raquel**, my sister from another mister. You are a force of nature, unapologetically blunt, and always speaking your mind without filters. I really enjoy trading hard-hitting questions on life and relationships with you. Thanks for pushing me to the limits, whether it's in board games or ping pong, with your borderline-psychotic competitive fire. Looking forward to playing chess with you!

The same gratitude goes to all great colleagues on the other end of the corridor and downstairs, **Elco**, **Sanne**, **Daphne**, **Lorena**, **Bea**, **Leah**, **Abel**, **Roosje**, **Laura**, **Mariah**, **Teresa**, **Giuliana**, **Paul**, **Kerri**, **Judith** and all the others I probably miss but had been fortunate enough to meet and share lunch, labuitjes and birthday cakes. Special thanks to **Jetti**, **Carla**, and **Richard**, for always being helpful and available whenever I needed assistance around the office. From the other side of the building in the department of Cardiothoracic Surgery, big thanks to **Luisa** for her incredible support with all the monthly administrative tasks.

My colleagues in Nicolab (too many to mention, which is a good thing), I'm grateful for the privilege of working with some of the most brilliant and committed individuals I know in our shared mission of saving lives. I can't wait to see what we'll accomplish in the future and I'm thrilled to be on this journey with you lot!

My paranymphs, **Bart** and **Praneeta**. **Bart**, the Kyle Gass to my Jables, we fought the devil together and now the guitars wail, the angels sing, the sky opens up, and the light shines upon us as we come up victorious in tattered clothes and bruised bodies. No, that's not me being overly dramatic at all, that actually happened. Thanks for filling all my PhD years with laughter, Tenacious D sing along, arbitrary arm wrestling, Paint.net advanced tutorials, long experiment of turning milk into cheese, being undefeated duo in agar.io, failed attempts in songwriting, masterclass in procrastination contemplation, and our latest trend: making congratulatory videos. Jokes aside, your constant support, pep talk, intellectual and honest feedback have contributed so much to my sanity and ultimately the success of this PhD. I am eternally indebted to you. **Praneeta**,

thanks for always encouraging my unfunny jokes and horrible puns. Your sarcastic laugh, side-eyes, and all the time when you called me out in disappointment, have challenged me to be a better person… and to find a better way to annoy you. You were there when I needed someone to validate my stereotypical Asian stories of suffering, or just simply be a listening ear when I sang Bollywood songs. I miss sharing an office with you and spending most of our time debating absurd topics, questioning our reality, and telling each other to shut up. I'm excited to see this new business venture you're about to kickstart!

I would be remiss if I didn't mention how massive of an impact the support I received from my family during this challenging venture. **Papa**, **Mama**, terima kasih untuk doa, dukungan dan nasihat-nasihat papa dan mama. Mendengar suara papa dan mama lewat telepon dan video call selalu menyuntikkan energi baru dan mendorongku untuk terus bekerja keras menyelesaikan studi. Menjadi kebanggaan orang tua dan keluarga selalu menjadi motivasiku, dan semoga gelar doktor yang dicita-citakan sejak aku TK, bisa membuat papa dan mama sedikit lebih berbahagia. **Kak Yan**, **Kaka Winni**, **Ichsan**, **Tanti**, **Yiyin**, dan **Ammar**, terimakasih buat update keluarga, berbagi foto-foto, tur keliling Eropa, dan permintaan THR tanpa henti yang selalu kutolak dengan senang hati. **Imam**, terima kasih sudah menjadi adek yang bijak dan dewasa. Kisah karirmu luar biasa inspiratif lho. Dan untuk semua keluarga di Indonesia, walaupun terpisah 11.000 kilometer, dukungan moral dan pesan-pesan positif melalui group message dan social media selalu membuatku melalui hari dengan sukacita. Terima kasih.

Now, dear my better half, **Aya**. Words cannot express the depth of my gratitude for being by my side through it all. Our life together in the Netherlands has been filled with ups and downs. You have been my rock, my anchor, my beacon of unrelenting support. Your smile, awkward dance, and soothing words carried me throughout our most difficult days. You're the laughter I need when things go wrong, and the steady in my chaos. Without you, I would not be sitting here today, counting on the days when this PhD journey will finally culminate: with you in the front row watching me defend my thesis, hopefully with the same passion I had when I pitched to you why we need a new TV. Thank you, and here's to happier times ahead. I love you.

Finally, my twinkle toes cuddlebug, **Milarose**. When the stork came over and dropped you gently on our porch four and a half years ago, it left a message: “Try finishing your PhD now.” And boy, how I love proving an imaginary animal wrong. For you, I could give the whole world so what is a mere PhD thesis? Thanks for all the hysterical scream and sprint every time I come home, your silly faces and random giggles, your validations for my dad jokes. They never fail to recharge my energy and fill my heart with pure bliss. If you ever read this, I hope you know how much I love you. I wish you a bright future, long-time happiness, and a world where reperfusion assessments in medical images are fully automated and quantified.